Electrocatalysis of noble metal alloys for denitrification in the hydrosphere

（水圏における脱窒素のための貴金属合金の電極触媒作用）

A thesis submitted

for

the degree of Doctor of Philosophy

by

Md. Motahar Hossain

in the

Division of Environmental Materials Science

Graduate School of Environmental Science

HOKKAIDO UNIVERSITY

March 2014

Table of contents

Chapter 1

Introduction

Nowadays groundwater is significantly contaminated with nitrate. It has become one of the key environmental issues to solve because nitrate causes damages to human health and ecosystem. Groundwater is the principal source of drinking water in many rural communities and some large cities [1]. About more than one-half of the population in the world is using groundwater as drinking water. According to FAO AQUSTAT database (AQUSTAT is FAO's global water information system, FAO stands for Food and Agriculture Organization of the United Nations) in 2005, in many countries such as Algeria, Bangladesh, India, Iran, Libya, Saudi Arabia, Syria and Yemen, groundwater is used rather than surface water in their agriculture sector. In the United State in 2005, 23 % of the freshwater has been supplied from groundwater and the rest was provided from surface water [2]. Water supply companies are predominantly using groundwater for the household and domestic purposes in the federal republic of Germany. Denmark also mostly relies on groundwater as a source for dinking water. In Danish, 98-100 percent of water for household and domestic purpose come from groundwater and 0-2% from surface water. In fact, groundwater is of great importance, as a water source throughout Europe. More than 65% of the drinking water comes from groundwater [3]. This chapter briefly describes the present situation of nitrate contamination, de-nitrification methods, summary of the pervious study of electrocatalytic reduction of nitrate ions as well as the objective and outline of the thesis.

1.1 Present situation of nitrate contamination

Nitrogen (N_2) is the main component of air, which we breathe [4]. Besides N_2, nitrogen can exists in many forms, such as N_2, N_2O, NO, NO_2, NH_3 in the atmosphere [5]. Most of them convert to nitrate and ammonium ions in solution through the

interaction with bacteria, rainwater, etc. These ions can be easily mixed with the soil to be a part of the soil ingredient, and consequently go into groundwater. Although there are many sources of nitrogen (both natural and anthropogenic) that could potentially lead to the pollution of the groundwater by nitrates, the anthropogenic sources cause the amount of nitrate to rise to a dangerous level. The main anthropogenic origin of nitrate contamination of the groundwater is waste materials, such as human and animal sewage, wastage from food processing industry, and improper disposal of manures. [6]. In densely populated areas, septic tank is another major anthropogenic source of nitrate contamination of the groundwater [6]. The utilization of chemical fertilizer in the agriculture sector is also the major source of nitrate pollution in the groundwater. In the agricultural farms, farmers extensively use nitrogen-containing fertilizer on their cultivated land to get maximum production [7]. The manure is another potential source of nitrate contamination. It is generally stored in large holes in the ground, and consequently massive leakage of nitrate to groundwater takes place.

The World Health Organization (WHO) standard is set at 50 ppm as NO_3^-, which corresponds to 11 ppm as nitrate-N [8]. United States Environmental Protection Agency (US-EPA) and Ministry of the Environment in Japan set the permissible limit of nitrate concentration at 10 ppm as nitrate-N (45 ppm as NO_3^-) based on the adverse effect on human health due to nitrate intake [3]. The nitrate concentration exceeds these standards in many areas of Europe (Great Britain, France, the Netherlands, Germany, and Switzerland, Italy, Belgium, Namibia), several areas of the United States, Israel and Japan as well as many areas of South East Asia (India, Bangladesh, Pakistan, Bangkok etc). Therefore, groundwater is significantly contaminated by nitrate (Figure 1.1) and it is a customary problem throughout the world.

The Ministry of Environment, Japan, regularly examines the nitrate contamination of the groundwater from 1999 to 2009. The Figure 1.2 shows the present situation of nitrate-nitrogen contamination of the groundwater ~~of~~ in Japan. Nitrate contamination is spreading into all over the country (Figure 1.2). The contamination level exceeds the permissible limit of 10 mg/L nitrate-nitrigen (NO_3-N). This high level of nitrate contamination of groundwater in Japan is also associated

with agricultural activity (extensive use of fertilizer, improper spreading and disposal of manure over farmland).

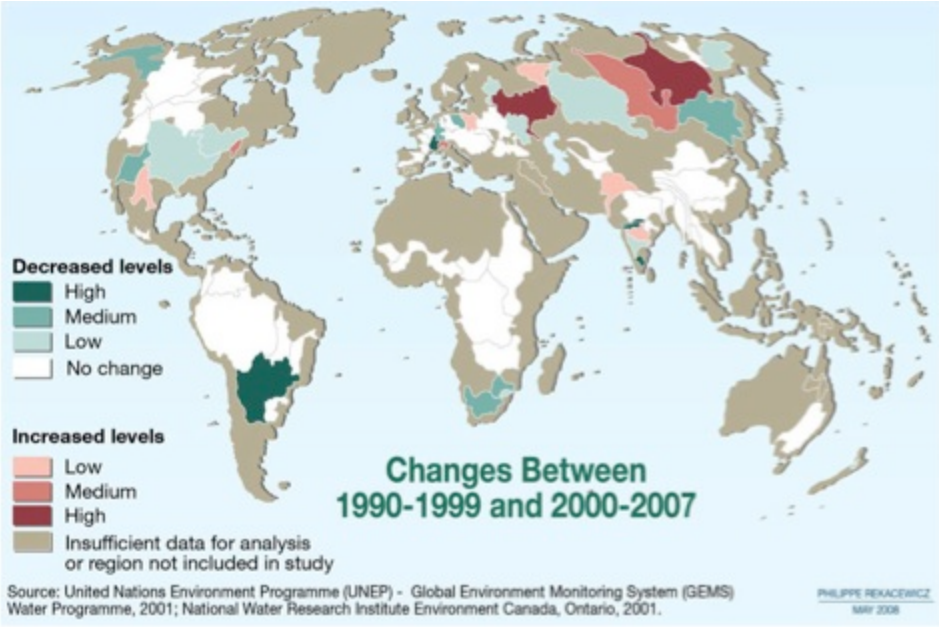

Figure 1.1 Nitrate contaminations in groundwater in the world *(Ref. water Quality for Ecosystems and Human Health, 2nd edition, UNEP, ERCE, UNESCO, 2008).*

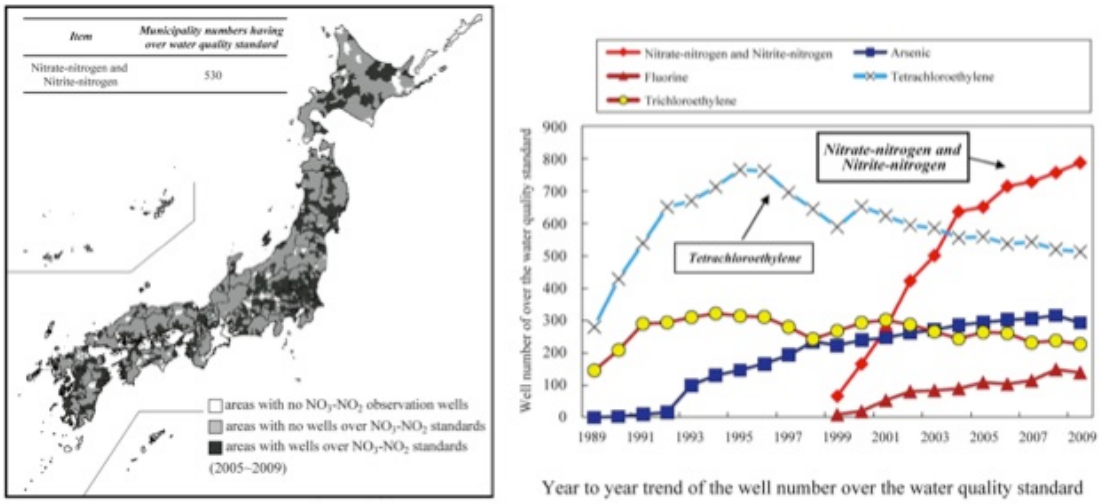

Figure 1.2 Nitrate contaminations in groundwater in Japan *(Source: http://www.maximsnews.com/news20120514ShimadaCREST11205140802.htm).*

Nitrate itself is less toxic. In the human stomach nitrate is reduced to nitrite by the microorganism under acidic condition. The nitrite is very toxic and can causes the following serious health problems:

Methemoglobinemia: Methemoglobinemia is one of typical disorders causing cyanosis. Infant cyanosis is called a blue baby syndrome. In the blood, two molecules of hemoglobin react with one molecule of nitrite to form methemoglobin [6]. This compound interferes with the blood's ability to carry oxygen. This leads to slow suffocation of the infant and consequently to death [7]. Because of the oxygen deficiency, the lip of the children turns into blue or purple, for this reason methemoglobiemia is referred to as blue baby syndrome [6]. Others symptoms of methemoglobinemia are gastrointestinal disturbance, such as vomiting and diarrhea, mental disorders (relative absence of distress when strictly cyanotic, and prickly when mildly cyanotic), and chocolate-brown colored blood [6, 8].

Carcinogenicity: In the human body, nitrites readily react with amide and amino compounds, especially secondary amines and alkyl amides, to generate N-nitroso compounds. This compound is a potential carcinogen for animal species [9, 10] and therefore probably carcinogenic for humans [11]. In numerous studies, it was concluded that exposure to high levels of nitrate and nitrite in drinking water has been linked to a variety of effects ranging from enlargement of the thyroid to fifteen types of cancer, two kinds of birth defects, and even hypertension. Since 1976 there have been a number of different epidemiological studies in eleven different countries that showed a definite relationship between increasing rates of stomach cancer and nitrate intake [12, 13, 14]. The National Academy of Science concluded that uptake of highly contaminated drinking water increases the possibility of human cancer risk [15]. Some other epidemiological studies also assessed that high intake of nitrate or nitrite-contaminated drinking water for a long time results in the increased risk of cancer. It is also reported that brain tumor in children has also positive correlation with nitrite intake from nitrate-contaminated drinking water or cured meat during pregnancy [114, 115].

1.2 Denitrification methods

Nitrate and nitrites are naturally occurring ions. Nitrate easily dissolves in water at ambient temperature and pressure and it is very difficult to remove. The

conventional household treatment methods such as boiling, filtration, disinfection and water softening are not effective for nitrate removal like other contaminants. There are several effective methods, which have already been established for removal of nitrate from drinking water. These methods are chemical denitrification, ion exchange, reverse osmosis, electrodialysis, catalytic denitrification and biological denitrification. These methods are concisely discussed from the viewpoint of the cost, maintenance requirements, efficiency and speed of treatment and drawbacks.

Chemical denitrification

Chemical processes for denitrification of water generally involve the treatment of nitrate with various reactive metals and compounds. These reactions can be understood to produce nascent hydrogen, which can then act as a reducing agent for anions such as nitrate and the reaction rate depends on pH of the solution. Using zero-valent metal like iron (Fe^0) and aluminum (Al^0), many studies has been investigated for removal of nitrate. Zero-valent iron Fe^0 is oxidized to ferrous ion (Fe^{2+}) whereas nitrate ion is reduced to ammonia or nitrogen gas in an aqueous solution of the acidic pH [eq. (i) and (ii)] [19]. In basic media (pH > 10.5), Al^0 also reduces nitrate to ammonium ion or nitrogen gas and itself is oxidized to Al^{3+} ion [eq (iii) and (iv)] [20, 21].

$$NO_3^- + 4Fe + 10H^+ \rightarrow 4Fe^{2+} + NH_4^+ + 3H_2O \quad \text{(i)}$$

$$2NO_3^- + 5Fe + 12H^+ \rightarrow 5Fe^{2+} + N_2 + 6H_2O \quad \text{(ii)}$$

$$3NO_3^- + 8Al + 18H_2O \rightarrow 3NH_3 + 8Al(OH)_3 + 3OH^- \quad \text{(iii)}$$

$$6NO_3^- + 10Al + 18H_2O \rightarrow 3N_2 + 10Al(OH)_3 + 6OH^- \quad \text{(iv)}$$

Chakrabarty studied the chemical denitrification using zero-valent magnesium [22]. In acidic media, magnesium produces hydrogen gas by donating two electrons to hydrogen ion [H^+]. This hydrogen gas can interact with nitrate to generate ammonia or nitrogen gas.

$$2H^+ + 2e^- \rightarrow H_2$$

$$2NO_3^- + 5H_2 \rightarrow N_2 + 4H_2O + 2OH^-$$

$$NO_3^- + 4H_2 \rightarrow NH_3 + 2H_2O + OH^-$$

There are many disadvantages in the chemical processes for the denitrification of water. It requires high capital investment because of the reaction should be done in the anaerobic condition. Most of the cases, the treatment produces a precipitate or sludge as by-products which is necessary to dispose. The disposal is associated with the further environmental concern as hazardous waste. Another most important disadvantage of this process is that it needs pretreatment as additional water treatment steps prior to the process. Another vital problem is that the metal ions are used in this process, which may exceed the maximum contaminant level for metal as specified by the U.S. Environmental Protection Agency, thereby increase the expenditure due to removal of the metal ion.

Ion-exchange

Ion exchange is the most frequently used treatment technology for nitrate removal. This technology removes nitrate ions from the aqueous phase by replacing them with the anion present in the ion exchange resin. Resin beds are consists of millions of tiny spherical beads, which usually are about size of medium sand grains [23]. Particular resins are used to substitute chloride ion for the nitrate ion (NO_3^-) in this process. Alternatively, nitrate-selective resins may also be used. As contaminated water is passed through the resin, contaminant ions are exchanged with other ions, mostly chlorides in the resin. The entire process is composed of the following four major steps to remove the selected ion.

1) Resin recharge
2) Anion exchange
3) Resin becomes exhausted
4) Resin regeneration

In the initial step of the process, the bed is recharged and reaching its utmost exchange capacity. The resin at this time has enough chloride ions to bring out the exchange as the solution passes through the complex [resin as for example Microporous nitrate selective strong base anion resin (triethylamin groups)]. The ion exchange is the next process. The resin bed commences to eliminate the sulfate radicals first. After the majority of SO_4^{2-} has been removed, the exchange of nitrate

with chloride starts. The completion of this phase is the third step. As all ionic exchange sites are occupied with anions from solutions, the resin is exhausted. At this

point no more anions leave the solution. Finally, in the fourth process, by passing a concentrated solution of sodium chloride over the resin the bed is regenerated by displacing the removed ions with the chloride ion [24].

The main problem is that the brines are generally either stored in landfills or discharged in the sea, which enhances the threat of future watershed pollution. Therefore the implementation of ion exchange process for denitrification is discouraged in many areas.

Electrodialysis

Electrodialysis is an electrically driven process where the voltage is used to drive charged ions through ion exchange membranes, reducing the TDS (total dissolved solids) in the source water. The source water flows between the cation and anion exchange membranes via flow spacers that are placed between the membranes. The spacers are used to provide a flow path for the water, support the membranes, and create turbulent flow. The DC (direct current) voltage potential induces the cations to migrate toward the cathode through the cation exchange membranes, and the anions to migrate toward the anode through the anion exchange membrane. The principle of the electrodialysis for the nitrate removal method is given below (Figure 1.3).

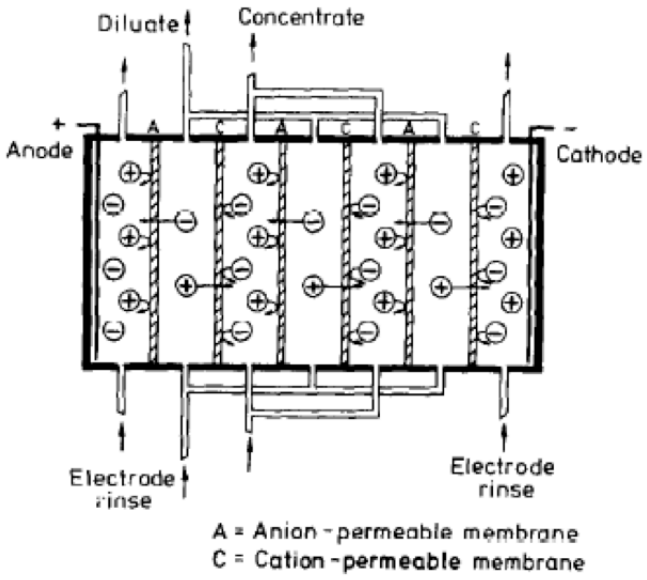

Figure 1.3. Principle of the electrodialysis for nitrate removal method from water. [*Ref. Distillation 65 (1987) 241]*.

The cations and anions get collected in the throw out waterside of the membranes and generate low TDS (total dissolve solids) product water on the dilute side of the membranes.

The polarity of the electrode is turned around two to four times an hour and changes the flow of ion movement in the electrodialysis reversal process [25]. Even though the process provides high recoveries, this process is applicable only for soft water treatment and need to control pH [26]. The cost of this process is very high and is impossible to establish for small-scale treatment [27, 28].

Reverse Osmosis

Reverse osmosis (RO) is a process for the removal of dissolved ions (nitrate ions) from water in which pressure is used to force the water through a semi permeable membrane element and to reject most of the dissolved materials [27, 28]. Removal of nitrates is achieved by putting the pressures exceeding its corresponding osmotic pressure upon RO cells. Pressures ranging from 300 to 500 psi (2070-10350 kPa) are applied to reverse the normal osmotic flow of water. The flow diagram of RO plant for nitrate separation from well water is given below (Figure 1.4).

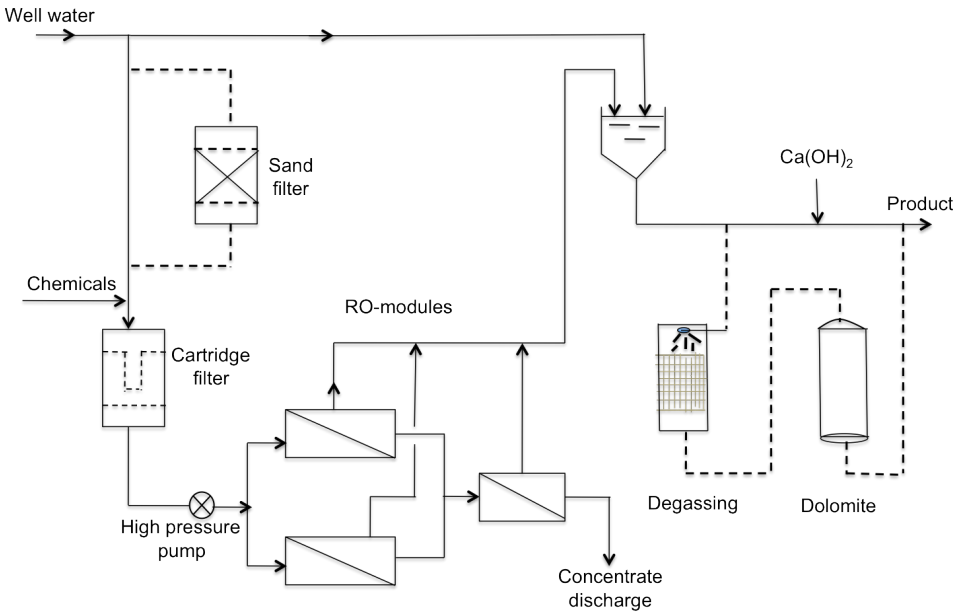

Figure 1.4 Flow diagram of reverse osmosis plant for nitrate separation from well water. [*Ref. Distillation 65 (1987) 241]*

Membranes commonly used are made of cellulose acetate, polyamides, and composite membranes are also available. These membranes do not show any preference for specific ions, but the degree of salt rejection is found to be proportional to the valence of ions present in the water supply. Though it is very cost effective technique, it has also some disadvantages. The main problems of this process are membranes fouling, compaction and deterioration with time. These problems occur due to deposition of soluble materials, organic matter, suspended and colloidal particles and other contaminants, pH variations and chlorine exposure, therefore pretreatment is required.

Biological denitrification

Biological denitrification exploits the ability of certain naturally occurring bacteria to use nitrate for respiration under anoxic conditions (absence of oxygen). The overall process is the reduction of nitrate to nitrogen gas occurs through a series of steps as follows [29]:

$$NO_3^- \rightarrow NO_2^- \rightarrow NO \rightarrow N_2O \rightarrow N_2$$

The range of the oxygen concentration from 0.1 to 0.2 mg/L has been indicated to have inhibitory effects on denitrification [30]. Denitrification can be employed in both heterotrophic and autotrophic bacterias. In heterotrophic bacterias under anoxic conditions, organic substrates such as methanol, ethanol, and acetic acid are used for the conversion of nitrate to nitrogen. The carbon monoxide was also used for the denitrification of water [31]. Autotrophic bacteria such as *Thiobacillus denitrificans* are proficient of denitrification [32]. Hydrogen or reduced sulfur compounds are used as substrates, and carbon dioxide or bicarbonate serves as the carbon source for cell synthesis in autotrophic denitrification. Autotrophic denitrification is significantly influenced by the ratio of the sulfur (S) and nitrogen (N). Various unit processes have been studied and used for biological denitrification. Fluidized and packed bed reactors are the commonly used reactor configurations, and immobilized microbial systems using alginate beads or other polymer matrix has been studied. Autotrophic organisms like *Micrococcus* are capable to reduce nitrate to

nitrogen and at the same time oxidize hydrogen to form water. Gross and Treutter developed a process known as DENITROPUR using hydrogenotrophic denitrification. The schematic diagram is given below (Figure 1.5).

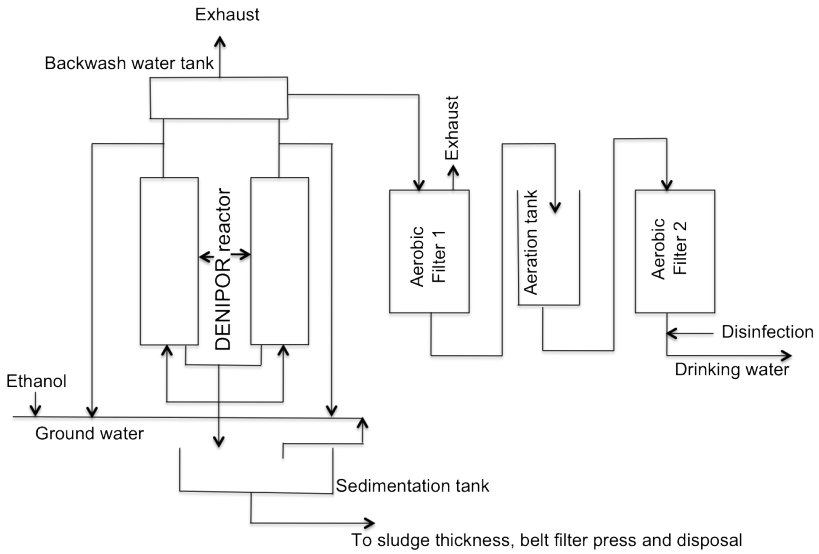

Figure 1.5 Schematic diagram of treatment plant using DENITROPUR process. [*Ref. J. Environ. Eng. 123(1997) 123]*.

The reproduction rate of autotrophic bacteria is low; therefore less biomass sludge needs to be disposed. In this method, post treatment is generally required to eliminate bacteria and enduring organic carbon. Biological denitrification method is reasonable but it has also several disadvantages such as

(1) Need to control temperature because the fermentation activity of the bacteria is declined at low temperature.

(2) Require a large reactor and need to control pH to increase the yield of the treatment.

(3) Further risk to contaminate water by bacteria

(4) Generate nitrite as byproduct, which is also toxic.

Catalytic denitrification

Horold et al. developed a catalytic process for reducing of nitrite and nitrate in drinking water remediation system [90]. The authors found that in the presence of hydrogen, palladium-alumina was the potential catalyst for reducing nitrite to nitrogen (98%) and ammonia. The lead (5%) copper (1.25%) Al_2O_3 catalyst was found to

completely remove nitrate from water containing an initial nitrate concentration of 100 mg NO_3^-/L. The reaction was completed in 50 min. The activity was 30 times greater than that of microbial denitrification. The process is also applicable and effective under certain conditions for ground water (temperature 10 ^{0}C, pH 6-8). The metal catalyzed denitrification can be split into four steps, which are described as follows:

$$NO_3^- + H_2 \rightarrow NO_2^- + H_2O \quad \text{(i)}$$

$$2NO_2^- + H_2 \rightarrow 2NO + 2OH^- \quad \text{(ii)}$$

$$2NO + H_2 \rightarrow N_2O + H_2O \quad \text{(iii)}$$

$$N_2O + H_2 \rightarrow N_2 + H_2O \quad \text{(iv)}$$

Ammonia is also generated according to the following reaction

$$NO_2^- + 3H_2 \rightarrow NH_4^+ + 2OH^- \quad \text{(v)}$$

This process works under specific conditions such as pH = 6 – 8, about 10 $^\circ$C and low nitrate concentration (up to 100 mg L^{-1}). The automation is easy to attain. Because of higher efficiency compared to biological processes as well as cost effectiveness, the catalytic denitrification might be also useful for small water treatment systems [33].

1.3 Electrochemical denitrification:

Electrocatalytic denitrification is a promising and effective approach to eliminate nitrate from drinking water. Basically, the electroreduction of nitrate is an complex process [39]. At the cathode, nitrates are principally reduced to relatively stable intermediates and various reduction products such as NO_2^-, NO, N_2O, N_2, NH_2OH NH_3 [132]. The type of the products and their relative production are dependent on the electrode materials, applied reduction potential, type of supporting electrolyte and the concentration of nitrate. In general, the main unfavorable reduction products are nitrite and ammonia because they are more toxic than nitrate so that their production reduces the potential applications of the electrochemical process for denitrification [40, 41, 42, 43]. Moreover, at the cathode the nitrite and ammonia is

oxidized to nitrate and nitrogen before their diffusion to the bulk electrode. The general reaction mechanism observed for the reduction of nitrate on metal electrodes as follows (Figure 1.6).

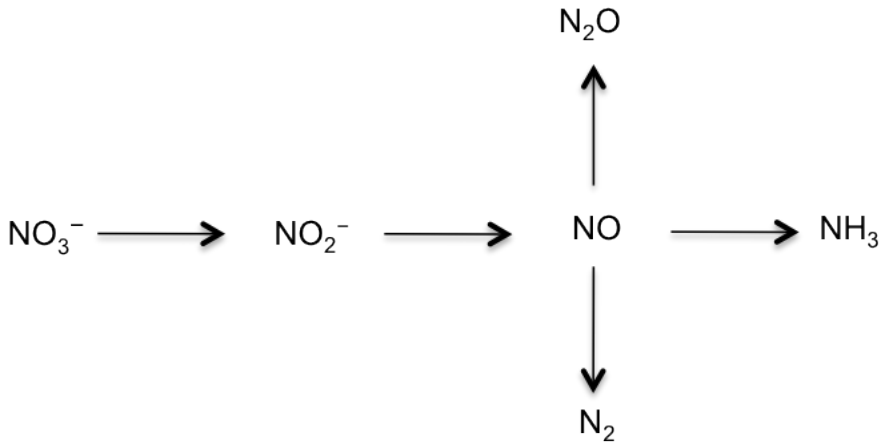

Figure 1.6 Reduction pathway for the reduction of nitrate on metal electrodes.

1.3.1 Advantages of electrochemical method

As discussed briefly in the previous section, there are various methods, which are useful for nitrate removal from dinking water. Among them, the electrocatalytic denitrification is the most effective and promising technique to reduce nitrates because of its superior advantages such as environmental compatibility, versatility, energy efficiency, safety, selectivity, amenability and cost effectiveness described the details of these advantages [44]. Based on their description, a brief summary of the advantages is noted as follows.

Environmental compatibility: Only electron and water are used as reagent, and no need to use extra reagent. Furthermore, most of the processes are highly selective and can be used to avoid the formation of unwanted side products.

Versatility: Electrochemical method is applicable in direct or indirect oxidations, phase separation and biocide functions. This process is effectively useful for many kinds of pollutants in different state such as gases, liquids and solids.

Energy efficiency: Electrochemical processes generally required low temperature compared to other non-electrochemical methods. The electrode and electrochemical cell can be easily designed and automation of applied voltage.

Therefore the power loss is reduced due to poor current distribution, voltage drop and side reaction.

Cost effectiveness: The necessary materials and operations are very simple and, and if properly designed also inexpensive.

1.3.2. Summary of the previous study

Numerous studies have been done during last hundred year on electrocatalytic reduction of nitrate. Electrocatalysts could be strategically applied for the purification of water treatment plant and industrial wastewater. Copper/palladium (Cu/Pd) were considered to be effective electrocatalysts for nitrate reduction until Sn-modified noble metals have been proved as very active cathode materials. Various metal cathodes have been extensively studied including Pt [45-50], Pd [47, 49, 51-54], Ni [48, 55-57], Pb, Zn, Fe [57], Cu [56, 58-62, 65], Ti [59, 63], Au [64-66], Au(Hg) [67], Ru, Rh, Ir [65, 68, 69], Bi[70], Sn [71, 72], vitreous carbon [73], pyrolytic graphic electrodes for electrocatalytic reduction of nitrate ions.

Vijh first attempted to compare the activity of various metals for the electrocatalytic reduction of nitric acid/nitrate [74] and concluded that metals having a high overpotential for hydrogen evolution also have a high overpotential for the reduction of nitrate. Dima et al. reported the electrocatalytic reduction of nitrate on five transition metals (Pt, Pd, Rh, Ru, Ir) and three coinage metals (Cu, Ag, Au) in acidic media [65]. Of the transition metals, the order of the catalytic activity for nitrate reduction is Rh > Ru > Ir > Pt > Pd when sulphuric acid was used as supporting electrode [76]. Rh showed the highest catalytic activity and this result is consistent with the results obtained by Wasberg and Horanyi [77, 78]. Based on the experimental results, the authors concluded that nitrate reduction on Rh reaches diffusion limited values. There are no gaseous products generated on Rh, in agreement with the observation by Brylev et al. [79]. The predominant products are ammonia and nitrite. Da Cunha et al. reported that the formation of gaseous products NO and N_2O was observed on Rh while using a high concentrated nitrate solution [47]. In this regards, the high activity of rhodium was confirmed to be due to high affinity of Rh for anions. The Tafel slope reported for the nitrate reduction on Rh was

close to 120 mV/decade, which implies that the rate-determining step is the conversion of nitrate to nitrite [78, 82]. The reaction rate may be hindered through the addition of chloride ion to the solution and may introduce galvanostatic potential oscillations [77]. Also the adsorption of the methanol chemisorption products, carbon monoxide has an inhibitive effect on nitrate reduction on Rh [78].

Considering the catalytic activity of the coinage metals, copper showed the very high activity for nitrate reduction, followed by silver and gold [82], whereas the rest of the metals showing very low activity. The elctrocatalytic activity for the reduction of nitrate on copper has been extensively investigated. Pletcher and Poorabedi observed that copper showed very fast reaction rate for the reduction of nitrate in acidic media to lead a diffusion-limited wave [81]. The predominant reduction product on copper was ammonia and the reduction was inhibited by the addition of chloride and bromide to the solution. Using online differential electrochemical mass spectroscopy (DEMS) the gaseous product (nitric oxide) was observed for the reduction of nitrate on copper in contrast to Pt and Rh, although no N_2O was formed [82]. It was also stated that copper is unstable and corrosive in acidic media that may influence the reduction of NO to N_2O [83]. Reyter et al. have studied the reduction of nitrate using activated copper which was prepared by using high-energy ball milling and alkaline pretreatment [89]. The reduction rate was 10 times greater for copper powder milled under air than that of copper milled under argon condition. This is happened due to the formation of more surface defects that may facilitate the nitrate adsorption on the electrode surface. The main reduction product was NH_3.

A very limited study has been done for nitrate reduction on “poor metals” such as mercury, [84] indium, [85] cadmium, [86] and tin in acidic media [87,71]. These metals have a high overpotential for the reduction of nitrate. Vijh found [74] that there is a relation between the overpotential for hydrogen evolution and nitrate reduction. Kyriacou and co-workers [71, 87, 88] obtained very attractive findings that tin is able to reduce nitrate to dinitrogen with very high selectivity (> 90%) at very negative potentials (–2.8 V vs Ag/AgCl), the rest of the products are nitrite and ammonia. At these very negative potentials, “cathodic corrosion” (destruction by hydride

formation) of tin takes place. Therefore this process is not useful for denitrification of water for practical application.

The main purpose of these past researches for nitrate reduction is to attain greater selectivity for the formation of hydroxylamine or nitrogen. Many studies have been accomplished using pure metal surfaces and none of them are proficient to reach such high selectivity. To achieve this aim, bimetallic alloys or monometals modified with foreign metal as adatoms or adions have been extensively studies for the reduction of nitrate. In this respect, numerous studies have been investigated for the catalytic activity of novel metals (Pd, Pt) modified with copper because copper itself is active for the reduction of nitrate and repercussion nitrite. Vorlope et al. investigated palladium-copper catalysts for nitrate reduction and suggested that copper was the selective catalyst for the reduction of nitrate to dinitrogen [90]. A systematic electrochemical investigation for the reduction of nitrate at palladium-copper electrodes was conducted by De Vooys et al. [91]. They observed that Pd has very low electrocatalytic activity for nitrate reduction and the activity drastically increased with the presence of copper on Pd surface. They also concluded that the activity and selectivity are dependent on the surface coverage of copper, whereas at the low Cu coverage, N_2 was produced with the highest selectivity (ca. 40%), while the highest activity was obtained at the highest Cu coverage with lower selectivity towards N_2. De Vooys et al. have made the following conclusion for the above observations. The copper sites on the surface are accountable for the reduction of nitrate to nitrite and NO because the Pd is inactive for nitrate reduction. Even though both copper and palladium is the efficient catalyst for the reduction of NO to N_2O but palladium is also highly active for the reduction of N_2O to N_2 [92], this reaction does not occur on pure copper metal electrode. It is also reported that N_2O was not generated on pure copper but on Pd surface fully covered by copper as the main reduction product. Pronkin et al. observed the similar enhancement effects in nitrate reduction using in situ prepared bimetallic PdCu nanoparticulate catalysts [93]. The different phenomena were observed between underpotentially deposited copper on platinum and Pd surfaces.

Pt has low activity in the reduction of N_2O, consequently less selective for the reduction of NO to N_2 compared to Pd. Therefore it is clearly attributed that PtCu electrode generates more ammonia and less N_2, which has been studied by Kerkeni et al. [94]. Palladium and platinum modified by silver has also the same enhancement effect for reduction of nitrate as like as Cu. On the other hand, Au modified Pd or Pt electrodes do not have the promotional effect [49, 94]. Whereas copper modified Au

electrode showed higher catalytic activity towards nitrate reduction. The general reaction mechanism for nitrate reduction on PdCu binary surface is given below (Figure 1.7).

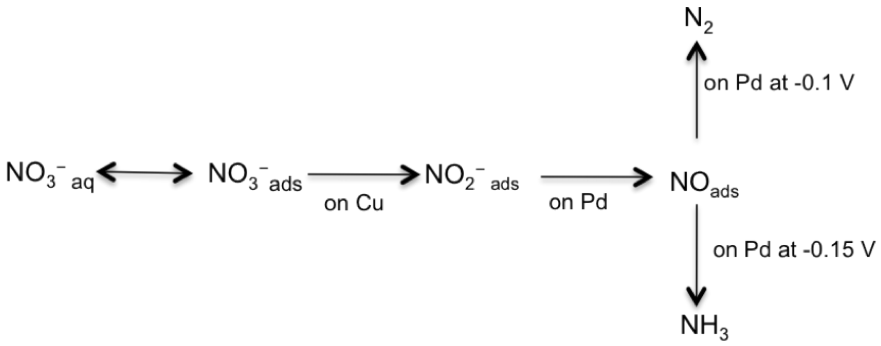

Figure 1.7 Reduction pathway for the reduction of nitrate on PdCu

Another most effective promoter for the reduction of nitrate on platinum or palladium is tin. The tin also enhances the selectivity toward N_2 formation [95, 96, 56]. Shimazu et al. have carried out electrochemical investigations of the tin-modified palladium and platinum deposited on Au [97]. They also found that without tin Pd and Pt has almost no activity for nitrate reduction whereas the activity abruptly increased by the addition of small amount of tin. The activity is dependent on the Sn coverage on Pd or Pt electrodes in acidic media. The maximum activity was observed at Pd surface with the Sn coverage was ≥ 0.75, in contrast the highest activity obtained on Pt at the Sn coverage of ca. 0.35-0.4 monolayer. The authors found that after a prolonged electrolysis at constant potential these electrodes, hydroxylamine was the predominant reduction product for tin/palladium, whereas the nitrogen dioxide (N_2O) was the most likely major products on tin/platinum/gold. They suggested that due to the stronger affinity of Sn towards oxygen compared with that of Pd and Pt, one or two oxygen atoms of nitrate most probably can easily coordinate with tin for Sn/Pd and Sn/Pt/Au electrodes thereby facilitated the reduction activity. A scheme for the mechanism of nitrate reduction on Pt-Sn binary metals is given below (Figure 1.8).

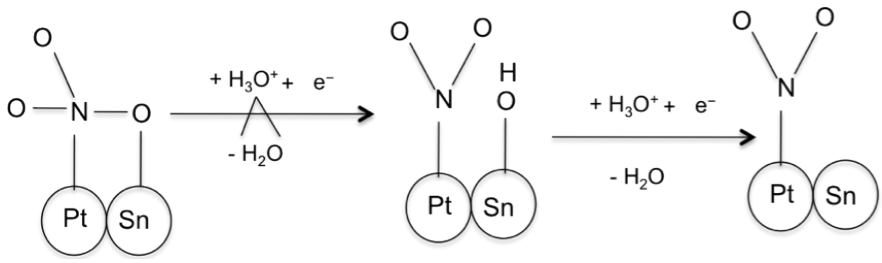

Figure 1.8 Nitrate reduction mechanism on Pt-Sn binary metal electrode.

The binding energies of Pd3d, Pt4f and Sn3d indicated that the oxidation state of Pd and Pt on the electrode surface is zero whereas Sn is most plausibly divalent. It is also observed that addition of Sn on the surfaces does not affect oxidation state of Pd and Pt. Shimazu et al. also concluded from the Tafel slope and pH dependence of the reaction rate that the reaction of adsorbed nitrate with the hydronium ion and an electron is the rate-determining step.

$$NO_3^- + H_3O^+ + e^- \rightarrow NO_2^-(a) + OH(a) + H_2O$$

The authors proposed the following reaction pathway for the production of N_2O and N_2 from NO_3^- (Figure 1.9).

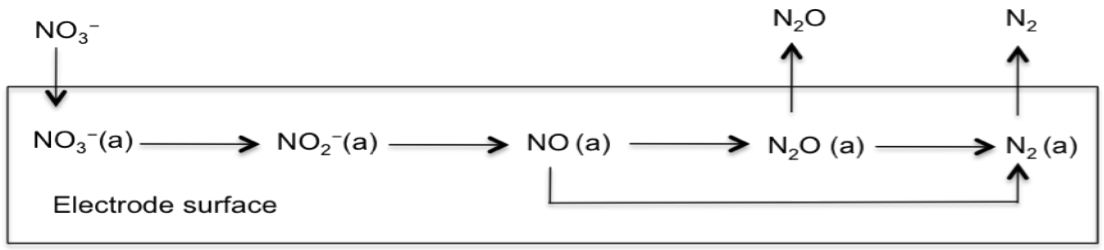

Figure 1.9 Nitrate reduction mechanism on Pt-Sn binary metal electrode.

Shimazu et al. also investigated the reduction of nitrate on gold electrodes modified with tin and palladium or platinum aiming to reduce overall loading of the noble-metal component [98, 95, 96]. A high electrocatalytic activity was obtained on the Pt-Sn electrodes for nitrate reduction but the selectivity was 97% ammonia. On the other hand, the highest activity and selectivity to gaseous products including 37% N_2 was observed on Pd-Sn electrode [98].

The thorough investigation was done in terms of the reduction activity as well as selectivity for nitrate reduction on tin modified rhodium, ruthenium and iridium electrodes in acidic media and compared with the previously reported tin modified Pd and Pt electrodes [68]. These electrodes exhibited very high catalytic activity toward nitrate reduction even though the activity was not as much as those of tin-modified Pd and Pt electrodes. The gaseous N_2O was highly produced on Sn/Pd (78%) whereas no gaseous products were generated on Sn/Ru. On the other hand, N_2O was the main product on Sn/Rh (59%). The products NH_3^+OH and N_2 were the same for Sn/Pt and Sn/Pd electrodes. The authors concluded that only the substrates of the period six

elements are able to produce N_2 as reduction product.

Germanium is one of the well-known promoters on platinum electrode for nitrate reduction. To accelerate the production of hydroxylamine from the nitrate in the industrial process, germanium is used as promoter on palladium + platinum catalysts [52,53]. Gootzen et al. suggested that germanium has the similar enhancement effect as described by Shimazu el al. for tin modified novel metals. The authors stated that like tin, germanium has a strong tendency to bind one of the oxygens of nitrate, consequently enhanced the activity [53, 97]. Gootzen also suggested that the higher activity of Pd+Pt is associated with the changes in the electronic structure of metals as results of alloy formation. However Dima et al. reported that germanium exhibited highest activity towards nitrate reduction in sulfuric acid but there is no significant effect in perchloric acid. In addition, the authors mentioned that in case of Sn, similar anionic effect was not observed. Furthermore Ge is covered by a hydride layer in the same potential region of nitrate reduction confirmed by FTIR measurement. According to the FTIR results, Dima et al. concluded that Ge does not directly promote nitrate reduction but hinder the adsorption of exclusively adsorbing anions like sulfate. However it plays a great role on the selectivity of the reaction. It is reported that with the addition of Ge on Pt the selectivity of hydroxylamine was 60% for the reduction of nitrate, in contrast there is no hydroxylamine produce in absence of Ge [53, 104].

Table 1.1 represents the summary of the results for nitrate reduction on binary metal electrodes based on methods, products, electrode materials and media of reaction.

Table 1.1 An overview based on method, products, electrode materials and reaction media for electrochemical reduction of nitrate on binary metal electrodes.

Methods	Electrode materials	Electrolyte solution	Products	Ref.
Cyclic voltammetry and quartz crystal microbalance (QCM) measurements, Ion chromatography, FIA and Mass spectroscopy for products analysis	Tin-modified noble metals (Pd, Pt, Rh, Ru, Ir) electrodes	0.1 M $HClO_4$	The predominant products were hydrogenated products such as NH_3OH^+, NH_4^+ for Ru, Ir, Pt and N_2O for Rh, Pd. There is N_2 was generated for Ru, Rh and Pd. A substantial amount of of N_2 was formed for Pt electrodes.	[96]
Cyclic voltammetry and electrolysis, electrode was characterized by SEM and XPS.	Copper-Palldium modified pyrolytic graphite electrodes	0.1 M and 1 M $NaNO_3$ + 1 M NaCl solution.	Products selectivity depends on electrolysis time, potential and surface composition. In neutral media the main product was nitrite and ammonia but N_2 was the selectivity in alkaline media.	[116]

Continued table 1.1

Cyclic voltammetry and galvalnostatic electrolysis	Rh-modified pyrolytic graphite electrodes	1 M NaCl, 1 M NaCl + 0.1 M $NaNO_3$ and 1 M NaCl + 0.1 M $NaNO_2$	Ammonia	[79]
Cyclic voltammetry, amperometry, rotating ring disk electrode, differential electrochemical mass spectroscopy	Palladium/Copper disk and platinum	M $HClO_4$ and H_2SO_4, pH=0.3	Predominant products were nitrogen and nitrous oxide. Products distribution depends on surface composition and pH	[62]
Electrochemical quartz crystal microbalance experiments and cyclic voltammetry	Sn modified palladium electrodes (Pd/Sn/Au)	0.1 M $HClO_4$	Nitrogen and ammonium ion	[95]
Electrochemical quartz crystal microbalance experiment, surface composition was evaluated by XPS	Sn modified platium electrodes (Pt/Sn/Au)	0.1 M $HClO_4$	The predominant product was ammonium ion	95
Square sinusoidal and triangular wave pulsing potential electrolysis	Bronze, $Cu_{68}Sn_{32}$	0.1 M K_2SO_4	Nitrogen and ammonium ion	[117]
Cyclic voltammetry and electrolysis	Bronze, $Sn_{85}Cu_{15}$	0.1 M K_2SO_4	The selectivity was nitrogen and intermediate was nitrite and ammonia.	[118]
Cyclic voltammetry, DEMS, X-ray diffraction	Palladium, Platinum and Palladium-Platinum activated with germanium	0.5 M H_2SO_4	Nitrogen and nitrous oxide	[52]
Cyclic voltammetry and electrolysis experiments, the characterization of the electrodes were evaluated by (SEM-EDX), XRD and XPS.	Nano-crystalline copper-palladium films by co-depostion on nickel electrodes	1 M NaOH	Ammonia and Nitrogen. Selectivity depends on composition of the electrode and reduction potential	[89]
Electrochemical cycling for activation of electrode, morphological modification by a change in the Hydrogen under-potential deposition	Rhodium film on titanium substrate	Alkaline, KCl electrolyte	Nitrogen	[69]

The electrocatalytic activity for nitrate reduction on platinum was examined in the presence of several inorganic cations (Ni^{2+}, Cd^{2+}, Co^{2+}, Ge^{4+}) in sulfuric acid solution by Safonova [99]. Out of these, Ge was indeed considered to be a good promoter for nitrate reduction. The other three cations also enhanced the nitrate reduction and forming ammonia as the reaction product. Only in case of germanium,

hydroxylamine was detected as a reaction product.

Single crystal electrodes have a surface of high regularity and can assist to make a detailed correlation between the macroscopic kinetics and microscopic properties of the interface. Several studies have been conducted for nitrate reduction on single-crystal platinum electrodes. In order to get more detailed view into the structure sensitivity and to understand in better-defined way the effect of hydrogen and anions on the reaction kinetics, Dima et al. investigated nitrate reduction on single crystal platinum electrodes [100]. The authors stated that the nitrate reduction is structure sensitive on single crystal platinum electrodes. They also proved that this structure sensitivity is largely caused by structure-sensitive co-adsorption of hydrogen and anions on the surface rather than by a structure-sensitive nitrate adsorption, dissociation or reduction. The authors also observed that in perchloric acid, the most active platinum surface for nitrate reduction is Pt(110) whereas in sulfuric acid the activity is lower than that on Pt (111) because of Pt(110) is strictly blocked by sulfate ion. Furthermore, Dima et al. presented some experimental evidence that NO tends to accumulate at the step sites on stepped electrode. The effect of the step density in the platinum single crystal for catalytic activity towards nitrate reduction was examined thoroughly by Taguchi et al. [101]. The authors observed that the electrocatalytic activity for nitrate reduction is dependent on the step density and the activity strongly increased with increasing the traces length is smaller than 5 atoms. In addition, the authors concluded that the electrocatalytically active nitrate does not adsorb on the Pt(111) terraces but on the Pt(111) monoatomic steps. Nitrate reduction is strongly influenced by the adsorption of anions and hydrogen due to weaker adsorption of nitrate on the electrode surface. Taguchi and Feliu have proposed two types of adsorbed upd hydrogen exist on Pt electrode: at low potential H_s adsorbed on Pt(110) whereas H_{nt} adsorbed at higher potential most probably on narrow (111) and the adsorbed H_s inhibit the nitrate reduction [45]. The authors stated that the activity of the electrocatalytic nitrate reduction was improved with the increase of the step density and therefore concluded that NO_3^- does not adsorb on the (111) terrace sites but on the step sites prior to its reduction in the hydrogen adsorption region. They also confirmed that NO is an important intermediate in nitrate reduction which is formed after rate determining step, presumably from nitrite. After that this NO was reduced to ammonia. The author also concluded that ammonia is the predominant product on a

platinum electrode because NO is adsorbed strongly on the electrode and does not desorb, and this strong adsorption consequently leads to the prohibition of the formation N_2O and N_2. Beltomo and Koper proposed the following mechanism for NO (ads) reduction to ammonia [102].

$$NO\,(ads) + H^+ + e^- \Leftrightarrow HNO\,(ads) \quad \text{Equillibrum}$$
$$HNO\,(ads) + H^+ + e^- \rightarrow H_2NO\,(ads) \quad \text{rds}$$
$$H_2NO\,(ads) + 4H^+ + 3e^- \rightarrow NH_4^+ + H_2O \quad \text{fast}$$

1.4 Reactivity to adsorbed species of metal ion

The catalytic and chemisorption properties of metal or bimetal or modified metal surfaces are governed by the electronic and geometric structures of the surface. As a result, the reactivity of a metal surface can be altered significantly by changing the surface structure, by alloying or by modifying with foreign metals or by introducing additional adsorbed species onto the surface. The electronic effects are generated from the local structure of the surface. It is generally proved that average energy of the *d* electrons of a metal is responsible for the electronic effect. The geometric effect is considered when the adsorb species interact with different metal surfaces with the indistinguishable electronic structures. In this case, the differences in bonding between adsorbed species and surface as well as potential energy barrier height are attributed to the differences in the bonding geometry [108].

The interaction energy between adsorbate and metal surface are governed by the coupling to the metal *d* bands, since the coupling to the metal s, p states is essentially the same for the transition metal and novel metals [107]. Therefore the center of the *d* band is an important factor characterizing the ability of surface *d* electrons to participate in bonding to the adsorbed species. The energy of *d* band (*d* band center) of a metal depends on its surrounding environment. The position of *d* band center alters by modifying the metal surface with foreign metals or by depositing it as an over layers [119] or making alloy with other metals [120], consequently change the reactivity. Alloying is extensively utilized to modify the activity of high surface area system [121,122].

Rodriguez and Goodman established that there is a strong correlation between the surface core level of overlayers and the CO chemisorption energy [119]. The change in the surface core level shifts for metal overlayers is directly associated with the shifts in the center of gravity of *d* band [122]. Hammer et al. concluded that the variation in the surface core level occurs due to change in the *d* band center [109]. The authors also reported that there is a relationship between variation in the *d* band center and the chemisorption energy. Stronger adsorption of CO becomes stronger for Pd surface was reported when the *d* band center shifts positive derection (upward) [110]. It is also proved that adsorption energy linearly increased with the increasing of *d* band center relative to the Fermi level. The linear relation between the adsorption energy and *d* band center was also reported for O_2 adsorption [126], but for the reduction of O_2, a volcano type variation in the electrocatalytic activity was observed against *d* band center of metal [109]. Pasti et al. reported that there is a correlation of H adsorption energy and the position of *d* band center of Pd and Pt overlayers on Au substrate [124]. The authors also observed a linear relationship between adsorption energy of hydrogen and *d* band center. Similar results were observed for O_2 adsorption on Pd, Rh, Ir and Pt (111) [127].

It has been reported that, the *d* band center of Pd and Pt downshits, by the modification of Sn. The *d* band centre of Pt shifts downward by the combination with Rh or Ru to form alloys [125]. The downshift of Pd *d* band center and upshit of Pt upon alloying between Pd and Pt were also reported [53]. Ruban et al. reported that *d* band center shifts downward when small element forms alloy with large element, whereas upshift of *d* band center occurs while the large element forms alloy with small element [107]. The change in the *d* band center of metals by modifying with foreign metal or alloying with other metal or its impurities, relative to pure metals have been extensively study by A. Ruban et al [107]. Table 1.2 demonstrated the shifting of *d* band center due to impurities or overlayers or making alloy with other metals

Table .1.2 Shifts in *d* band centers of metal surface impurities and overlayers relative to the pure metal values *[Reference: J. Mol. Cat. A: Chemical 115 (1997) 421]*.

	Fe	Co	Ni	Cu	Ru	Rh	Pd	Ag	Ir	Pt	Au
Fe	*-0.92*	0.05 0.14	-0.20 -0.04	-0.13 -0.05	-0.29 -0.73	-0.54 -0.72	-1.24 -1.32	-0.83 -1.25	-0.36 -0.95	-1.09 -1.48	-1.42 -2.19
Co	0.01 -0.01	*-1.17*	-0.28 -0.20	-0.16 -0.06	-o.24 -0.70	-0.58 -0.95	-1.37 -1.65	-0.91 -1.36	-0.36 -1.09	-1.19 -1.89	-1,56 -2.39
Ni	0.09 0.96	0.19 0.11	*-1.29*	0.19 0.12	-0.14 -0.63	-0.31 -0.74	-0.97 -1.37	-0.53 -1.14	-0.14 -0.86	-0.80 -1.53	-1.13 -2.10
Cu	0.56 0.25	0.60 0.38	0.27 0.18	-2.67	0.58 -0.22	0.32 -0.27	-0.64 -1.04	-0.70 -1.21	0.58 -0.32	-0.33 -1.15	-1.09 -1.96
Ru	0.21 0.30	0.26 0.37	0.01 0.29	0.12 0.30	*-1.41*	-0.17 -0.12	-0.82 -0.47	-0.27 -0.40	0.02 -0.13	-0.62 -0.61	-0.84 -0.86
Rh	0.24 0.31	0.34 0.41	0.16 0.34	0.44 0.22	0.04 0.03	-1.73	-0.54 -0.39	0.07 -0.08	0.17 0.03	-0.35 -0.45	-0.49 -0.57
Pd	0.37 0.36	0.54 0.54	0.50 0.54	0.94 0.80	0.24 -0.11	0.36 0.25	*-1.83*	0.59 0.15	0.53 0.31	0.19 0.04	0.17 -0.14
Ag	0.72 0.55	0.84 0.74	0.67 0.68	0.47 0.62	0.84 0.50	0.86 0.67	0.14 0.27	*-4.30*	1.14 0.80	0.50 0.37	-0.15 -0.21
Ir	0.21 0.33	0.27 0.40	0.05 0.33	0.21 0.56	0.09 -0.01	-0.15 -0.03	-0.73 -0.42	-0.13 -0.09	*-2.11*	-0.56 -0.49	-0.74 -0.59
Pt	0.33 0.35	0.48 0.53	0.40 0.54	0.72 0.78	0.14 0.12	0.23 0.24	-0.17 0.02	0.44 0.19	0.38 0.29	*-2.25*	-0.05 -0.08
Au	0.63 0.53	0.77 0.74	0.63 0.71	0.55 0.70	0.70 0.47	0.75 0.67	0.17 0.35	0.21 0.12	0.98 0.79	0.46 0.43	

The impurities/overlayer atoms are listed horizontally and the host entries are listed vertically. For each combination of the two numbers listed is first the isolated surface impurities given and than the overlayer. The surfaces considered are the most close packed and the overlayer structures are pseudomorphic. No relaxation from the host lattice positions are included. All values are in eV and the elemental d band centers are relative to the Fermi level.

It is reported that when the *d* band centre of metal moves up (higher energy) or down (lower energy) and become close to or a little bit far from the energy state of antibonding orbital of the adsorbed species, the stronger or weaker interaction is

occurred between the *d* band and antibonding orbital of adsorbed species (here nitrate ion) to form the bond [53]. It is believed on the basis of electrochemical reduction of nitrate, weak or moderate adsorption facilitated faster reduction of nitrate i.e., accelerate reduction rate whereas strong adsorption leads slower reduction rate and weaker adsorption has tendency to dissolute from the surface, resulting slowest reduction rate. Therefore downshift in the *d* band center of noble metal is a measuring tool and plays an important role for accelerating nitrate reduction and product selectivity.

1.5 Objective and outline of the thesis

1.5.1 Objective of the thesis

In the research about the electrocatalysts for denitrification, tin-modified novel metals show the high electrocatalytic activity in the past reports [68]. Particularly, Sn-modified Pd exhibits the high catalytic activity [96], and Sn-modified Pt has the high nitrogen selectivity [97]. In order to understand an electrocatalytic function of these electrodes, it is essential to evaluate the role of novel metals in denitrification system. In addition, the tin coverage illustrates the unique curve that shows the highest catalytic activity around the middle coverage. It is assumed that this tendency implies the alloying of novel metals and tin.

According to the rigid band model [105], electrons in *5s* orbital transfer from tin atoms to holes of the 4d orbitals of the Pd atom on the alloying process of Pd-Sn [105]. Finally, *d* band of Pd atom is fully filled due to the hybridization of *d* band of Pd with the partner element band [106]. It is also concluded that hydrogen sorption ability of Pd is totally lost, if the *d* band could be filled [112, 113].

The profile of the collective band is very complicated, although it is considered that the collective band is highly related to its catalytic activity. Hence, I consider the approximation by considering the *d* band center. The *d* band center is also important parameter characterizing the capability of electrons to take part in bonding to the adsorbed species [107]. Of course, the catalytic activity highly depends on its surrounding environment. That is why this is the approximation to clarify the

mechanism from the viewpoint of "energy". Based on calculation of the electron density function, the *d* band center of novel metal shifts to positive (upshift) or negative direction (downshift) upon alloying with other foreign metal (see Figure 1.10 and 1.11) [107, 109].

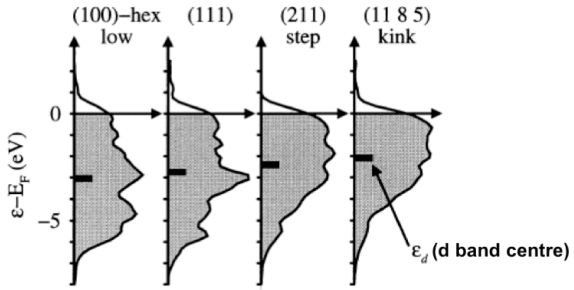

Figure 1.10 The d density of states (d band center) of Pt metal

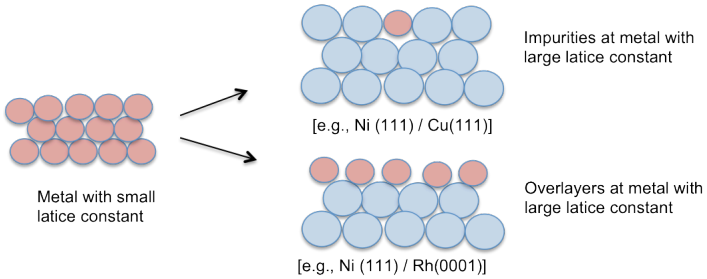

Figure 1.11. When a metal atom (small grey circle) with a small lattice constand (and fd > 0.5) is put as an impurity or overlayer at the surfacc of a metal (light blue circle) with a large lattice constant, the embedding density and therefore the local d-band width are lowered and the center of d band is caused to shift up in order to preserve the degree of d band filling . For a large metal atom on a small metal atom substrate the opposite is found [107]

When the *d* band center of metal moves up (close to Fermi level), and it overlaps or close to the energy of anti-bonding orbital of adsorbed species like CO, it leads to strong interaction between metal *d* electron and adsorbed species. The opposite is also true, or weaker interaction is expected for downshift of d-band center. (Figure 1.12) [53,108].

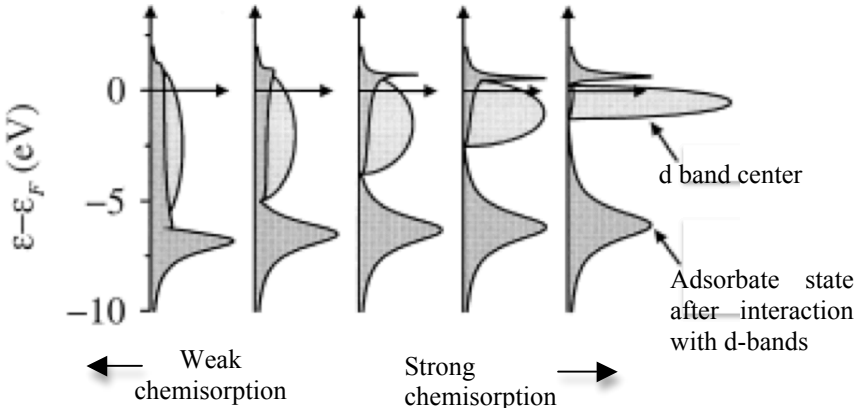

Figure 1.12. The locat density of states projected onto an adsorbate state interacting with d bands at a surface. the strength of the d bands is shifted up towards the Fermi energy and the width W of the d bands is decreased to keep the number of electrons in the band constant. As shifts up, the antibonding states are emptied above and the bond becomes stronger (bottom). The calculation was done by using the Newns-Anderson model [6]. Adapted from Hammer [111].

It is expected that the interaction between downshifted *d* band of novel metal and adsorbate (here nitrate ion) causes a weak adsorption of nitrate on the electrode surface, and consequently accelerates the nitrate reduction. In the other hand, the opposite phenomenon ~~is~~ happens by the upshift of *d* band. Therefore, the *d* band shift is a key role to measure the reactivity of the electrocatalyst to the adsorbed species.

In case of Pd-Sn alloy, *d* band center shows downshift as alloying. In the contrast, *d* band center of Pt shifts up or down upon alloying with Pd and Rh. In addition, to complicate thing, alloying with Sn also alters the *d* band center and therefore influences on the interaction between metal surface and adsorbed species. On the other hand, industrial Sn plating uses the electrochemical reduction with the current of 1 mA m^{-2} in pretreatment in order to improve the reflectivity. Reflectivity is highly related to the free electron at the metal surface. It means its band structure has been changed by the electrochemical reduction. Shining of plate can be directly translated to the high dielectric constant. I believe that the electrocatalytic activity must be improved.

On the basis of the above discussion, in order to improve the catalytic activity and product selectivity to N_2, the aim of the research is to clarify the electron state of alloy, and to understand the role of novel metals in Sn alloy on the catatytic activity for nitrate reduction. In addition, to understand the role of novel metals, PdPt and PtRh alloys have been examined, because I think that the effect of the *d*-band center shift on the electrocatalytic properties could be clarified. Further, the production analysis could give a useful insight into the mechanism of electrocatalytic reactions. As a result, I can extract the key factors to prepare new electrodes that heve the excellent catalytic activity and N_2 selectivity for nitrate reduction.

1.5.2 Outline of the Thesis

The main body of the thesis comprises 6 chapters.

Chapter 1 describes present situation of nitrate contamination, its adverse effects on human beings, currently used denitrification methods as well as the advantages of electrochemical method, previous studies of electrochemical reduction of nitrate ions and reactivity of metals. The objective and outline of the thesis has been described in this chapter.

In chapter 2, the experimental procedures of electrochemical measurements such as the electrochemical cleaning of electrode surface, cyclic voltammetry, analytical techniques for products, XPS and STM and surface enhanced infrared absorption spectroscopy spectral (SEIRAS) are briefly discussed.

In chapter 3 the reduction of nitrate on electrochemical pre-reduced tin-modified palladium electrodes was described. The characterization of the thus prepared tin-modified electrodes was carried out by cyclic voltammetry, STM and XPS. The tin coverage dependence and the effect of the electrochemical pre-treatment on Sn/Pd electrode for the catalytic activity and product distribution towards nitrate reduction have been examined in detail. Finally the origin of the observed enhanced effects has been discussed.

Chapter 4 describes the reduction of nitrate on Sn-modified PdPt/Au. As did in chapter 3, the characterization of the electrodes and nitrate reaction were examined using cyclic voltammetry, STM, XPS and product analysis. Tin coverage, surface composition dependence and electrochemical pre-treatment effect on these electrodes for nitrate reduction has been examined. In addition, the role of novel metals in alloy for nitrate reduction has also been described. Moreover the adsorption behavior of NO_3^- on these electrodes was examined using SEIRAS techniques, and results were compared with pure Pd and Pt have also been discussed

In chapter 5, described are the preparation, characterization, and electrocatalytic properties of Sn modified PtRh (Sn/PtRh) electrodes. Sn coverage and surface composition dependence of the nitrate reduction activity of the Sn/PtRh electrodes have also been described. The reduction products distribution on this electrode has been examined and compared to Sn modified Rh and Pt electrodes. In addition, the role of novel metals for catalytic activity and product selectivity and the adsorption behavior of NO_3^- on Rh, Pt and PtRh alloy and those modified by Sn have also been examined.

In chapter 6, The general conclusion obtained throughout the present study is described based on the experimental results. The future prospect of this study for denitrification from nitrate contaminated water has also been discussed.

1.6 References

[1] Solley, Wayne B., Pierce, Robert R., and Howard A. Perlman, "Estimated Use of Water in the United States in 1990," U.S. Geological Survey Circular 1081, 1993.

[2] Groundwater use, the USGS water Science School (http://ga.water.sugs.gov/edu/wugw.html)

[3] Martin, D.F., Martin, B.B., Alldredge, R. Bull. Hist. Chem. 33 (2008) 17-24.

[4] Berner, E., Berner, R., 1987, The Global Water Cycle, Prentice Hall, New Jersey, p. 102-119.

[5] J.F. Gaillard,., February, 1995, Lecture on Nitrogen Cycle.

[6] G.R.Hallberg, and D.R Keeney, 1993, Nitrate, Alley, William A., ed., *Regional Ground-water Quality,* Van Nostrand Reinhold, New York, p.297-322.

[7] Behm, Don 1989, Ill Waters: The Fouling of Wisconsin's Lakes and Streams (Special Report), *The Milwaukee Journal,* p. 2.

[8] WHO "Guideline for drinking water quality, Recommendations, World Health Organization, Geneva, Switzerland, 3rd ed., Vol.1, 2004.

[9] H. H. Comly, J. Am. Med. Assoc. 257 (1987) 2788.

[10] D. I. Gustafoson, 1993, Pesticides in Drinking Water, Van Hostrand Reinhold, New York, p. 241.

[11] C. J. Johnson, P. A. Bonrud, T. L. Dosch, A. W. Kilness, K. A Senger, C.D Busch, M. R. Meyer, J. Am. Med. Assoc. 257 (1987), 2796.

[12] P. Fraser, IARC Sci. Publ. 65 (1985) 183.

[13] D. Forman, S. Al-Dabbagh, R. Doll, Nature 313 (1985) 620.

[14] H. A. Risch, M. Jain, N.W. Choi, J.G. Fodor, C.F. Pfeiffer, G.R. Howe, I. W. Harrison, K.J.P. Craib, A. B. Miller, Am. J. Epidemiol. 122 (1985) 947.

[15] M. C. Dutt, H.Y. Lim, R.K.H. Chew, Food Chem. Toxicol. 25 (1987) 515.

[16] Nitrate and Nitrite in Drinking Water. National Research Council, National Academy of Sciences. National Academy Press, 1995.

[17] J. M. Pogoda, S. Preston-Martin, Public Health Nutr. 4 (2001) 183.

[18] B. A. Muller, S.S. Niesen, S.Preston-Martin, Int. J. Epidemiol. 33 (2004) 1209.

[19] G.C.C Yang, H. Lee, Water Res. 39 (2005), 884.

[20] J.C. Fanning, Coord. Chem. Rev. 199 (2000) 159.

[21] A.P. Murphy, Nature 350 (1991) 223.

[22] K. Manish, C. Saswati, J. Haz. Mat. 135 (2006) 112.

[23] A. P. Morphy, Chemical process for the denitrification of water, US Patent 5069800, 1991.

[24] G.A. Guter, Removal of Nitrate from contaminated water supplies for public use, Environmental Protection Agency, Cincinnati. 1981

[25] L. R. Siwak, "Here's How Electrodialysis Reverse and Why EDR works." Int'l Desalination & Water Reuse Quarterly, vol. 2/4, 1993

[26] R. Rautenbach, W. Kopp, G. V. Opbergen, R. Hellekes, Desalination 65(1987) 241.

[27] S. Harmon,"Nitrate removal: Searching for the ideal in an imperfect world," Water Technology, November 2002.

[28] D. Elyanow, J. Persechino, Advanced in Nitrate removal, GE Water & Process Technologies, 2005.

[29] R. Knowles, Microbiological Rev. 46 (1) (1982) 43.

[30] B. E. Rittmann, P. M. Huck, CRC Critical Rev. Environ. Control. 19(2) (1989) 119.

[31] B. P. Gayle, G. D. Boardman, J. H. Sherreard, R. E. Benoit, J. Environ. Engr. ASCE, 115(5) (1989) 930.

[32] K. M. Hiscock, J. W. Lloyd, D. N. Lerner, Water Res. 25(9) (1991) 1099.

[33] S. Horold, T. Tacke, K. D. Vorlop, Environ. Technol. 14 (1993), 931.

[34] A. Kapoor, T. Viraraghavan, J. Environ. Eng.123 (1997) 371.

[35] Y. Fernandez-Nava, E. Maranon, J. Soons, L. Castrillon, Bioresour. Technol. 99 (2008) 7976.

[36] J. Virkutyte, V. Jegatheesan, Bioresour. Technol. 100 (2009), 2189.

[37] S. Samatya, N. Kabay, U. Yuksel, M. Rda, M. Yuksel,. React. Funct. Polym. 66 (11) (2006) 1206.

[38] J. Flora, A. Hayes, J. Khan, Water Res. 32 (1998) 2830.

[39] W. J. Plieth, A. J. Bard, Encyclopedia of Electrochemistry of the Elements, vol. 8, Marcel Dekker, New York, 1978.

[40] L. M. Devkota, D. S. Willian, J. H. Matta, O. E. Albertson, D. Grasso, P. Fox, Water Environ. Res. 72(5) (2000) 610.

[41] Z. Macova, K. Bouzek, J. Appl. Electrochem. 35 (2005) 1203.

[42] I. Katsounaros, D. Ipsakis, C. Polatides, G. Kyriacou, Electrochim. Acta 5 (2006) 1329.

[43] O. Brylev, M. Sarrazin, L. Roue, D. Belanger, Electrochim. Acta 52 (2007) 6237.

[44] K. Rajeswar, J. G. Ibanez, G. M. Swain, J. Appl. Electrochem. 24 (1994) 1077.

[45] S. Taguchi, J. M. Feliu, Electrochim. Acta 53 (2008) 3626.

[46] de Groot, M. T.; Koper, M. T. M., J. Electroanal. Chem. 2004, 562, 81.

[47] M. C. P. da Cunha, M. Weber, F. C. Nart, J. Electroanal. Chem. 163 (1996) 414.

[48] H. L. Li, D. H. Robertson, J. Q. Chambers, D. T. Hobbso, J. Electrochem. Soc. 135 (1988) 1154.

[49] F. Gauthard, F. Epron, J. Barbier, Catalysis 220 (2003) 182.

[50] G. Tchobanoglous, F. L. Burton, Biological unit processes, wastewater engineering, treatment, disposal, and reuse, 3rd Edition, McGraw-Hill, Singapore, 1991, p. 359.

[51] F. V. Andrade, L. J. Deiner, H. Varela, J. F. R. de Castro, I. A. Rodrigues, F. C. Nart, J. Electrochem. Soc. 154 (2007) F159.

[52] J. F. E. Gootzen, L. Lefferts, J. A. R. Van Veen, Appl. Catalysis A: General 188, (1999) 127.

[53] J. F. E. Gootzen, P. G. J. M. Peeters, J. M. B. Dukers, L. Lefferts, W.Visscher, J. A. R. van Veen, J. Electroanal. Chem. 434 (1997) 171.

[54] U. Prusse, K. D. Vorlop, J. Mol. Catalysis 173 (2001) 313.

[55] F. Armijo, M. Isaacs, G. Ramirez, E. Trollund, J. Canales, M. J. Aguirre, J. Electroanal. Chem. 566 (2004) 315.

[56] K. Shimazu, R. Goto, K. Tada, Chem. Letters (204) 2002.

[57] Li, H. L.; Chambers, J. Q.; Hobbso, D. T. J. Appl. Electrochem. 18 (1988) 454.

[58] G. E. Badea, Electrochim. Acta 54 (2009) 996.

[59] M. Li, C. Feng, Z. Zhang, N. Sugiura, Electrochim. Acta 54 (2009) 4600.

[60] D. Reyter, D.; Belanger, L. Roue, Electrochim. Acta 53 (2008) 5977.

[61] T. R. L. C. Paixao, L. Cardoso, M. Bertotti, Talanta 71 (2007) 186.

[62] A. S. Koparal, U. B. Ogutveren, J. Hazard. Mat. 89(2002) 83.

[63] Wang, Y.; Qu, Water Environ. Res. 2006, 78, 724.

[64] S. M. El-Deab, Electrochim. Acta 49 (2004) 1639.

[65] G. E. Dima, A. C. A. de Vooys, M. T. M. Koper, J. Electroanal. Chem. 554 (2003) 15. .

[66] T. Ohmori, M. S.; El-Deab, Osawa, M. J. Electroanal. Chem. 1999, 470, 46.

[67] H. L. Li, W. C. Anderson, J. Q. Chambers, D. T. Hobbs, Inorg. Chem. 28 (1989) 863.

[68] S. Piao, Y. Kayama, Y. Nakano, K. Nakata, Y. Yoshinaga, K. Shimazu, J. Electroanal. Chem. 629 (2009) 110.

[69] M. Tucker; J.; Philip, Waite, Hayden, M.; Brian, E. J. Appl. Electrochem. 2004, 34, 781.

[70] M. Dortsiou, G. Kyriacou, J. Electroanal. Chem. 630 (2009) 69.

[71] I. Katsounaros, G. Kyriacou, Electrochim. Acta , 52 (2007) 6412.

[72] I. G. Casella, M. Gatta, J. Electroanal. Chem. 568 (2004) 183.

[73] B. R. Scharifker, J. Mostany, A. Serruya, Electrochem. Comm. 2 (2000) 448.

[74] A. K. Vijh, J. Catal. 32 (1974) 230.

[75] N. E. Khomutov, U. S. Stamkulov, Elektrokhimiya 7 (1971) 332.

[76] S. Ureta-Zanaru, C.Yanez, Electrochim. Acta 11 (1997) 1725.

[77] M. Wasberg, G. Horanhi, Electrochim Acta 40 (1995) 615.

[78] G. Horanhi, M. Wasberg, Electrochim Acta 42 (1997) 615.

[79] O. Brylev, M. Sarrazin, L. Roue, D. Belanger, Electrochim. Acta 52 (2007) 6237.

[80] M. Wasberg, G. Horanhi, Electrochim Acta 385 (1995) 63.

[81] D. Pletcher, Z. Poorabedi, Electrochim Acta 24 (1979) 1253.

[82] G. E. Dima, A. C. A. de Vooys, M. T. M. Koper, J. Electroanal. Chem. 2003 (554) 15.

[83] Schmid, G. Z. Elecktrochem. 63 (1959) 1183.

[84] S. W. Boese, V. S. Archer, J. Electroanal. Chem. 138 (1982) 273.

[85] N. A. Hampson, R. J. Piercy, Electroanal. Chem. 45 (1973) 326.

[86] Davenport, R. J.; Johnson, D. C. Anal. Chem. 45 (1973) 1979.

[87] I. Katsounaros, D. Ipsakis, C. Polatides, G. Kyriacou, Electrochim. Acta 52, (2006) 1329.

[88] I. Katsounaros, G. Kyriacou, Electrochim. Acta 53 (2008) 5477.

[89] D. Reyter, D. Belanger, L. Roue, J. Phy. Chem. 113 (2009) 290.

[90] S. Horold, K-D. Vorlop, T. Tacke, M. Sell, Catal. Today 17 (1993) 21.

[91] A.C.A. de Vooys, R.A. van Santen, J.A.R. van Veen, J. Mol. Catal. 154 (2000) 203.

[92] A.C.A. de Vooys, M.T.M Koper, R.A. van Santen, J.A.R. van Veen, J. Catal.

202 (2001) 387.
[93] S. N. Prokin, P.A. Simonov, V.I. Zaikovkskii, E.R. Savinova,. J. Mol. Catal. A 265 (2007) 141.
[94] Kerkeni, S.; Lamy-Pitara, E.; Barbier, J. Catal. Today 75 (2002) 35.
[95] K. Shimazu, T. Kawaguchi, K. Tada, J. Electroanal. Chem. 529 (2002) 20.
[96] K. Shimazu, R. Goto, S. Piao, Y. Kayama, K. Nakata, Y. J. Yoshinaga, Electroanal. Chem. 601 (2007) 161.
[97] K. Tada, K. Shimazu, J. Electroanal. Chem. 577 (2005) 303.
[98] K. Tada, T. Kawaguchi, K. Shimazu, J. Electroanal. Chem. 572 (2004) 93.
[99] T. Y. Safonova, O.A. Petrii, J. Electroanal. Chem. 448 (1998) 211.
[100] G.E. Dima, G.L. Beltramo, M.T.M. Koper, Electrochimica Acta 50 (2005) 4318.
[101] S. Taguchi, J. M. Feliu, Electrochim. Acta 52 (2007) 6023.
[102] G.L. Beltramo, M.T.M. Koper, Langmuir 16 (2003) 8907.
[103] H. H. Francisco, H.G. Ressler, C. E. Roberts, R. G. Snyder, US Patent 3082157 (1963).
[104] G. E. Dima, V. Rosca, M. T. M. Koper, J. Electroanal. Chem. 559 (2007) 167.
[105] I. R. Harris, M Cordey-Hayes, J. Less-Common Met. 16 (1968) 223.
[106] J. C. Fuggle, F. U. Hillebrecht, R. Zeller, Z. Zolnierek, P. A. Bennett, Ch. Freburge, Phys. Rev. B 27 (1982) 2145.
[107] A. Ruban, B. Hammer, P. Stoltze, H. L. Skriver, J. K. Norskov, J. Mol. Catal. A: 115 (1997) 421.
[108] B. Hammer, J. K. Norskov, Advance in Calalysis 45 (2000) 70.
[109] B. Hammer, O.H. Nielsen, J. K. Norskov, Catal. Lett., 46 (1997) 31.
[110] M. Valden, X. Lai, D. W. Goodman, Science 281(1998) 1647.
[111] B. Hammar, Faraday Discuss 110 (1998) 323.
[112] D. A. J. Rand, R. Woods, J. Electroanl. Chem. 36 (1972) 57.
[113] W. M. H. Sachtler, R. A. Van Santen, Adv. Catal. 26 (1977) 69.
[114] Pogoda, J.M., Preston-Martin, S. Public Health Nutr. 4 (2001) 183-189.
[115] Muller B.A., Niesen S.S., Preston-Martin, S. Int. J. Epidemiol. 33 (2004) 1209-1216.
[116] O. Ghodbane, M. Sarrazin, L. Roue, D. Belanger, J. Electrochem. Soc. 155 (2008) F117.

[117] C. Polatides, M. Dortsiou, G. Kyriacou, Electrochimica Acta 50 (2005) 5237.

[118] C. Polatides, G. Kyriacou, J. Appl. Electrochem. 35 (2005) 421.

[119] J.A. Rodriguez and D.W. Goodman, Science 257 (1992) 897.

[120] M. Holmblad, J.H. Larsen, I. Chorkendorff, L. Pleth Nielsen,F. Besenbacher, I. Stensgaard, E. Loegsgaard, P. Kratzer, B.Hammer and J.K. Nørskov, Catal. Lett. 40 (1996) 131.

[121] J.H. Sinfelt, Bimetallic Catalysts: Discoveries, Concepts and Applications, Wiley publishers, New York, 1983..

[122] V. Ponec, Adv. Catal. 32 (1983) 149.

[123] M. Weinert, R.E. Watson, Phys. Rev. B 51 (1995) 17168.

[124] I. A. Pasti, N. M. Gavrilov, and S.V.Mentus, Advance in Physical Chemistry, Volume 2011, Article ID 305634, 8 pages.

[125] F. H. B. Lima, E. R. Gonzalez, Electrochimica Acta 53 (2008) 2963.

[126] M. H. Shan, T. Huang, P. Liu, J. Zhang, K. Sasaki, M.B. Vukmirovic, R. R. Adzic, Langmuir 22 (2006) 10409.

[127] Spencer D. Miller, Nilay ˙Ino˘ glu, John R. Kitchin, J. Chem. Phys. 134, (2011) 104709.

Chapter 2

Experimental

2.1 Materials and chemicals

Palladium, platinum and palladium-platium alloy (Pd/Pt = 31/69) targets for sputtering were purchased from JOEL co., Japan. The platinum-rhodium alloy (PtRh) wires were obtained form Nilaco Co., Japan. Chemicals, such as $PdCl_2$ (Wako Pure Chemicals), K_2PtCl_6 (Aldrich Chem. Co.), $SnCl_2.2H_2O$ (Kanto Chemicals), and $NaNO_3$ (Kanto chemicals), were of reagent grade. Perchloric acid (Kanto Chemicals) was of ultrapure grade. The other chemicals used for the product analyses were of reagent grade. Milli-Q water was used throughout the experiments. All the aqueous solutions were sufficiently deaerated with 5 N purity argon prior to use.

2.2. Electrochemical measurements

This research mainly used electrochemical methods to examine the catalytic reaction and to characterize alloy electrodes. The electrochemical method monitors the relation between the voltage and the current, which associates with the behavior of electrons at the electrode/electrolyte interfaces. Consider the simple configuration of the electrolysis. When the electron transfer takes place from the electrode to the solution

species (reduction), the potential of electrode should be high (or low) enough to oxidize (or reduce) the chemical species in the solution. Therefore, it is very important to consider the energy profile at the interface in order to understand the electrochemical reaction. Figure 2.1 shows the electron transfer based on the energy level profile at the interface [1]. When the more negative potential is applied to the electrode than the vacant molecular orbital (MO) of the solution species, an electron can transfer from the electrode to the vacant MO. The flow of electrons in this direction is called

"cathodic current" and the solution species is reduced. To initiate the oxidation

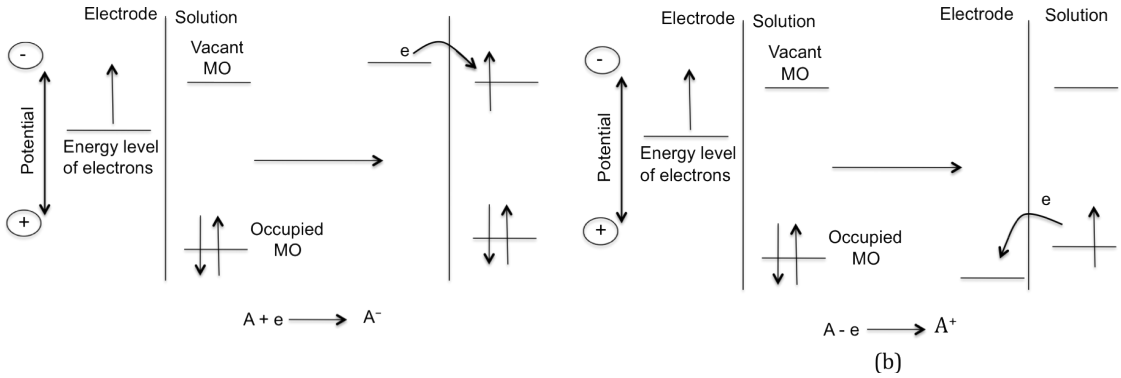

Figure. 2.1 Representation of (a) reduction and (b) oxidation process of a solution species, A in solution. The molecular orbital (MO) of species A shown are highest occupied MO and the lowest vacant MO. This corresponds in an approximate way to the E^0 of A/A^- and $A^{+/}A$ couples, respectively [1]

reaction, the more positive potential should be applied than the occupied MO of the solution species. This type of the current is known as "anodic current". The applied potential by which these processes occur is associated with the standard electrode potential of the specific chemical substances in the system.

Generally three kinds of electrode are used in an electrochemical system to conduct the experiment such as a working electrode (W.E), a counter electrode (C.E) and a reference electrode (R.E) as shown in Figure 2.2. These electrodes are connected to the potentiostat, which is used as a power source and for monitoring the potential and current.

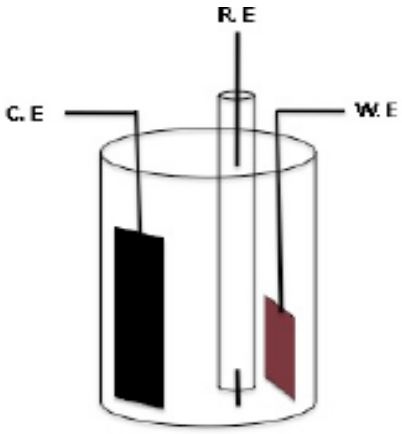

Figure 2.2 A typical electrochemical cell.

The electrochemical measurements in this study were performed in a three-electrode cell settled in an Ar-filled box to prevent the interference from air. All solutions were sufficiently deaerated with argon of 5N purity prior to use. To control the potential a Toho model 2001 potentiostat, a Toho model PS-07 polarization unit with a Toho model FG-02 function generator, or a Hokuto Denko HZ-5000 automatic polarization system was used. The cell used for the constant potential polarization experiments for the product analysis had a Nafion membrane to separate the working and counter electrode compartments to isolate products from the counter electrode. A platinized Pt foil served as the counter electrode. The reference electrode was an Ag/AgCl (saturated KCl) electrode, and all potentials in the text are referred to this electrode. Data were acquired using a personal computer.

2.3 X-ray photoelectron spectroscopy

The principle of X-ray photoelectron spectroscopy (XPS) is based on the photoelectric effect, or the interaction between an electromangnetic wave and atoms of the materials. Since the XP spectrum directly reveals the electronic structure of the

material, it provides information about the elemental composition, empirical formula, and chemical and electronic states of elements that exist within a material. The process of photoelectron emission from a solid is divided into three stages (three step model)

1. First, the electron of the element absorbs energy from X-ray. When the energy overcomes the energy level of the orbital in which electron exists, the electron is released, or photoelectrons are emitted (Photoelectron emission process).
2. The photoelectrons generated within the element move toward the surface. However, the escape possibility exponentially decays with the depth. [Electron attenuation length (escape depth)]
3. Finally these photoelectrons reaches surface, and are emitted into vacuum. These photoelectrons are collected by the photomultiplier located above the sample stage. (related to work function)

As shown in Figure 2.3, the binding energy of electron E_b is expressed using the energy of the excitation X-rays, hν, the kinetic energy of the emitted photoelectrons, E_k and work function ∅, based on the energy conservation law, the binding energy stated by the following equation.

$$E_b = h\nu - Ek - \varnothing,$$

Zero binding energy is defined at the Fermi level. The binding energy, E_b is defined as the difference between the total energy at the initial and the final state of the photoelectron emission process. The binding energy is estimated by measuring the kinetic energy of the emitted photoelectrons.

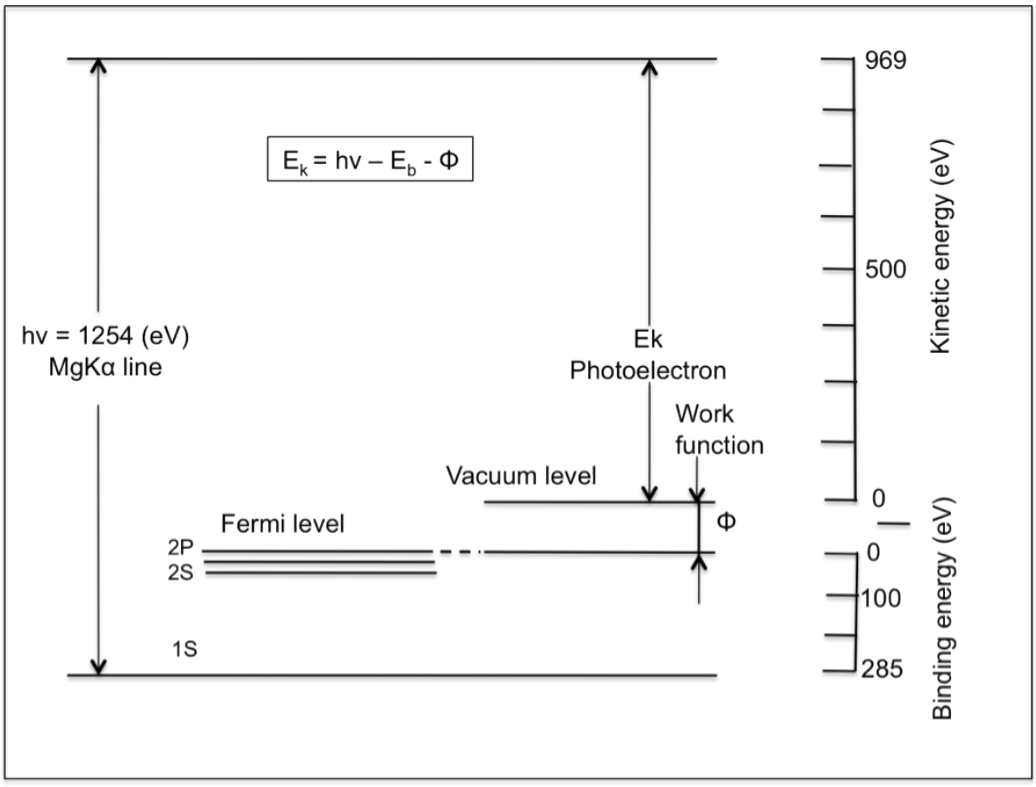

Figure 2.3 Energy diagram of photoelectron emission on carbon atom in XPS.

The surface composition of the elements on the electrode surface can be calculated from the XPS peak intensity using the following equation

$In(d) = S \times I_x \times N_n \times \sigma i \times \exp [-d/\lambda_i \cos (\theta)]$ ……(1)

Here, S = Machine function

I_x = Intensity of incident X-ray

N_n = Number of the certain atoms, n, per the certain surface area.

σ_i = Photoemission cross section area of i-state in the certain atom

λ_i= Mean free path length of i-state in the certain atom n.

θ = Angle between the detector and the sample

In normal mode, θ = 90

Integrated Ini(d) in the region of peak shows the total number of atom at depth d (Å). Considering all the atoms are located at the surface, d is zero. Mean free path can be ignored.

Here, I_x = Intensity of incident X-ray = 300 W, which is calculated from 30 kV × 10 mA = 300 W. From the above equation (1), by using the XPS peak intensity for each element, the number of atoms (Nn) for individual element can be calculated. After calculating the number of atoms for individual element exists on the surface, the surface composition was estimated.

In this research, the X-ray photoelectron spectra were obtained using a Rigakudenki model XPS-7000 X-ray photoelectron spectrometer with monochromic Mg Ka radiation at 300 W. The take-off angle was 90^o. The Au4f7/2 emission was used as an internal reference (83.98 eV) to determine the binding energy of the elements.

2.4 Scanning Tunneling Microscope

A scanning tunneling microscope (STM) provides images of the sample by scanning the sample surface by the probe (tip). The XYZ positioning at a nanometer is performed by means of piezoelectric material of the scanner (Figure 2.4). The tip is positively or negatively biased with a small current with a small current, called “the tunneling current” that flows between the tip and the surface. The tunneling current is amplified with a picoamperometric amplifier. At a constant current mode, to keep the tunneling current at the preset value, the distance between the tip and the sample surface is changed when the tunneling current is changed during the scan. The tip is scanned line by line, resulting in the topographical image of the surface.

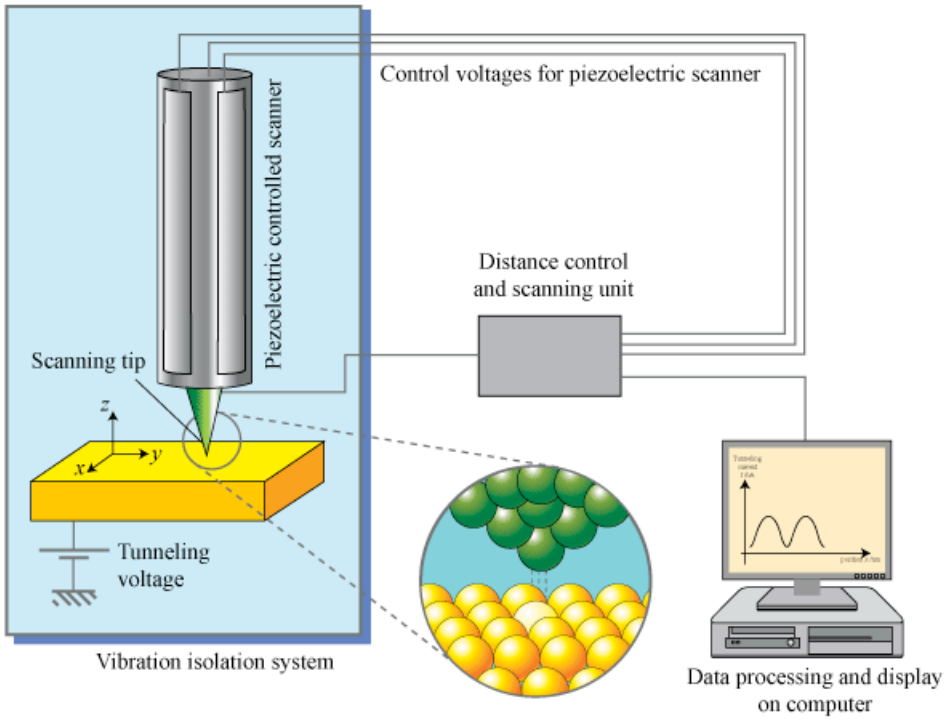

Figure 2.4 Basic principle of Scanning Tunneling Microscope
(Source: http://en.wikipedia.org/wiki/Scanning_tunneling_microscope)

In this study, all STM images were obtained from a Nanoscope III STM (Digital Instruments, USA) under the laboratory ambient atmosphere. For imaging, Pt-Ir tips were used. The instrument was equipped with a low-current converter MMS-STMLC. All images were acquired at constant tunneling current (10-100 pA) with bias voltages of 0.7-1.0 V.

2.5 Products analysis

The nitrate reduction products were analyzed using High Performance Liquid Chromatography (HPLC), Flow Injection Analysis (FIA) for solution products. The

gaseous species were analyzed by using a quadruple mass spectrometer. The principle of these above instrument is briefly discussed here.

2.5.1 High-performance liquid chromatography (HPLC)

High-performance liquid chromatography **(HPLC)** is a chromatographic technique that can separate a mixture of compounds, and is used in order to identify, quantify and purify individual component species from the mixture. An HPLC system consists of four units: a pumping unit, sample-injection unit, separation unit, detection unit, and data-processing unit. The flow diagram of HPLC is shown in Figure 2.5. As an usual chromatographic separation mechanism, chemical species are separated due to the difference in the interaction with the stationary phase between chemical species. The concentration of the individual chemical species can be determined using the corresponding peak area and calibration curve.

In this study, the HPLC system was used to estimate nitrate, nitrite and ammonia. The nitrate and nitrite were analyzed using an RP-18 GP 250-4.6 column (Kanto Chemical Co., Inc.) as stationary phase, a 10 mM NaCl aqueous solution containing 10 μM [3-(N,N'-dimethylmyristylammonio) propanesulfonate] as the mobile

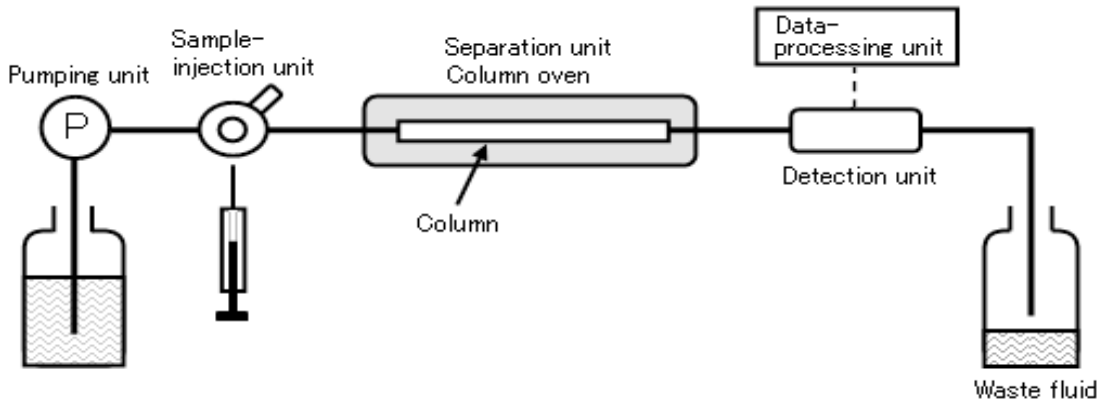

Figure 2.5 Configuration of an HPLC system

phase and a JASCO model 870-UV as the detector. For the analysis of ammonium ion, a Showa Denko ICY-521 column as stationary phase, a 0.004 M HNO_3 as mobile phase and a Shimazu model CDD-10A vp conductivity as the detector were used [2].

2.5.2 Flow Injection Analysis (FIA)

A simplest flow injection analyzer (FIA) assembles with a pump, which is utilized to drive the carrier stream through a narrow channel; an injection port, through which a well-defined volume of sample (analyte) solution is injected into the carrier stream in a reproducible manner; and a microreactor in which the sample zone disperses and reacts with the components of the carrier stream, forming a species which is sensed by a flow through detector and recorded.

The principle of FIA is very simple. Sample (analyte) is injected into a continuous flow of reagent solution (carrier), dispersed, and transported to detector. Sample dispersion is controlled and depends on volume of injected sample, flow rate of carrier, length of the reaction coil, and diameter of the tubing used. Figure 2.6 shows schematic representation of the basic FIA system.

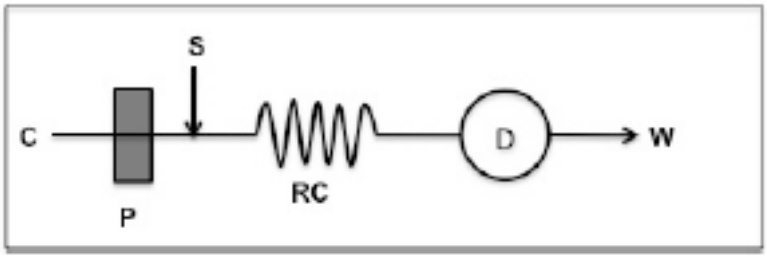

Figure 2.6 Schematic representation of the basic FIA system (C= carrier, P= Pump, S= Point of sample injection, RC= Reaction coil and D = Detector)

In this study, FIA was utilized to estimate the hydroxylamin using the indophenol method and spectroscopic analysis was accomplished at the wavelength of 625 nm. In alkaline media, the anlalyte, hydroxylamine was mixed with phenol, Na_2HPO_4, trisodium citrate and EDTA 2Na. The final product was indophenol, which was analyzed using the visible detector or at 625 nm [3]. The standard curve was calibrated by standard ammonium chloride solution.

2.5.3 Quadrupole Mass spectrometry (QMS)

A quadrupole mass spectrometer composts of an ionizer (bombardment through electrons from a hot filament), an accelerator, and a mass filter four parallel rodes assembled as in the Figure 2.7. Two opposite rods have an applied potential of (U+ Vcos(ωt)) and others have a potential of – (U+ Vcos(ωt)), where U is a DC voltage and Vcos(ωt) is an AC voltage. The applied potentials on the opposed pairs of rods

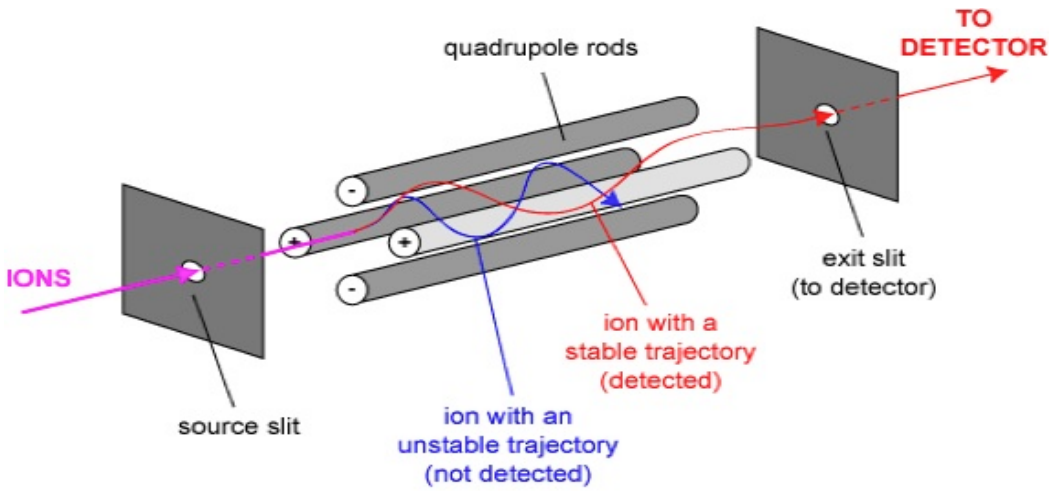

Figure 2.7 Schematic representation of quadrupole mass spectrophotmeter. (Source: http://www.chm.bris.ac.uk/ms/theory/quad-massspec.html)

varies sinusoidally as cos(wt) cycles with time 't'. This results in ions being able to traverse the field free region along the central axis of the rods but with oscillations amongst the poles themselves. These oscillations result in complex ion trajectories dependent on the m/z of the ions.

The route of ions traveling through the flight path centre depends on applied potential. Only those ions have specific mass to charge (m/z) ratio are allowed to pass through the quadrupole filter to the detector and the rest of the ions will have unstable trajectories and hit the quadrupoles and not to be detected. The mass range and resolution of the instrument is determined by the length and diameter of the rods.

In this study, the electrolysis was done for reduction of nitrate for five hours and entire gaseous phase of the cell such as N_2, NO, and N_2O were collected in a pre-evacuated sampling vessel. The gaseous samples were analyzed using Canon-Anelva model M- 201QA-TDM quadrupole mass spectrometer at a background pressure below 8×10^{-6} Pa. The mass spectra were corrected for the fragmentation.

2.6 Surface enhanced infra-red absorption spectroscopy (SEIRAS)

Surface-enhanced infrared absorption spectroscopy (SEIRAS), developed by Osawa and co-workers, is a superior method to obtain the information about the adsorbed species [5, 6], which has some features as follows.

(1) SEIRAS is highly sensitive to the electrode surface. The signal enhancement is 10-100 times.

(2) The contribution of the solvent and solution species is essentially neglected.

(3) The cell used for the SEIRAS measurements is free from any unexpected exhaustion and/or accumulation because of the sufficient solution volume at the

electrode.

In addition to these features, the surface selection rule gives the information on the adsorption states. According to the surface selection rule, only the molecular vibrations that have dipole changes perpendicular to the metal surface are observed.

There are two different mechanisms, the electromagnetic and chemical mechanisms, are considered to contribute to the total enhancement. An important electromagnetic effect is perturbation of the optical properties of the metal island film with adsorbed species. The topology of the metal surface potentially contributes to the enhancement properties. To simplify the explanation, it is considered that the metal surface is formed by the metal nano-particles, as shown in Figure 2.8. By the radiation of infrared light, the metal particle is polarized and the dipole (*P*) is induced in an island. The local electric field is formed around the particles, which induces the excitation of oscillation of the adsorbed molecule. The exited oscillation gives the perturbation to the

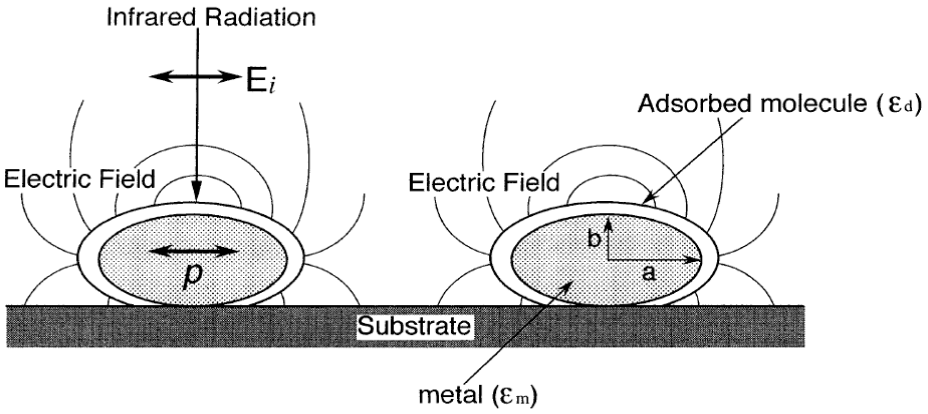

Figure 2.8 Polarization of metal particle in the incident electric field. The thin lines represent the electric field produced by the induced dipole *P* in the particle. The metal particle is modified by a prolate ellipsoid. The adsorbed molecule is modified by t thin layer covering the metal core *[Reference; Bull. Chem.Soc. Jpn 70 (1997) 2861]*.

polarization of the metal particle and the absorption of the metal is changed [4]. The effect of the adsorbed species is remarkable at the frequency of the molecular oscillation. From the difference between the metal adsorptions the oscillation of the adsorbed molecules can be observed indirectly. Since the absorption by metal is larger than that of the adsorbed molecule, the absorption of the molecule is observed as enhanced.

The chemisorbed molecules shows larger enhancement compared to physisorbed molecule. A possible origin of the chemical mechanism is the orientation effect. The orientated molecules show larger intensities than randomly orientated molecules for the vibration, which gives the dipole change perpendicular to the surface, since the component of the vibration parallel to the surface is not observed on the randomly orientated surface due to the surface selection rule [7].

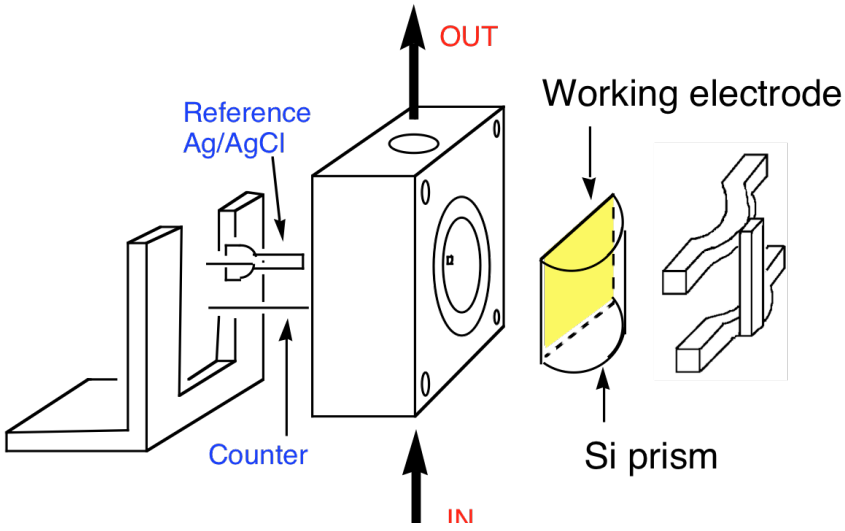

Figure 2.9 Sketch of the experimental setup for Surface Enhanced Infrared Spectroscopy (SEIRAS) with the prism for attenuated total reflection and the spectrochemical cell.

Figure 2.9 shows the typical experimental setup for SEIRAS. A flow cell made of polychlorotrifluoroethylene (PCTFE) was used for the electrochemical and infrared measurements. Both a platinized Pt foil counter electrode and a Ag/AgCl (saturated KCl) reference electrode were assembled in the cell. The prism was attached to the cell via an O-ring. The electrode was electrically connected to a TOHO model PS-7 potentiostat with a TOHO model FG-02 function generator via a copper foil inserted between the cell body and the edge of the electrode (prism). Prior to the measurements, the cell was cleaned in a mixed acid (HNO_3 + H_2SO_4) in order to minimize any organic contaminants, followed by sufficient rinsing with Milli-Q water. The PCTFE cell was connected to solution reservoirs via a valve and the solution in the cell (volume: 1.8 ml) was easily replaced with another solution as described previously [4].

In this research study, all SEIRA spectra were measured using a Bio–Rad FTS60A/896 Fourier transform infrared spectrometer equipped with an HgCdTe detector and a home-built single-reflection accessory (incident angle of 70°) [5]. The spectral resolution was 4 cm^{-1}. The solution in the cell was replaced to 0.1 M $HClO_4$ after the adsorption of nitrate using 0.1 M $HClO_4$ solution containing 0.01 M $NaNO_3$. All spectra are shown in absorbance unit.

2.7 References

[1] Electrochemical Method (Fundamental and Applications), 2nd edition, Allen J Bard and Larry R Faulkner, John Wiley and Sons, Inc. 2001, USA.

[2] K. Shimazu, R. Goto, S. Piao, Y. Kayama, K. Nakata, Y. Yoshinaga, J. Electroanal. Chem. 601 (2007) 161.

[3] C. Lu, S. Lu, W. Qiu, Q. Liu, Electrochim. Acta 44 (1999) 2193.

[4] F. R. Rima, K. Nakata, K. Shimazu, M. Osawa, J. Phys. Chem. C 114 (2010) 6011.

[5] M. Osawa, Bull. Chem. Soc. Jpn. 70 (1997) 2861.

[6] M. Osawa, Appl. Phys. 81 (2001) 163.

[7] K. Ataka, S.T. Stripp, J. Heberle, Biochimica et Biophysica Acta 1828 (2013) 2283

Chapter 3

Reduction of Nitrate on Electrochemically Pre-reduced Tin-modified Palladium Electrodes

3.1 Objective

Noble metal-based binary metal electrodes often exhibit a higher electrocatalytic activity than single noble metal electrodes. Particularly the tin-modification of platinum and/or palladium can drastically enhance their activity for important reactions such as the reduction of nitrate and the fuel cell reactions. The reduction of nitrate has received considerable attention from the viewpoint of the electrochemical remediation of nitrate-contaminated water systems [1-3]. In the previous studies [4-6], It is reported that tin-modified Pt and Pd electrodes (Sn/Pt and Sn/Pd) showed an extremely high catalytic activity for nitrate reduction, while unmodified Pt and Pd showed a negligible activity. Particularly, the maximum activity of Sn/Pd obtained at a Sn coverage greater than 0.65 is the highest among the already reported electrodes [7-17]. The study of the oxidation of methanol has a long history, and still is one of the most important current issues because this is the anode reaction of the methanol-fuel cell. It is well known that the Sn/Pt electrodes enhanced the electrocatlytic activity of Pt by 50-100 times for this reaction [18-21].

During the study of such binary electrodes, however, we often face the problem that data are not very consistent with those reported by other groups. For example, the addition of Sn to Pt electrodes always enhanced the catalytic activity for the oxidation of methanol, but the magnitude of the enhancement varied from report to report. Similar phenomena were also observed for Sn modified noble metal electrodes for the reduction of nitrate, although the data variation was not as significant compared to the oxidation of methanol. There are several factors to consider which affect the electrocatalytic properties of binary metals. Surface composition is the most important factor. Particularly, in the case when a second metal, which is easily oxidized when

exposed to air, was used, the surface composition often changed under the reaction conditions from that when it was determined because the electrode was usually exposed to air between the characterization and reaction experiments. However, in the case of the Sn modified noble metal electrodes, this is not the case because Sn is very stable and is not removed from the surface even if it was exposed to air. It is already reported that the surface coverage of Sn is an important factor in determining the activity for the reduction of nitrate [4-6]. The activity also depends on the Pd layer thickness [6]. In the present study, it will be demonstrated that an electrochemical pretreatment, or reduction of the as-prepared Sn/Pd, prior to the electrode reaction is another important factor and has an enhancement effect on the reduction of nitrate.

3.2 Preparation of Pd and tin-modified electrodes

Glass slides (Matsunami Glass Ind., Ltd. BK7, 20 mm x 13 mm x 0.7 mm^t), sonicated in soap water (5 vol.% solution of CONTRAD 70) for 1 h and then rinsed with water, were used as underlying substrates of the Pd film electrodes. After the plasma treatment at 20 mA under about 2 Pa for 300 s, 75 nm of Au and 5 nm of Pd (JEOL Co., Japan) were successively deposited onto the glass slides under about 2 Pa by a sputtering instrument (JFC-1600, JEOL Co., Japan). The electrode potential was repeatedly scanned in the range of –0.2 to 1.2 V at the scan rate of 0.05 V s^{-1} until a reproducible cyclic voltammogram was recorded. Although the Au substrate was used, this Pd film electrode is simply cited as a Pd electrode or more simply Pd.

The Pd electrodes were immersed in a 0.12 mM $SnCl_2$ + 0.1 M $HClO_4$ solution for various periods of time ranging from 2 to 20 min, followed by rinsing with copious amounts of water. The tin was spontaneously adsorbed onto the electrode surface by this procedure. This prepared tin modified electrode is labeled as the as-prepared Sn/Pd.

3. 3 Results and discussion

3.3.1 Reduction of nitrate on tin modified Pd electrodes

3.3.1.1 Tin-coverage dependence of electrocatalytic activity of as-prepared Sn/Pd electrodes

Figure 3.1 shows cyclic voltammograms of the Pd electrodes in 0.1 M $HClO_4$

before and after the tin modification.

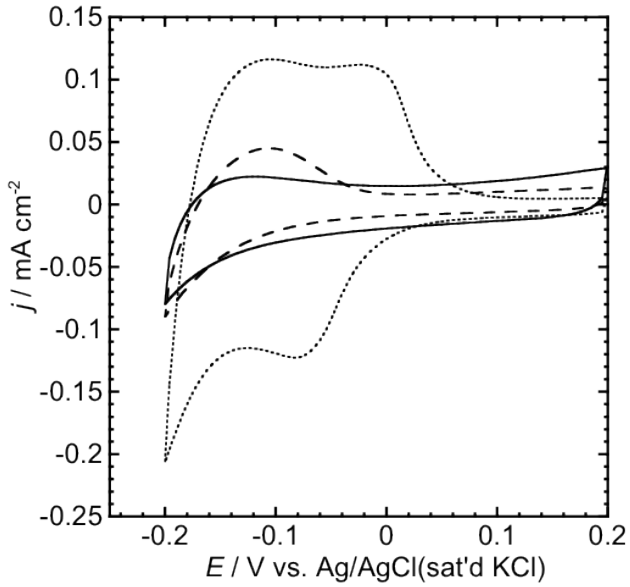

Figure 3.1 Cyclic voltammograms of (dotted curve) Pd, (dashed curve) as-prepared Sn/Pd, and (solid curve) pretreated Sn/Pd electrodes in 0.1 M $HClO_4$ at the scan rate of 0.05 V s^{-1}. Tin was adsorbed by immersing a Pd electrode in a 0.12 mM $SnCl_2$ solution for 15 min. The tin coverage was 0.89. The electrochemical pretreatment was conducted at -0.35 V for 60 s.

The hydrogen wave of the as-prepared Sn/Pd (dashed curve) is much smaller than that of Pd (dotted curve), showing the blocking of the adsorption sites for hydrogen atoms by the tin. The tin coverage, θ_{Sn}, was determined from the charges obtained by integrating the oxidation waves of Pd and as-prepared Sn/Pd, Q_H° and Q_H, respectively, and the equation of $\theta_{Sn} = (Q_H^\circ - Q_H)/Q_H^\circ$. For the particular case shown in Figure 3.1, $\theta_{Sn} = 0.89$. It should be mentioned that the determined θ_{Sn} is not very correct because the contribution of absorbed hydrogen atoms in the bulk Pd cannot be neglected. However, the contribution is considered to be much smaller than that of the bulk Pd because of the Pd layer thickness (5 nm). Therefore, the present θ_{Sn} should be taken as the value at first approximation. The cyclic voltammogram of the as-prepared Sn/Pd (Figure 3.1, dashed curve) corresponds to the reference for electrochemically pretreated Sn/Pd electrodes described later. It should be emphasized that the hydrogen wave still appeared for the as-prepared Sn/Pd electrode, which almost completely disappeared after the pretreatment (see section 3.3.2.3 for details).

As described in the experimental section, electrodes with different θ_{Sn} values were prepared by changing the adsorption time of tin. The electrocatalytic activity on the apparent area basis increased with the increasing θ_{Sn} from 0.32 to 0.82 (Figure 3.2). As shown in the inset of Figure 3.2, however, the nitrate reduction current at -0.1 V did not significantly increase until θ_{Sn} reached 0.45, beyond which it abruptly increased and reached the maximum at around 0.8. At an extremely high θ_{Sn}, it had a tendency to decrease. Such a θ_{Sn} dependence is consistent with the previously reported one for Sn/Pd electrodes, which were prepared by electrochemical Pd deposition followed by the spontaneous tin adsorption [6].

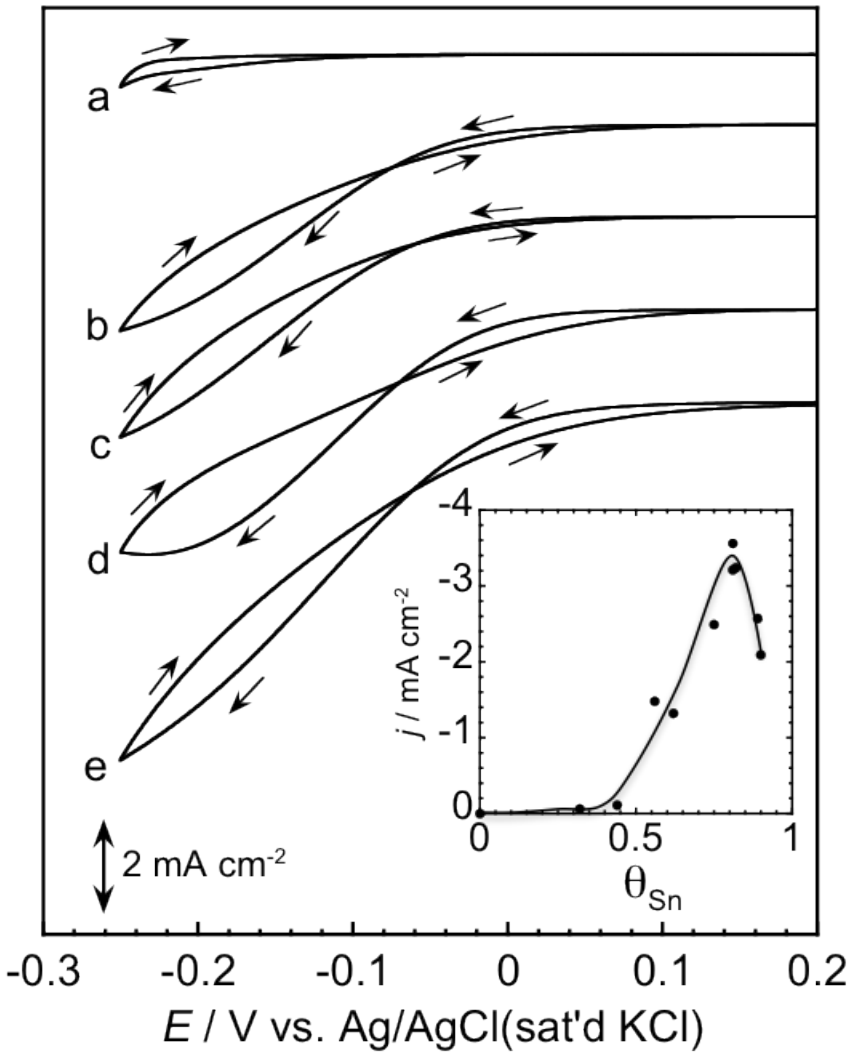

Figure 3.2 Cyclic voltammograms for the reduction of nitrate on as-prepared Sn/Pd electrodes in 0.01 M $NaNO_3$ + 0.1 M $HClO_4$ at the scan rate of 0.01 V s^{-1}. Sn coverage: (a) 0.32, (b) 0.56, (c) 0.62, (d) 0.75, and (e) 0.82. Inset shows tin coverage dependence of the reduction current at -0.1 V on the as-prepared Sn/Pd electrodes during the potential sweep at the scan rate of 0.01 V s^{-1}.

However, the magnitude of the maximum current is less than half of the previously reported value [6]. This is neither due to the difference in the surface roughness, 1.6 - 2.0 and 1.2 - 1.6 for the present and previous cases, respectively, nor the thickness of Pd (the Pd layer thickness of both electrodes is greater than 3 layers, under which activity is not dependent on the thickness) [6].

3.3.1.2 Pretreatment effect on the electrocatalytic activity of Sn/Pd electrode

As described in a previous report [6], the electrocatalytic activity is dependent on the tin-coverage and Pd layer thickness. Another factor is considered, if it exists, would be the adsorption state of tin. In most of our previous reports regarding the tin-modified noble metal electrodes, the electrode was used for the reaction immediately after the spontaneous adsorption of tin without any further intended pretreatment, and the XPS measurements showed that tin mostly exists in the divalent state.

In the present study, the tin-modified Pd electrodes were electrochemically reduced at the constant potential in the range between -0.10 V and -0.45 V for 60 s in a pure 0.1 M $HClO_4$ solution prior to the reduction of nitrate in order to reduce the divalent tin to more reduced states.

Figure 3.3 shows the cyclic voltammograms for the reduction of nitrate at the electrodes without and with the electrochemical pretreatment of Sn/Pd (θ_{Sn} = 0.89) at –0.35 V. By this pretreatment, the potential, at which the nitrate reduction current starts increasing, shifted to more positive potentials by about 0.06 V, and the reduction current became higher in almost the entire potential region. The enhancement, defined by the ratio of the nitrate reduction current at both electrodes, is about 5 at 0.1 – 0 V and 2.5 at –0.10 V. The enhancement or the nitrate reduction current was independent of the pretreatment time from 10 s to 300 s at -0.35 V (Figure 3.4), but dependent on the pretreatment potential.

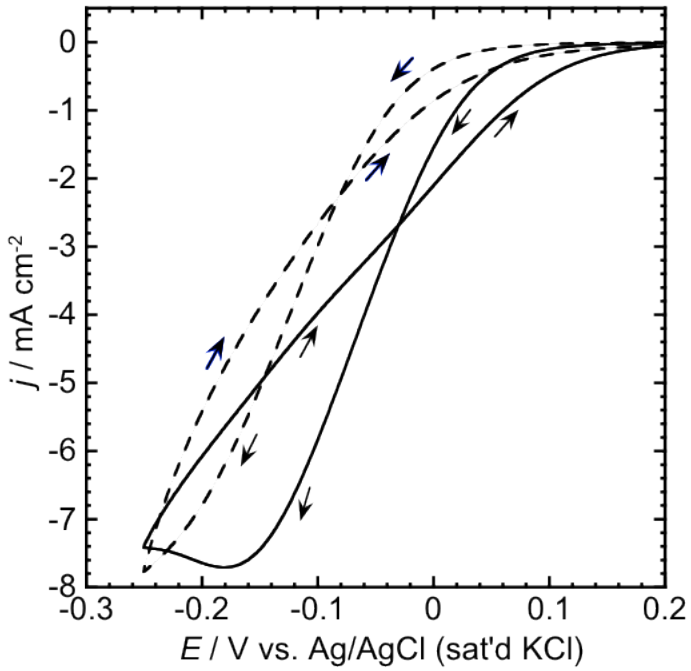

Figure 3.3 Cyclic voltammograms of (dashed curve) as-prepared Sn/Pd, and (solid curve) pretreated Sn/Pd electrodes in 0.01 M $NaNO_3$ + 0.1 M $HClO_4$ at the scan rate of 0.01 V s^{-1}. The tin coverage was 0.89. Electrochemical pretreatment was conducted at -0.35 V for 60 s.

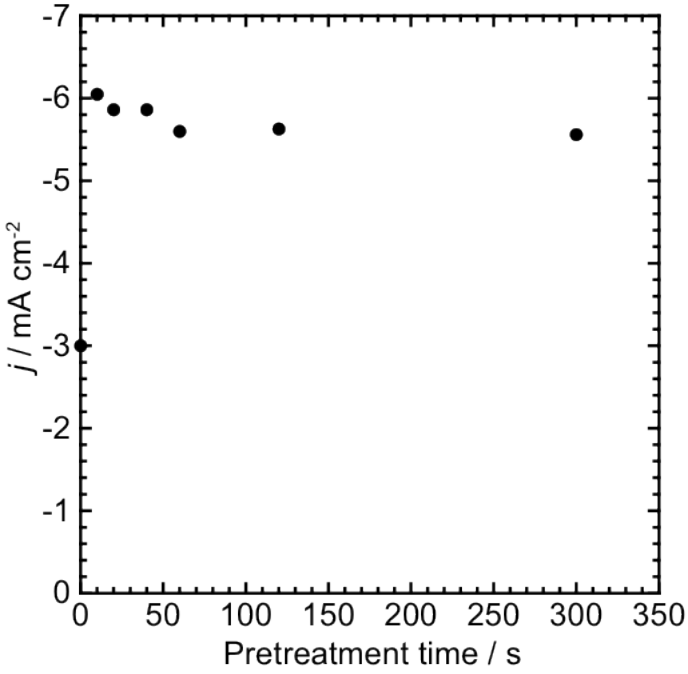

Figure 3.4 Pretreatment time dependence of the reduction current at -0.1 V on Sn/Pd. Sn coverage: 0.89, pretreatment potential: -0.35 V.

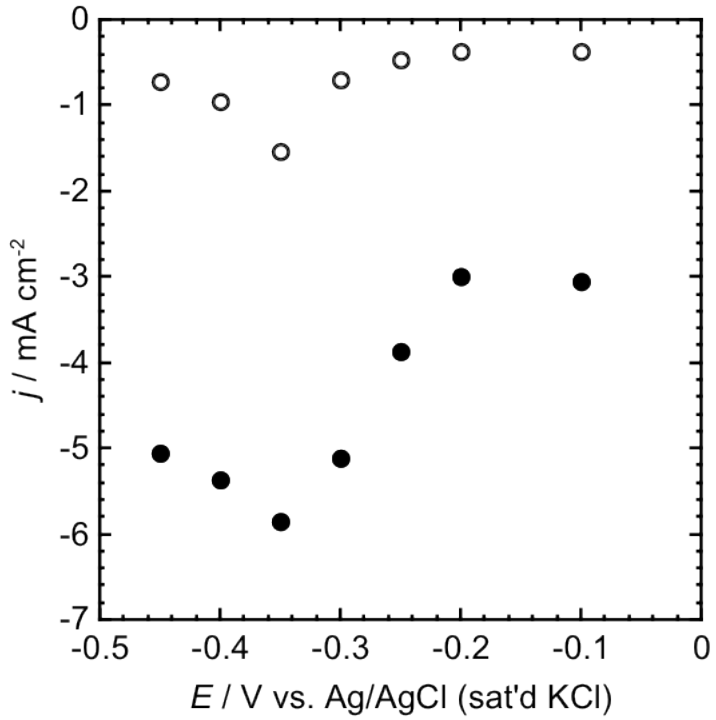

Figure 3.5 Pretreatment potential dependence of the reduction current for the reduction of nitrate at (open circle) 0 V and (solid circle) –0.1 V. Sn coverage: 0.89, pretreatment time: 60 s.

Figure 3.5 shows that the nitrate reduction currents of the pretreated electrodes increased with the decreasing pretreatment potential from –0.2 V to –0.35 V, beyond which it started to decrease. The latter decrease is probably due to the partial detachment of the electrode from the substrate by the generation of a massive amount of hydrogen gas. Actually, many holes were observed by STM after the pretreatment at very negative potentials.

3.3.1.3 Product distribution

To examine the electrochemical pretreatment effect on the reaction selectivity, the products as well as nitrate were quantitatively analyzed as described in Chapter 2. The product distribution (Table 3.1) is shown as a percentage of each product among all products with a standard deviation based on three independent experiments. The nitrite concentration initially increased but then decreased with time, showing that nitrite behaves as an intermediate. For this reason, the product distributions on the as-prepared and pre-treated Sn/Pd electrodes were compared at approximately the same

conversion.

Table 3.1 Distribution of products for the reduction of nitrate at –0.2 V in 0.01 M $NaNO_3$ + 0.1 M $HClO_4$

Electrode	θ_{Sn}	Conv. %	Product Distribution / %				
			NO_2^-	N_2O	N_2	NH_3OH^+	NH_4^+
As-prepared Sn/Pd	87-88	46-52	14.1 ± 4.6	29.0 ± 4.5	28.6 ± 7.9	10.6 ± 4.5	17.8 ± 5.1
Pretreated Sn/Pd	82-86	33-41	17.5 ± 5.1	13.3 ± 5.2	51.3 ± 6.0	1.1 ± 0.5	16.7 ± 4.7

Pretreatment of as-prepared Sn/Pd electrode was performed at –0.35 V for 60 s.

As shown in Table 3.1, the nitrite selectivity is almost the same on both electrodes. Although the standard deviation is not very small, clear differences in the selectivity can be seen for the other products. The hydroxylamine formation drastically decreased by the pretreatment of the electrode, while the production of ammonium ion remained unchanged. The nitrous oxide (N_2O) almost became half, and the nitrogen gas formation doubled. As an environmental aspect, harmless nitrogen gas is the most preferable product. Therefore, the present results, or the enhanced activity together with increased nitrogen gas selectivity, are very important in electrochemical remediation technology.

In our previous reports [22, 23], the product selectivity was discussed based on the number of formed and cleaved bonds. For example, hydroxylamine is formed as a result of the cleavage of two N-O bonds of the nitrate followed by the formation of two N-H and one O-H bonds. In the case of nitrogen gas, all the N-O bonds should be cleaved from two nitrate ions, and one N-N bond is formed. Although such a description does not describe the reaction mechanism, it was useful to derive the characteristics of the electrode. We will now briefly conduct a similar consideration to obtain what bond formation or cleavage the electrochemical pretreatment has an effect on. The decrease in the hydroxylamine and N_2O selectivity is indicative of the acceleration of the N-O bond cleavage by the electrochemical pretreatment of Sn/Pd. Because the sum of the N_2O and N_2 production increased from 58 % for the as-prepared electrode to 65 % for the pretreated electrode, the N-N bond formation is somewhat accelerated. Another important effect of the electrochemical pretreatment is to reduce the hydrogenation ability of the electrode, because the N-H and O-H bond

formation is suppressed as shown by the decreased hydroxylamine selectivity.

In order to more quantitatively express the abilities of N-O bond cleavage, N-N bond formation as well as N-H (and O-H) bond formation, the following parameters, n_{N-O}, n_{N-N}, and n_{N-H}, are introduced in our previous paper [22],

$$n_{N-O} = \frac{f_{NO_2^-} + 5f_{N_2O} + 6f_{N_2} + 2f_{NH_2OH} + 3f_{NH_3}}{f_{NO_2^-} + 2f_{N_2O} + 2f_{N_2} + f_{NH_2OH} + f_{NH_3}} \quad (1)$$

$$n_{N-N} = \frac{f_{N_2O} + f_{N_2}}{f_{NO_2^-} + 2f_{N_2O} + 2f_{N_2} + f_{NH_2OH} + f_{NH_3}} \quad (2)$$

$$n_{N-H} = \frac{3f_{NH_2OH} + 3f_{NH_3}}{f_{NO_2^-} + 2f_{N_2O} + 2f_{N_2} + f_{NH_2OH} + f_{NH_3}} \quad (3)$$

where f_i represents the molar fraction (or percentage) of the species i among all products. n_{N-O}, n_{N-N}, and n_{N-H} represent the average numbers of cleaved N-O bonds, formed N-N and N-H bonds per reacted nitrate ion, respectively. n_{N-H} includes the number of formed O-H bonds. The maximum numbers of n_{N-O}, n_{N-N}, and n_{N-H} are 3.0, 0.5, and 3.0, respectively. When the harmless N_2 is the only product, n_{N-O}, n_{N-N}, and n_{N-H} are 3.0, 0.5, and 0.0, respectively. Then a new parameter has been introduced, P_{N2}, which expresses the potential of the electrode for the selective N_2 production, defined by the following equation,

$$P_{N2}(\%) = 100 \times \left\{ n_{N-O}/3 + n_{N-N}/0.5 + \left(1 - n_{N-H}/3\right) \right\} / 3 \quad (4)$$

When only N_2 is formed, the P_{N2} becomes 100%. Thus P_{N2} shows the capability of the selective N_2 production evaluated from the bond formation and cleavage. The values of n_{N-O}, n_{N-N}, n_{N-H}, P_{N2} calculated from the observed product distributions are summarized in Table 3.2.

Table 3.2 Average number of cleaved N-O bonds and formed N-H & N-N bonds per reduced nitrate and potential for the selective N_2 production.

Electrode	Conversion %	N-O	N-H	N-N	P_{N2} %
As-prepared Sn/Pd	46-52	2.57	0.54	0.37	80.22
Pretreated Sn/Pd	33-41	2.70	0.32	0.39	85.89

By the pretreatment, both $n_{N\text{-}O}$ and $n_{N\text{-}N}$ increased, and $n_{N\text{-}H}$ decreased. As a result, the P_{N2} increased from 80.2% for untreated Sn/Pd to 85.9% for treated electrode. Therefore, the enhanced effect of the pretreatment was confirmed based on the number of bond formation and cleavage.

3.3.2. Characterization of Sn/Pd electrodes before and after the pretreatment

Because the standard electrode potential of $Sn^{2+/0}$ is –0.14 V vs. SHE [24] or –0.337 V vs. Ag/AgCl used in this study, and the pretreatment potentials were close to this potential, it is strongly suggested that the pretreatment caused a change in the oxidation state of tin. To examine such a change and any other change, cyclic voltammetric, STM, and XPS measurements were performed.

3.3.2.1 Scanning Tunneling Microscope (STM)

Figure 3.6 shows typical STM images of a Pd electrode and Sn-modified Pd electrodes without and with pretreatment at –0.35 V (θ_{Sn} before the pretreatment was 0.90). It is generally known that the sputtered metal surface consists of nanometer scale islands. Using six different images, the average diameter of the islands and depth between the neighboring islands were obtained. The average diameter of 30 nm and depth of 1.12 nm were obtained for the Pd electrode.

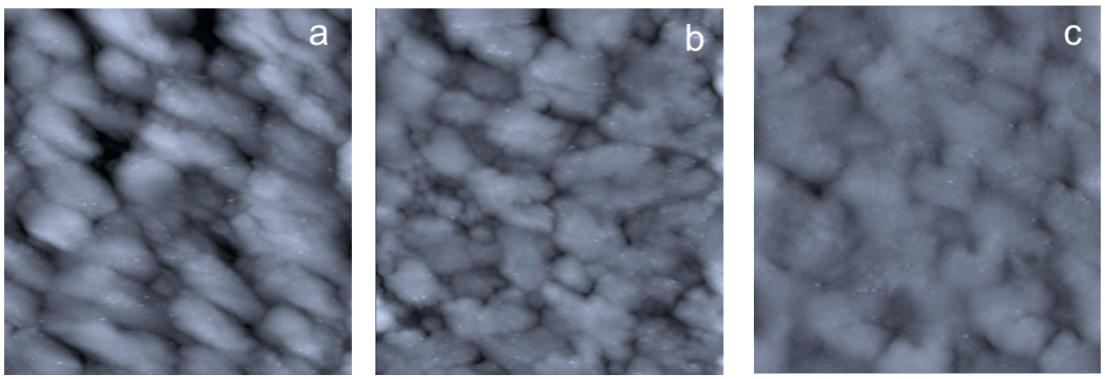

Figure 3.6 STM images of (a) Pd, (b) as-prepared Sn/Pd, and (c) pretreated Sn/Pd electrodes. The scan size is 200 nm x 200 nm. A tip bias voltage of typically 800 mV and a tunneling currents of 300 pA were used.

By the adsorption of tin, the average diameter tended to increase (34 nm) and the depth to decrease (0.99 nm), but the change is not so significant that it suggests the surface reconstruction. Therefore, it is considered that tin is simply adsorbed on the Pd surface without changing the surface structure. However, the electrochemical treatment caused a significant change as demonstrated by increased diameter (45 nm) and much smaller depth (0.63 nm). By performing the electrochemical pretreatment, therefore, the as-deposited Pd islands were merged with neighbors, and formed a large-scale island. Based on these results, it is concluded that the electrochemical pretreatment promoted the reconstruction of the as-deposited islands structure.

3.3.2.2 X-ray Photoelectron Spectroscopy (XPS)

In order to evaluate the oxidation state of Sn and Pd in the Sn/Pd electrodes before and after the electrochemical pretreatment, the XP Sn3d and Pd3d spectra were measured. The XP Sn3d spectrum of an as-prepared Sn/Pd electrode showed a set of two single peaks at 495.0 and 486.3 eV (Figure 3.7a) as previously reported for tin-modified electrochemically deposited Pd electrodes [6]. These peaks are assigned to divalent tin by reference to the literature values [25]. For the pretreated sample, a large shoulder appeared on the negative side of the peak to make the peak-shape flat, indicating the formation of reduced tin. The deconvolution of the peaks was accomplished by fitting the spectral profile with Gaussian shapes in order to determine the peak position and intensity of each component peak. A set of peaks at 495.1 eV and 486.7 eV were assigned to the divalent tin according to literature values [25], and similarly another set of peaks at 493.6 eV and 485.2 eV to zero-valent tin (Figure 3.7a). The average composition of zero-valent tin for three independent electrodes is 38%. This value is probably underestimated, because zero-valent tin is easily oxidized when the electrode was exposed to air before the introduction into the XPS chamber. Knowing the existence of zero-valent tin for the pretreated electrode, looked carefully at the peak shape for as-prepared electrode. Because the peak is not very sharp, it is not simulated as a single peak. The deconvolution, using the same parameters of peak position and width of half maximum as those for the pretreated electrode, shows a small amount of zero-

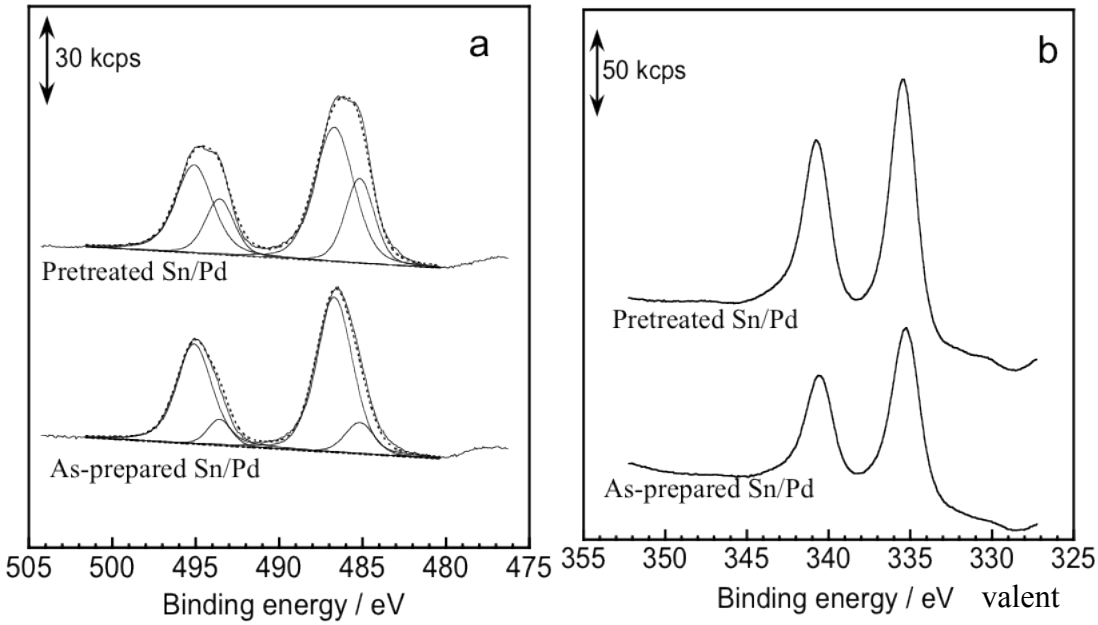

Figure 3.7 XP (a) Sn3d and (b) Pd 3d spectra of as-prepared Sn/Pd (Sn coverage: 0.90) and pretreated Sn/Pd (Sn coverage before the pretreatment: 0.90) electrodes. Results of the deconvolution are also shown for the Sn3d spectra.

tin (<14%). It is concluded that the reduction of divalent tin to zero-valent tin was accelerated by the pretreatment as expected.

Figure 3.7b also shows the XP Pd3d spectra before and after pretreatment at -0.35 V. The peak of $Pd3d_{5/2}$ is partially overlapped with the Au 4d peak so that only the $Pd3d_{3/2}$ peak was analyzed. The binding energy of 340.7 eV is assigned to the zero-valent Pd. This binding energy was not changed before and after the pretreatment, showing that the pretreatment did not affect the Pd oxidation state.

The fractions of Pd and Sn between these two elements were estimated to be 0.69 and 0.31 for the as-prepared Sn/Pd, and 0.76 and 0.24 for the pretreated Sn/Pd, respectively, by integrating only the $d_{3/2}$ peaks, using their relative sensitivity factors calculated from the photoionization cross sections and spectrometer factors. The Sn fractions are much smaller than the electrochemically determined θ_{Sn} values (0.85–0.89 for these samples). This is definitely due to the fact that Sn is only in the outermost layers, while Pd exists both in the surface and bulk. From the comparison

of the fractions before and after the pretreatment, it is concluded that the surface Sn fraction decreased by the pretreatment of the Sn/Pd electrodes.

3.3.2.3 Hydrogen adsorption properties

In order to investigate the electrochemical characteristics of the electrodes, cyclic voltammograms of the hydrogen adsorption/desorption were measured as shown in Figure 3.1 (solid curve). By the electrochemical pretreatment, the hydrogen wave almost disappeared. If Sn atoms simply block the adsorption of hydrogen atoms on Pd, these results are indicative of the increase in the surface Sn coverage. However, this is not supported by the XPS data as already described. Therefore, it is reasonable to assume that the surface Pd lost its hydrogen adsorption ability. The change in the electronic state of Pd expected from this phenomenon is not observed in the XP spectra, because the contribution from the bulk Pd is much greater in the XPS signals. This loss of hydrogen adsorption ability will be due to *d*-band filling as described later.

3.3.2.4 Stability

The change in the surface state as observed in the hydrogen adsorption ability may affect the other surface phenomena, such as the formation of surface oxide, removal of tin, etc. To examine this, continuous potential cycling was applied to the as-prepared and pretreated electrodes. With the increasing number of cycles, the shape of the cyclic voltammogram became close to that of pure palladium for both electrodes (Figure 3.8) due to the oxidative dissolution of the surface tin atoms. However, the pretreated electrode changed its shape (magnitude of hydrogen waves and peak potential due to surface oxide reduction) much slower than the as-prepared electrode (Figure 3.8c). These different electrochemical behaviors also suggest that something more than morphology change, like an electronic interaction between Sn and Pd, took place by the pretreatment.

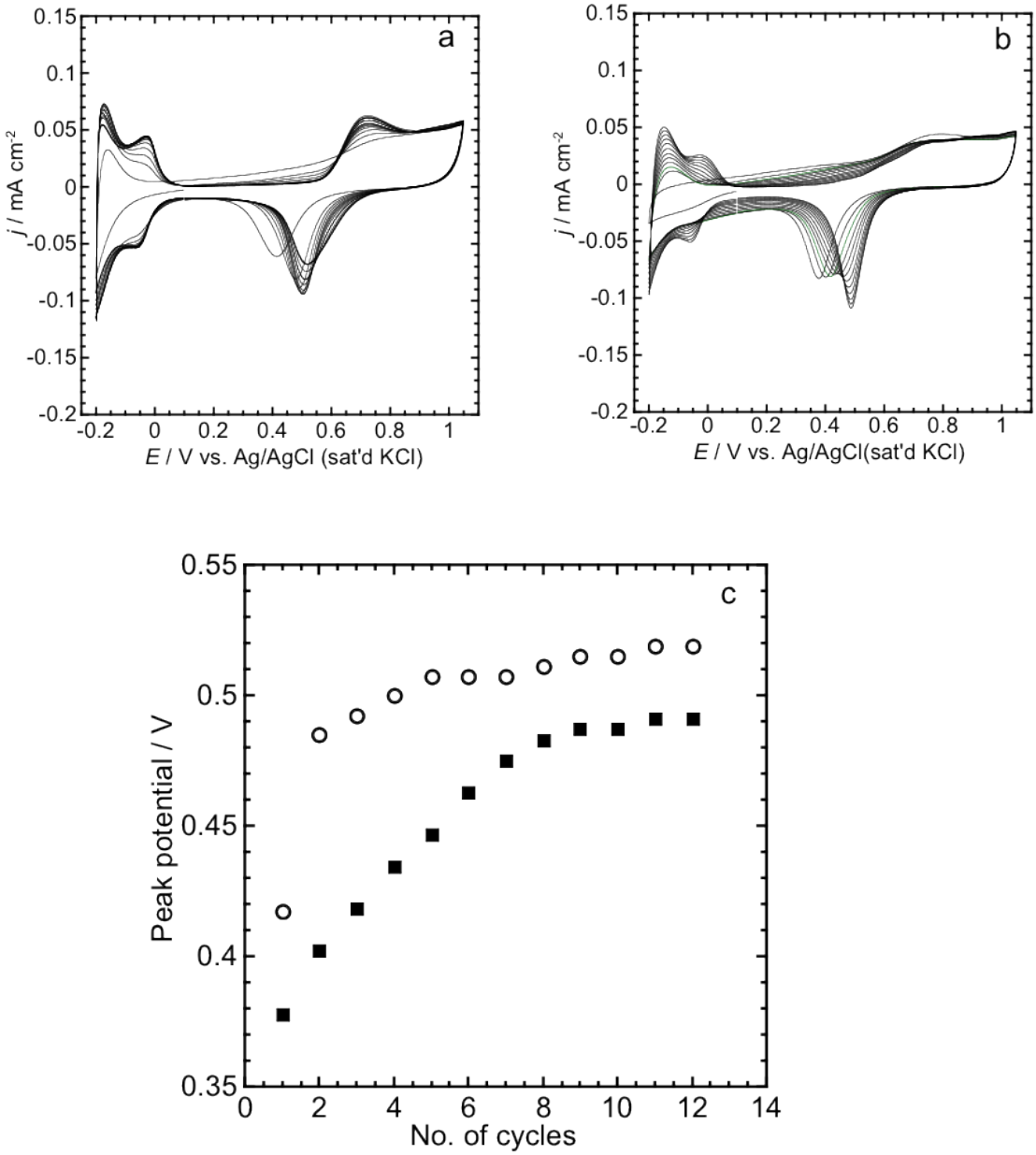

Figure 3.8 Continuous cyclic voltammograms of (a) as-prepared Sn/Pd (Sn coverage: 0.90) and (b) pretreated Sn/Pd (Sn coverage before the pretreatment: 0.90) electrodes in 0.1 M $HClO_4$ at the scan rate of 0.025 V s^{-1}, and (c) cycling time dependence of surface oxide reduction peak potential on (open circle) as-prepared Sn/Pd and (solid circle) pretreated Sn/Pd electrode. The electrochemical pretreatment was conducted at -0.35 V for 60 s.

3.3.3 Pretreatment effect on Sn/Pd and Sn/Pt electrodes

The XP spectra demonstrated that the reduction of divalent tin was promoted by

the electrochemical pretreatment. As evidenced by the STM and electrochemical measurements, it caused a further change in the morphology and adsorption properties of the electrodes. These results suggest that tin and palladium, which initially exist more independently, more electronically interact with each other to form an alloy, although the STM images at the scale shown in this study do not necessarily show a direct relation between the surface structural change and alloy formation. More importantly, tin and palladium are well known to form an alloy [26]. In early studies, it was considered that the 5s electrons are transferred from the tin atoms to holes in the 4d shell of the palladium, consistent with a simple rigid band model [27]. In the review on electronic structure of Pd alloys with electropositive elements [28], however, Fuggle et al. concluded that the Pd *d*-band is being filled and it is largely due to changes in hybridization of the Pd *d*-band with the partner element band. It is also known that the hydrogen sorption (both absorption and adsorption) ability of Pd is lost when the *d*-band is filled [29, 30]. Therefore, the observed loss of the hydrogen adsorption ability is consistent with the *d*-band filling. The *d*-band filling occurs because the *d*-band center moved away from the Fermi level to higher binding energies [28]. Based on the density functional calculations, Norskov et al. have shown that the *d*-band center varies dependent on the surface structure [31, 32]. For the surface metal impurities and overlayers on the other metals, or surface alloys, up to about a 2 eV shift in the *d*-band center was reported. They have also shown that the adsorption energy of CO linearly increased with the increasing *d*-band center relative to the Fermi level. It was claimed that the *d*-band center is an important parameter characterizing the ability of the surface *d*-electrons to participate in bonding to the adsorbate, not only CO, but also other molecular adsorbates [30]. Actually, the linear dependence between the adsorption energy and *d*-band center was also reported for the adsorption of O_2 [33]. A similar trend has been expected for the adsorption of nitrate [8], or the upshift of the *d*-band center causes a stronger interaction between the *d*-band and nitrate. On the contrary, the downshift produces a weaker interaction. The reaction is facilitated at the surface showing a moderate interaction with the adsorbates. For the reduction of O_2, a volcano-type variation in the electrocatalytic activity was observed against the *d*-band center [33]. Therefore, the change in the adsorption state of nitrate by the pretreatment of the as-prepared Sn/Pd may be a plausible reason for the enhanced activity.

Preliminary experiments have been conducted to examine the adsorption state of nitrate using the surface-enhanced infrared absorption spectroscopy (SEIRA). However, none of electrodes (Pd, as-prepared Sn/Pd, pretreated Sn/Pd) showed the existence of adsorbed nitrate. These results further required to examine whether there exists infrared-inactive adsorbed species or not.

Fuggle et al. [28] also concluded that as the electronegativity difference between the elements is decreased there is greater overlap in band energies of Pd and second metal. The electronegativities of Pd and Sn are 2.0 and 1.7 [33], respectively. Conversely, smaller overlap and hence smaller change in electronic structure are expected for the alloy composed of elements having greater difference in the electronegativity. Platinum has a greater electronegativity (Pt 2.1-2.2 [33]), and the Sn/Pt electrode also shows the high catalytic activity for the reduction of nitrate. To examine the effect of electronic structure on electrocatalytic properties, the pretreatment effect was examined for the Sn/Pt electrode. This electrode was prepared following a procedure similar to Sn/Pd, or by successively sputtering Au and Pt followed by the spontaneous adsorption of tin. The electrocatalytic activity for the reduction of nitrate was enhanced by the pretreatment.

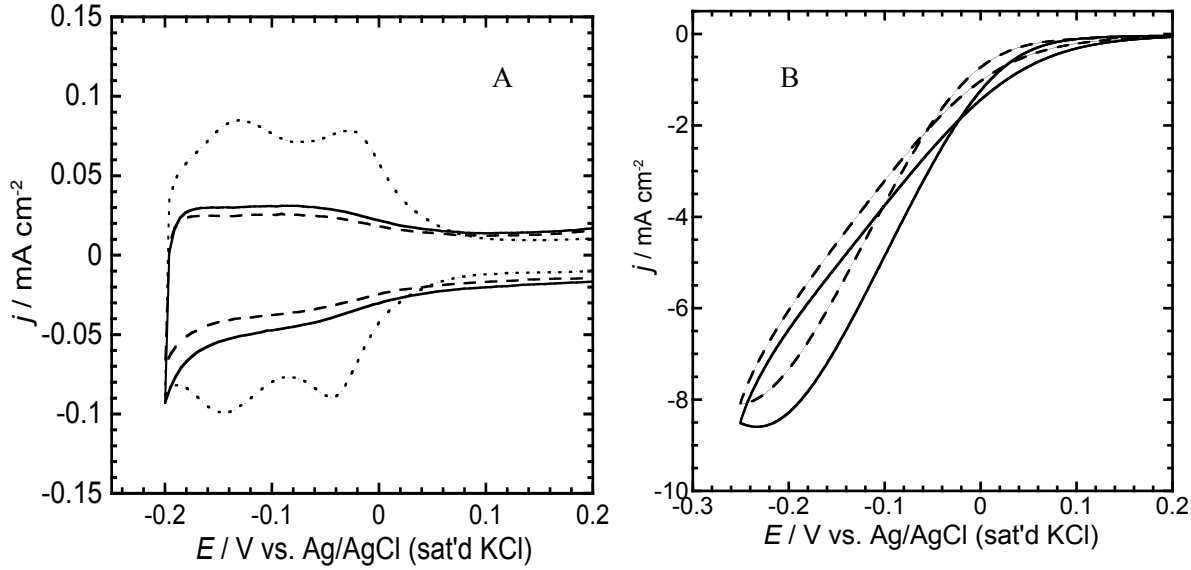

Figure 3.9 (A) Cyclic voltammograms of (dotted curve) Pt, (dashed curve) as-prepared Sn/Pt, and (solid curve) pretreated Sn/Pt electrodes in 0.1 M $HClO_4$ at a scan rate of 0.05 V s^{-1}. Tin coverage was 0.83. (B) CVs of (dashed curve) as-prepared Sn/Pt and (solid curve) pretreated Sn/Pt electrodes in 0.01 M $NaNO_3$ + 0.1 M $HClO_4$ at a scan rate of 0.01 V s^{-1}. The electrochemical pretreatment was conducted at -0.35 V for 60s.

However, the enhancement of current is insignificant (1.3 times) (Figure 3.9 B). The hydrogen wave in the cyclic voltammogram in 0.1 M $HClO_4$ remained unchanged after the pretreatment at –0.35 V for 60 s (Figure 3.9 A).

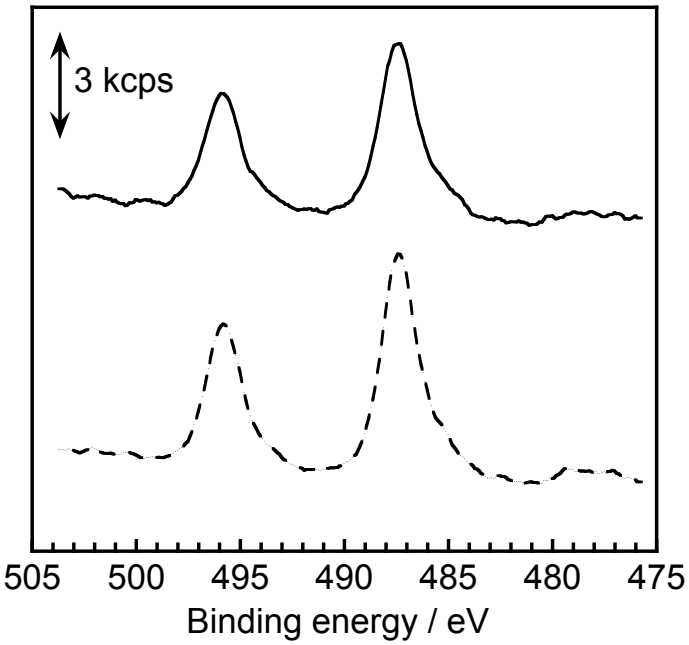

Figure 3.10 XP spectra of Sn3d of (dash curve) as-prepared Sn/Pt and (solid curve) pretreated Sn/Pt electrodes. Sn coverage before pretreatment was 0.90. The Sn/Pt electrode was pretreated at -0.35 V for 60s.

XP Sn $3d_{5/2}$ and $3d_{3/2}$ peaks for Sn/Pt electrode appeared at 495.83 and 487.41 eV, respectively (Figure 3.10), which are assigned to divalent tin as observed previously [5]. Contrary to Sn/Pd, neither clear band nor shoulder is observed after the pretreatment. These results suggest that the interaction between Sn and Pt is weaker compared with Sn/Pd. Consequently, the effect of pretreatment on the electrocatalytic properties of Sn/Pt is much smaller.

3.4 Conclusion

The pretreatment of tin-modified Pd electrodes at negative potentials enhanced the electrocatalytic activity for the reduction of nitrate. The formation of N_2, the preferable product from an environmental aspect was also enhanced to about 50% of

the products. By the pretreatment, spontaneously adsorbed tin, which was originally in the divalent state, was at least partially reduced to the zero-valent state. Although a clear change in the electronic state of palladium was not observed by XPS, palladium lost its hydrogen adsorption ability, showing the change in the surface electronic state. STM showed that the pretreatment caused a surface reconstruction. The most plausible explanation for these observations would be the formation of an alloy on the surface. The resulting change in the surface electronic state will enhance the N-O bond cleavage via modification of the adsorption strength of the adsorbates. Acceleration of the N-O bond cleavage results in the decreased hydroxylamine and N_2O selectivity. The loss of the hydrogen adsorption ability also leads to the decline in the hydrogenation ability of the electrode.

3.5 References

[1] K. Rajeshwar, J. G. Ibanez, Environmental Electrochemistry-Fundamentals and Applications in Pollution Abatement, Academic Press, San Diego, CA, 1997.

[2] V. Rosca, M. Duca, M. T. de Groot, M. T. M. Koper, Chem. Rev. 109 (2009) 2209.

[3] M. Duca, M. T. M. Koper, Energy Environ. Sci. 5 (2012) 9726.

[4] K. Shimazu, R. Goto, K. Tada, Chem. Lett. 2002, 204.

[5] K. Tada, K. Shimazu, J. Electroanal. Chem. 577 (2005) 303.

[6] K. Shimazu, R. Goto, S. Piao, R. Kayama, K. Nakata, Y. Yoshinaga, J. Electroanal. Chem. 601 (2007) 161.

[7] A.C.A. de Vooys, R.A. van Santen, J. A. R. van Veen, J. Mol. Catal. 154 (2000) 203.

[8] J. F. E. Gootzen, P. G. J. M. Peeters, J. M. B. Dukers, L. Lefferts, W. Visscher, J. A. R. van Veen, J. Electroanal. Chem. 434 (1997) 171.

[9] J. F. E. Gootzen, L. Lefferts, J. A. R. van Veen, Appl. Catal. A: Gen. 188 (1999) 127.

[10] T. Ya. Safonova, O. A. Petrii, J. Electroanal. Chem. 448 (1998) 211.

[11] S. Kerkeni, E. Lamy-Pitara, J. Barbier, Catal. Today 75 (2002) , 35.

[12] X-K. Xing, D.A. Scherson, J. Electroanal. Chem. 199 (1986) 485.

[13] J. Garcia-Domenech, M. A. Climent, A. Aldaz, J. L. Vazquez, J. Clavilier, J. Electroanal. Chem. 159 (1983) 223.

[14] C. Lu, S. Lu, W. Qiu, Q. Liu, Electrochim. Acta 44 (1999) 2193.

[15] S. Ureta-Zanartu, C. Yanez, Electrochim. Acta 42 (1997) 1725.

[16] M. C. P. M. da Cunha, J. P. I. De Souza, F. C. Nart, Langmuir 16 (2000) 771.

[17] J. Yang, M. Duca, K. J. P. Schouten, M. T. M. Koper, J. Electroanl. Chem. 662 (2011) 87.

[18] M. M. P. Jassen, J. Moolhuysen, Electrochim. Acta 21(1976) 869.

[19] M. R. Andrew, J. S. Drury, B. D. Mcnicol, C. Pinnington, R. T. Short, J. Appl. Electrochem. 6 (1976) 99-106.

[20] K. J. Cathro, J. Electrochem. Soc. 116 (1969) 1608.

[21] M. M. P. Jassen, J. Moolhuysen, Electrochim. Acta 21 (1976) 861.

[22] S. Piao, Y. Kayama, Y. Nakano, K. Nakata, Y. Yoshinaga, K. Shimazu, J. Electroanal. Chem. 629 (2009) 110.

[23] K. Nakata, Y. Doi, S. Kubota, K. Shimazu, J. Electroanal. Chem. 647 (2010) 187.

[24] A. J. Bard, R. Parsons, J. Jordan (eds), Standard Potentials in Aqueous Solution, Dekker, New York, 1985.

[25] A. V. Naumkin, A. Kraut-Vass, S. W. Gaarenstroom, C. J. Powell, NIST X-ray Photoelectron Spectroscopy Database 20 (web edition) version. 4.1.

[26] H. Okamoto, J. Phase Equilib. Diffus. 33 (2012) 253.

[27] I. R. Harris, M. Cordey-Hayes, J. Less -Common Met. 16 (1968) 223.

[28] J. C. Fuggle, F. U. Hillebrecht, R. Zeller, Z. Zolnierek, P. A. Bennett, Ch. Freiburg, Phys. Rev. B 27 (1982) 2145.

[29] D. A. J. Rand, R. Woods, J. Electroanal. Chem. 36 (1972) 57.

[30] W. M. H. Sachtler, R. A. Van Santen, Adv. Catal. 26 (1977) 69.

[31] R. Ruban, B. Hammer, P. Stoltze, H. L. Skriver, J. K. Norskov, J. Mol. Catal. A: Chem. 115 (1997) 421.

[32] B. Hammer, O. H. Nielsen, J. K. Norskov, Catal. Lett. 46 (1997) 31.

[33] M. H. Shao, T. Huang, P. Liu, J. Zhang, K. Sasaki, M. B. Vukmirovic, R. R. Adzic, Langmuir 22 (2006) 10409.

Chapter 4

Electrochemical Reduction of Nitrate on Tin Modified Palladium-Platinum Electrodes

4.1 Objective

The reduction of nitrate and nitrite has been extensively studied on various metal electrodes in the past decades [1-14, 30, 31]. Bimetallic electrodes generally composed of a noble metal and a second base metal have been widely investigated [1-7, 9-11, 13]. Some of these electrodes are very active for the nitrate reduction, but the only problem is their low selectivity for the formation of nitrogen gas. Palladium or platinum based bimetallic electrodes, such as Cu modified Pd [10], and Ge modified Pd, Pt and PdPt [13] showed a high catalytic activity for the nitrate reduction. In our previous studies [15-20], it was found that Sn modification on a novel metal electrode increased the electrocatalytic activity for the nitrate reduction in an acidic solution. The effect of the Sn modification was higher in the order of Sn/Ir < Sn/Ru ≈ Sn/Rh < Sn/Pt < Sn/Pd [20]. Particularly, Sn/Pd showed the highest activity among so far reported electrodes [17]. For the electrochemical denitrification process, it is important to control not only the activity but also the product selectivity. The selective formation of harmless nitrogen gas is the best from the environmental viewpoint. It is generally considered that the product distribution is determined by subsequent reactions after the reduction of the nitrate to nitrite [10, 21]. In determining the distribution of the products, such as NO_2^-, N_2O, N_2, NH_2OH, and NH_3, the hydrogenation ability to form the N-H bond and the N-O bond

cleavage ability of the electrodes play an important role. To selectively form N_2, it is essential to control these abilities.

In the previous study, it has been reported that the main reduction products were NH_3^+OH and NH_4^+ (57%) for the Sn/Pt electrodes and N_2O (78%) for the Sn/Pd electrodes [20]. The hydrogenation ability of the Sn/Pt electrodes is too high and the N-O bond cleavage ability of the Sn/Pd electrodes is not enough to produce N_2. It is simply hypothesized that a higher N_2 selectivity would be obtained by enhancing the N-O bond cleavage ability of the Sn/Pd and/or decreasing the hydrogenation ability of the Sn/Pt. One of the simple solutions is to harmonize these abilities by mixing Pt and Pd. Based on this idea, it is conducted the reduction of nitrate on Sn-modified PdPt electrodes in this study. The electrodes were prepared by the sputtering and deposition methods. To examine the effect of the surface Pd/Pt composition and Sn-modification on the adsorption state of nitrate, the surface enhanced infrared spectroscopic (SEIRAS) measurements were conducted and spectra were analyzed based on our previous studies on nitrate [34], nitrite [35], and nitric oxide [35] adsorption on the Pt electrodes.

4.2 Preparation of electrodes

4.2.1 Preparation of electrodes by sputtering

Glass slides (Matsunami glass Ind. LTD., BK7 type, 20 mm x 13 mm x 0.7 mm) used as substrates were ultrasonically cleaned in soap water (5 vol. % solution of CONTRAD 70) for one hour and rinsed with water. Seventy five nm of gold was sputtered onto the glass slides under a vacuum at room temperature after plasma cleaning at 20 mA under about 2 Pa for 300 s using JFC-1600 sputtering device (JEOL Co., Japan). Then 5 nm of Pd, Pt, or PdPt (Pd/Pt = 31/69 in molar ratio) was sputtered onto the gold film on the glass slide. These electrodes are referred to as Pd(sp), Pt(sp), or PdPt(sp) electrodes, respectively ("sp" in parentheses stands for "sputtering"). The electrodes were used immediately after the preparation.

Sn modification was carried out by the immersion of the electrode into 0.1 M $HClO_4$ containing 0.025-0.25 mM $SnCl_2$. The prepared Sn-modified Pd(sp), Pt(sp), and PdPt(sp) are referred to hereafter as the Sn/Pd(sp), Sn/Pt(sp) , and Sn/PdPt(sp) electrodes, respectively. The Sn coverage (θ_{Sn}) was determined using the equation $\theta_{Sn} = (Q_H^0 - Q_H)/Q_H^0$, where Q_H^0 and Q_H are the charge due to the oxidation of the adsorbed hydrogen atoms before and after the adsorption of Sn^{2+}, respectively, as described in previous report [17]. These charges were obtained from cyclic voltammograms in 0.1 M $HClO_4$.

4.2.2 Preparation of electrodes by electrochemical deposition

Gold films used as substrate electrodes were prepared by vacuum deposition according to a previously described method [18]. The gold electrodes were electrochemically cleaned by cycling the electrode potential in the range between 0 to 1.48 V vs. Ag/AgCl (saturated KCl) in a 0.1 M $HClO_4$ solution at a sweep rate of 0.1 V s^{-1}. The roughness factor of the Au electrodes was determined to be 1.2 to 1.6 from the charge required for the reduction of the oxide monolayer on the Au [22]. The deposition of Pd and Pt on the Au was conducted at 0.4 V for 60 s in 1 mM $PdCl_2$ and K_2PtCl_6 + 0.1 M $HClO_4$, respectively. The codeposition of Pd and Pt on the Au was conducted under the same conditions, but in a mixed $PdCl_2$ and K_2PtCl_6 solution, where total noble metal concentration was kept in 1 mM. For the electrodes used for the constant potential electrolysis, the deposition period was extended to 600 s. Tin modification was carried out by the same method as for sputtered electrodes. These electrodes are described using "dep" in parentheses such as Sn/Pd(dep), Sn/Pt(dep) , and Sn/PdPt(dep) electrodes.

Similar electrochemical deposition conditions were applied for the preparation of electrodes for IR measurements except elongated deposition time of 900s. To obtain optical response, the gold thin film was deposited on the total reflecting plane of a Si hemicylinder prism by the previously described electroless deposition technique [31].

4. 3. Results and Discussion

4.3.1 Sputtered electrodes

4.3.1.1 Characterization

Cyclic voltammograms in 0.1 M $HClO_4$ were used to examine the surface states of the electrodes. The shape of them changed with the number of cycles for PdPt (sp)

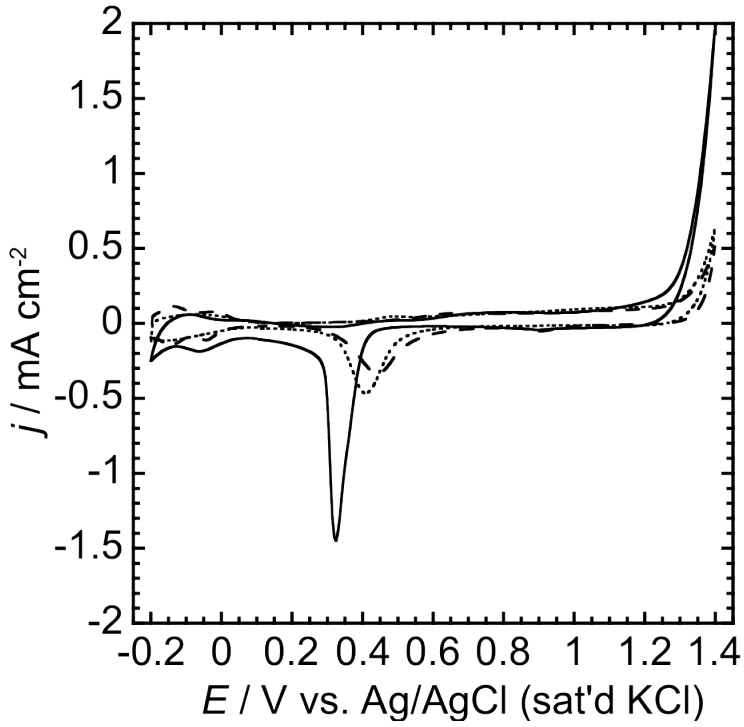

Figure 4.1. Cyclic voltammogram Pd (solid line) , Pt (dash line) and PdPt (dot line) in 0.1 M $HClO_4$. Scan rate: 50 mV s^{-1}. The surface composition of Pd/Pt was 30/70.

electrodes. Figure 4.1 shows the second cycle of cyclic voltammograms for a PdPt(sp) electrode together with those of Pd(sp) and Pt(sp) electrodes (the first cycle voltammograms did not show typical characteristics of these electrodes even for single Pd(sp) and Pt(sp) metal electrodes). These voltammograms show that Pd(sp) and Pt(sp) electrodes were of polycrystalline, and that Pd and Pt were well mixed in a PdPt(sp) electrode rather than they formed independent islands because a single oxide reduction

peak was observed. Capon and Parsons reported that there is a linear relationship between the reduction peak potential of the surface oxide and the surface composition for the Pd-Pt electrodes [23]. Using the relationship, therefore, the surface composition of the PdPt(sp) electrodes can be determined. The oxide reduction peaks of Pd(sp) and Pt(sp) electrodes were observed at 0.325 ± 0.007(5) V and 0.449 ± 0.005(4) V, respectively. The high reproducibility in the peak potential for the single component Pd(sp) and Pt(sp) electrodes provides the accurate terminal points of the linear relationship. From the average peak potential for four different PdPt(sp) electrodes, 0.441 ± 0.005(4) V, the surface composition was determined to be Pd/Pt = 31/69, which is the same as that of a PdPt target used for the sputtering (Pd/Pt = 31/69)

The sputtered PdPt electrode having the surface composition of Pd/Pt = 31/69 is refereed hereafter as PdPt(sp, 31/69). With increasing number of cycles, the oxide reduction peak of the PdPt(sp) electrode shifted in a positive direction, reflecting a preferential dissolution of Pd from PdPt. The surface compositions are Pd/Pt = 23/77, 16/84, and 12/88 after 3rd, 6th, and 10th cycles, respectively.

The X-ray photoelectron spectroscopy will be an alternate technique to obtain the information about the surface composition. Because the $Pd3p_{3/2}$, $Pd3d_{5/2}$, and $4f_{5/2}$ peaks were close to or overlapped with the O1s, $Au4d_{5/2}$, and Au5p peaks, respectively, the Pd $3d_{3/2}$ and $4f_{7/2}$ peaks were used to calculate the surface composition. Results using a linear background or a Shirley background (in parenthesis) were Pd/Pt = 34/66 (28/72), 33/67 (29/71), 35/65 (27/73), and 30/70 (26/74) after 2nd, 3rd, 6th, and 10th cycles, respectively. These values are close to that of a PdPt target, and are almost independent of the number of cycles. The result that the surface composition was not changed until the 6th cycle is not consistent with the shift of the surface oxide reduction peak. Such a discrepancy between electron spectroscopy and electrochemistry has been reported for a Pt-Rh alloy electrode [25]. Based on the depth profile of the Auger electron spectrum and quantitative analysis of the electrochemical data, Capon and Parsons concluded that the electrochemically determined composition most reliably reflects that of the outermost

layer of the surface [25]. Therefore, I will hereafter use the electrochemically determined surface composition.

The Sn coverage, θ_{Sn}, increased with the immersion time and the concentration of a $SnCl_2$ solution. Figure 4.2 shows the immersion time dependence of the Sn coverage of the PdPt(sp) electrode at the fixed $SnCl_2$ concentration (0.05 mM). The inset shows cyclic voltammograms of PdPt(sp) in 0.1 M $HClO_4$ before and after the immersion for 360 s, at which the θ_{Sn} is 0.70.

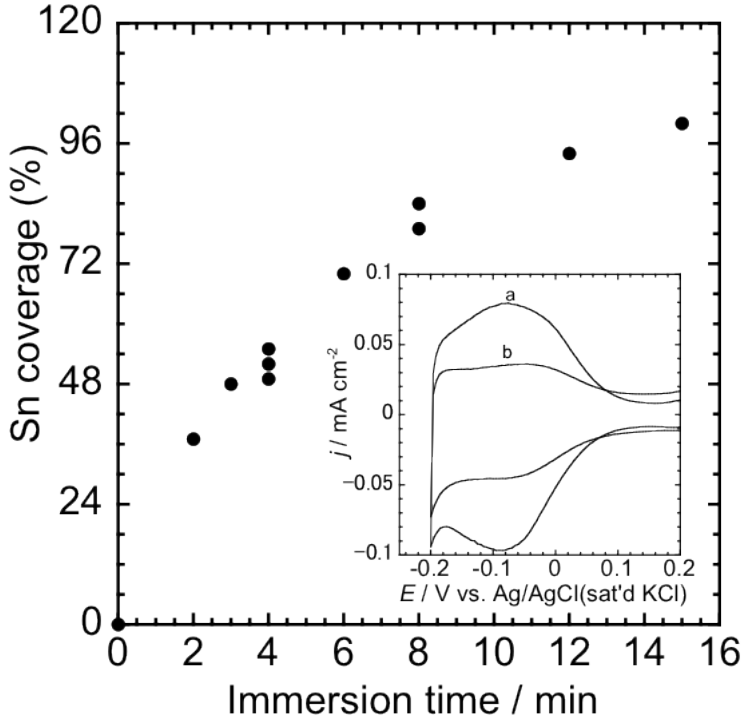

Figure 4.2 Plot of Sn coverage (θ_{Sn}) on PdPt(sp) vs. immersion time. The inset shows cyclic voltammograms of PdPt (a) before and (b) after the immersion in a 0.1 M $HClO_4$ solution containing 0.05 mM $SnCl_2$ for 360s. The scan rate was 0.05 V s^{-1}. The surface Pd/Pt composition was 31/69 and the θ_{Sn} was 0.70.

The binding energies of XP Pd $3d_{3/2}$ and Pt $4d_{7/2}$ peaks are summarized in Table 4.1 for Pd(sp), Pt(sp) and PdPt(sp) electrodes before and after Sn modification. The Pd $3d_{3/2}$ binding energies of PdPt(sp, 31/69) and PdPt(sp, 12/88), which correspond to the electrodes after 2nd and 10th cycles of as-sputtered electrodes, are very close to that of

Pd(sp) and also the reported values for Pd (0) (339.3 – 341.1 eV). Similarly all Pt $4d_{7/2}$ binding energies are within the reported values for Pt (0) (70.83 - 71.9 eV) [21, 31, 32].

Table 4.1 Binding energy of $Pd3d_{3/2}$, $Pt4f_{7/2}$ and $Sn3d_{3/2}$ in Pd, PdPt, Pt (sp) electrodes and their Sn modified derivatives.

Electrode	Binding energy / eV		
	$Pd3d_{3/2}$	$Pt4f_{7/2}$	$Sn3d_{3/2}$
Pd	340.81 ± 0.09		
PdPt (sp, 31/69)	340.79 ± 0.04	71.25 ± 0.03	
PdPt (sp, 12/88)	340.77 ± 0.03	71.21 ± 0.02	
Pt		71.21 ± 0.02	
Sn/Pd	340.73 ± 0.15		486.59 ± 0.20
Sn/PdPt(sp, 31/69)	340.71 ± 0.04	71,19 ± 0.04	486.54 ± 0.27
Sn/PdPt (sp, 12/88)	340.68 ± 0.06	71.20 ± 0.03	486.49 ± 0.23
Sn/Pt		71.17 ± 0.03	487.04 ± 0.34

By the tin modification, both Pd $3d_{3/2}$ and Pt $4f_{7/2}$ binding energies remained almost unchanged. Therefore, Pd and Pt exist as zero-valent state both before and after the tin modification. The $Sn3d_{5/2}$ binding energy shows that the plausible oxidation state of the Sn is divalent.

Figure 4.3 shows typical STM images of PdPt(sp, 31/69) and Sn/PdPt(sp, 31/69). The PdPt particles are uniformly sized (diameter: 7 nm, depth: 0.63 nm) and are much smaller than Pd (diameter: 30 nm) and Pt particles (diameter: 30 nm). By the adsorption of tin (θ_{Sn} = 0.90), such features disappeared to apparently form much greater and more flat islands (diameter: 31 nm, depth: 0.48 nm). This change is consistent with the high coverage of tin, but detailed structural change of the PdPt particles is unclear.

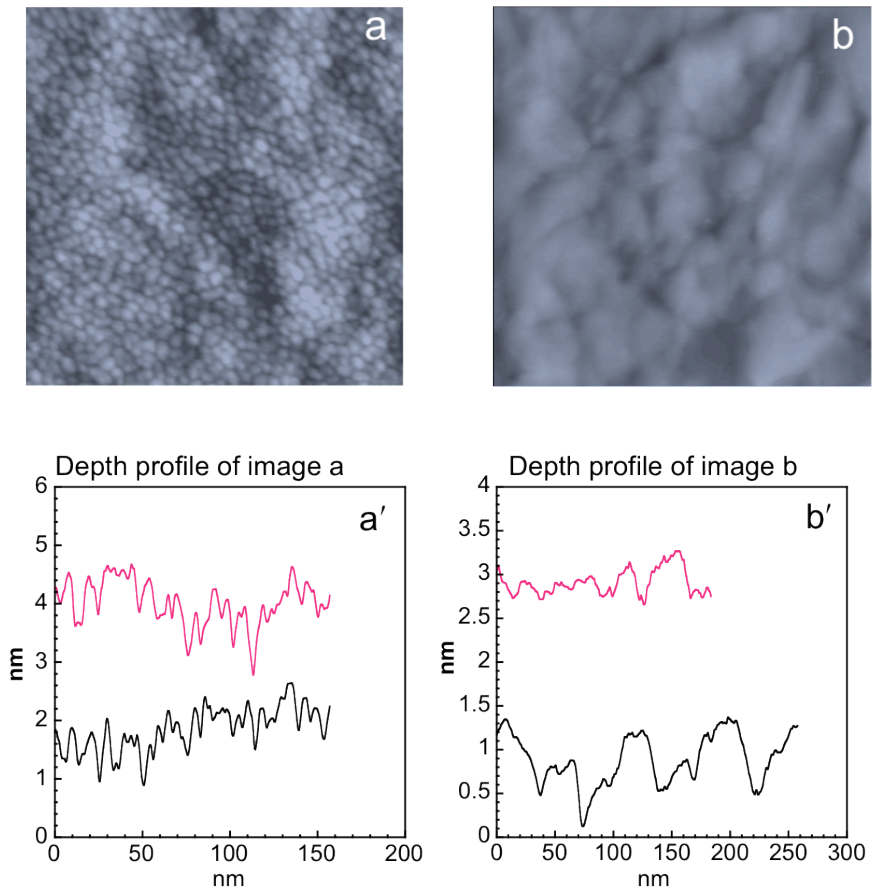

Figure 4.3 STM images of (a) PdPt(sp) and (b) Sn/PdPt(sp) electrodes. a′ and b′ are the depth profile of image a & b, respectively. The scan size is 200 × 200 nm. A tip bias voltage of typically 800 mV and a tunneling currents of 300 pA were used.

4.3.1.2 Nitrate Reduction

As usually observed for tin-modified noble metal electrodes [17, 20], nitrate reduction activity of Sn/PdPt(sp) was strongly dependent on the tin coverage. Figure 4.4 shows the θ_{Sn} dependence of the cyclic voltammograms of Sn/PdPt(sp, 31/69) in 0.1 M $HClO_4$ containing 0.01 M $NaNO_3$.

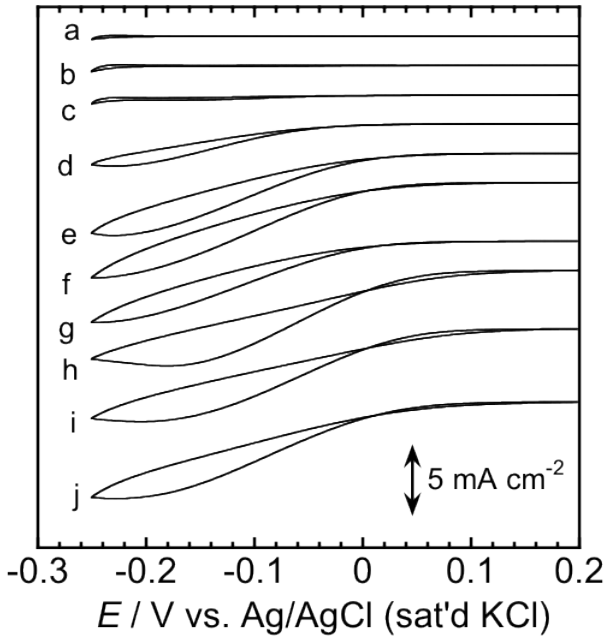

Figure 4.4 Cyclic voltammogarams for reduction of nitrate on Sn/PdPt electrodes in 0.01 M $NaNO_3$ + 0.1 M $HClO_4$. θ_{Sn}: (a) 0, (b) 0.21, (c) 0.31, (d) 0.40, (e) 0.52, (f) 0.60, (g) 0.72, (h) 0.86 and (i) 0.89 and (j) 0.98. The scan rate was 0.01 V s^{-1}. The surface composition of Pd/Pt was 31/69.

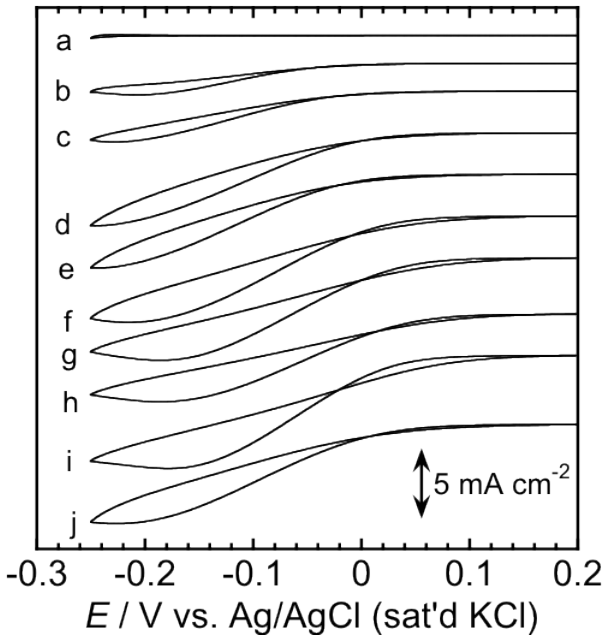

Figure 4.5 CVs for reduction of nitrate on Sn/PdPt electrodes in 0.01 M $NaNO_3$ + 0.1 M $HClO_4$. θ_{Sn}: (a) 0, (b) 0.37, (c) 0.52, (d) 0.59, (e) 0.63, (f) 0.69, (g) 0.79, (h) 0.84 and (i) 0.90 and (j) 1.0. The scan rate was 10 mV s^{-1}. The surface composition of Pd/Pt was 12/88.

All electrodes, Sn/PdPt(sp, 31/69) (Figure 4.4), Sn/PdPt(sp, 12/88) , (Figure 4.5) Sn/Pd (sp), and Sn/Pt(sp), showed the similar trend, or the reduction current was very low at low tin coverages, and gradually increased from θ_{Sn} = 0.3 – 0.4 to finally reach the maximum at θ_{Sn} = 0.8 – 0.9. [Figure 4.6] Such a θ_{Sn} dependence has been observed for Sn/Pd electrodes [17].

For Sn/Pt film quartz crystal electrodes, however, the current linearly increased with θ_{Sn}, and reached the maximum value at θ_{Sn} = 0.35 [15]. Therefore, the reduction activity seems to be dependent on the surface state of metal (the thickness of metal layers used in these studies were quite different). The maximum current densities for the Sn/PdPt(sp, 31/69 and 12/88) was higher than those of Sn/Pd(sp) and Sn/Pt(sp), showing the synergetic effect of Pd and Pt (Figure 4.6). The maximum current densities, 3.6 and 4.1 mA cm^{-2} for the Sn/Pd(sp) and Sn/Pt(sp) electrodes, respectively, were close to those in our previous reports using electrochemically deposited Pd [15] and Pt thin film electrode [16].

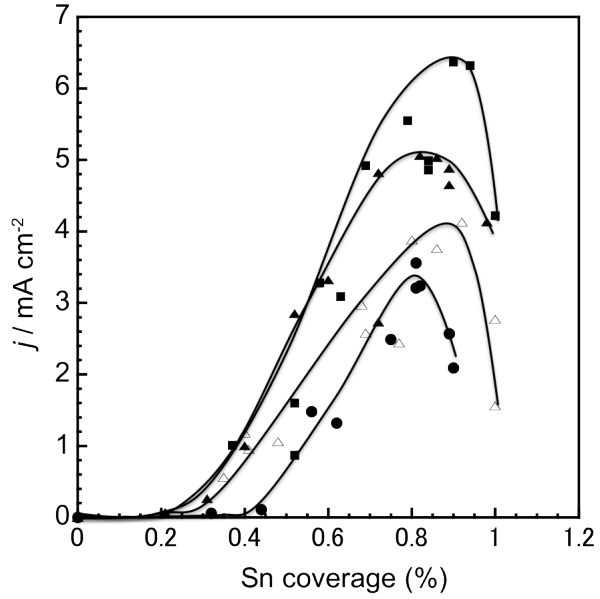

Figure 4.6 Tin coverage dependence nitrate reduction activity on Sn/Pd (solid circle), Sn/Pt (open triangle), Sn/PdPt (solid triangle, Pd/Pt = 31/69) and Sn/PdPt (solid square, Pd/Pt = 12/88).

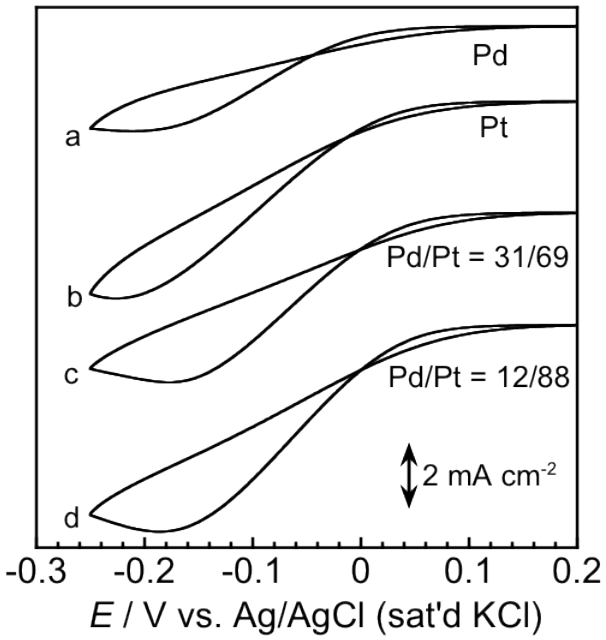

Figure 4.7 Reduction of nitrate in 0.01 M $NaNO_3$ + 0.1 M $HClO_4$ on Sn modified (a) Pd, (b) Pt, (c) PdPt (Pd/Pt = 31/69) and (d) PdPt (Pd/Pt = 12/88) electrodes. The Sn coverage was 0.80-0.82 and the scan rate was 0.01 V s^{-1}.

For the Sn/Pd electrodes, the value of the reduction current was sensitive to not only the tin coverage but also the Pd layer thickness and the surface electronic state [17]. As a result, the maximum current in the θ_{Sn}-dependence ranged from about 3 to 10 mA cm^{-2}. Among the previously reported maximum currents, 6.45 mA cm^{-2} for Sn/PdPt(sp, 12/88) is the second highest. Figure 4.8 shows the maximum current densities based on the real surface area as a function of the PdPt ratio. Again the higher reduction current was observed for Sn/PdPt(sp) electrodes than Sn/Pd(sp) and Sn/Pt(sp) electrodes. Therefore, the observed increase in the reduction current is not due to the difference in the surface area.

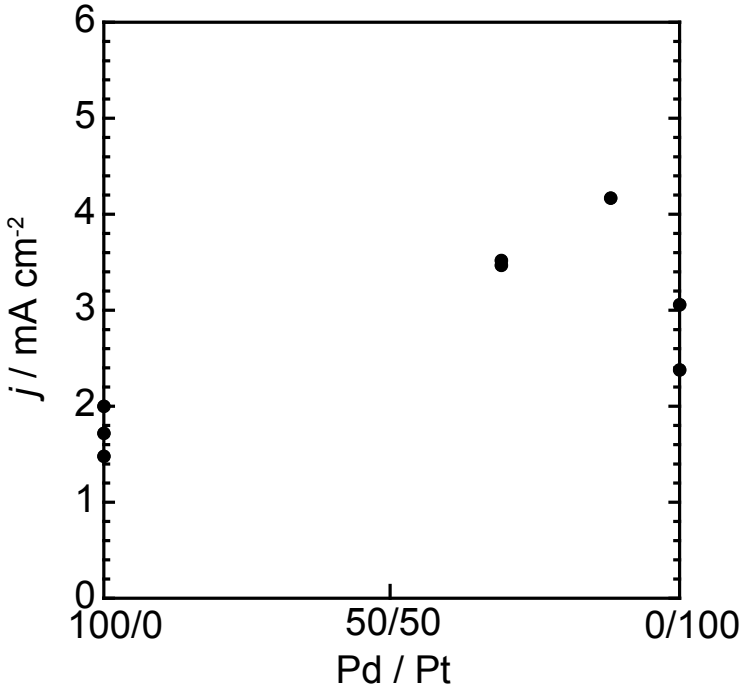

Figure 4.8 Composition dependence nitrate reduction activity on Sn modified PdPt eletrodes. The Sn coverage was 0.81-0.86. Reduction current was taken at -0.1V from the cyclic voltammograms in Figure 4.7.

The bulk electrolysis was conducted on Sn/PdPt(sp, 31/69) at –0.2 V for 5 hours in 0.1 M $HClO_4$. The θ_{Sn} was adjusted to 0.90 ± 0.01 where the maximum activity was obtained. In the time-course of nitrate reduction, the nitrite was initially formed, and decreased with time, showing a typical behavior of an intermediate product. The product distributions after 5 hour electrolysis on Sn/PdPt(sp, 31/69), Sn/Pd(sp), and Sn/Pt(sp) are summarized in Table 4.2 together with that expected for a physical mixture of Sn/Pd(sp) and Sn/Pt(sp) (Pd/Pt = 31/69). The main product on Sn/PdPt(sp, 31/69) was N_2 gas, and the product selectivity of 44% is very high among the reports for the noble metal-based electrodes. Both N_2 and N_2O were greater than those expected for the physical mixture. Therefore, the N-N bond formation was accelerated by the use of the PdPt alloy. The total hydrogenation ability of Sn/PdPt(sp, 31/69), exemplified by a sum of NH_3OH^+ and NH_4^+ production, decreased.

Table 4.2 Distribution of products for nitrate reduction at -0.2 V.

Electrode	Composition Pd/Pt	Sn coverage	Conversion (%)	Products (%)				
				NO_2^-	NH_3OH^+	NH_4^+	N_2O	N_2
Sn/Pt	0/100	0.85-0.91	25-46	25.12 ± 9.14	2.71 ± 1.46	32.86 ± 6.12	6.90 ± 4.77	32.41 ± 11.64
Sn/PdPt	31/69	0.89-0.91	52-64	4.71 ± 3.07	13.59 ± 5.14	12.74 ± 0.48	24.99 ± 2.78	43.97 ± 2.46
Sn/Pd	100/0	0.87-0.88	46-52	14.1 ± 4.6	10.6 ± 4.5	17.8 ± 5.1	29.0 ± 4.5	28.6 ± 7.9
Mixture)	31/69			21.70	5.16	28.18	13.74	31.22

Mixture: Calculate for physical mixture of Sn/Pd and Sn/Pt

To more quantitatively express these features, average number of cleaved N-O bonds, formed N-N bonds, and formed N-H(O-H) bonds per reduced nitrate has been calculated. The results are given in the Table 4.3.

Table 4.3 Average number of formed and cleaved bonds per reduced nitrate and the potential for the selectivity N2 production (P_{N2})

Electrode	Composition Pd/Pt	N-O	N-N	N-H	P_{N2}(%)
Sn/Pt	0/100	2.57	0.28	0.78	72
Sn/PdPt	31/69	2.72	0.41	0.46	86
Sn/Pd	100/0	2.57	0.36	0.55	80
Mixture	31/69	2.57	0.31	0.68	75

Data were taken from above table for calculation

The maximum number is 3 for the N-O bond (corresponding to the case that all N-O bonds of nitrate are cleaved), 0.5 for the N-N bond (corresponding to the case that N_2 is the only product), and 3 for the N-H(O-H) bond (corresponding to the case that only hydrogenated products such as NH_3OH^+ and NH_4^+ are produced). The number of the cleaved N-O bonds, $n_{N\text{-}O}$, is 2.72, which is greater than 2.57 for Sn/Pd(sp), Sn/Pt(sp), and their physical mixture (the same value for these electrodes), showing the enhancement of the cleavage of N-O bonds. Compared with values for Sn/Pd(sp), Sn/Pt(sp), and their

physical mixture, the number of N-N bond and N-H bond formation, n_{N-H} increased and decreased, respectively, (for example, the number of N-N bond formation, n_{N-N} of 0.41 is greater than 0.31 for the mixture, and the number of N-H bond formation of 0.46 is much smaller than 0.68 for the mixture), coinciding with the consideration based on the product selectivity. In the previous study, the following new parameter was also introduced to show the total ability of N_2 formation.

$$P_{N2}(\%) = 100 \times \left\{ n_{N-O}/3 + n_{N-N}/0.5 + \left(1 - n_{N-H}/3\right) \right\} / 3 \quad (1)$$

P_{N2} is referred to as the potential of the electrode for the selective N_2 production. This equation was derived on the basis of the fact that n_{N-O}, n_{N-N}, and n_{N-H} are 3.0, 0.5, and 0.0, respectively, when the harmless N_2 is the only product. Thus the P_{N2} becomes 100% when only N_2 is formed. The P_{N2} for Sn/PdPt(sp) was 86%, and was greater than those of Sn/Pt(sp) (72%), Sn/Pd(sp) (80%), and their physical mixture (75%). Therefore, the effect of alloying between Pd and Pt was clear on the product selectivity.

4.3.2 Deposited electrode

As described in the previous section, the PdPt(sp) electrodes showed the enhanced activity and product selectivity for the reduction of nitrate. This motivates us to examine electrodes of different Pd/Pt compositions. Although the surface composition is tunable by cycling the potential, only the PdPt electrodes whose surface composition is smaller than Pd/Pt = 31/69 can be prepared due to the preferential dissolution of Pd. In addition, no other target than Pd/Pt = 31/69 used in this study is commercially available. Therefore, an alternative method is required to prepare PdPt electrodes of small Pd/Pt ratios. The need for the alternative preparation method also became obvious during the infrared spectroscopic measurements to examine how the change in the electronic state of the surface by alloying affects the adsorption state of the reactant; the sputtered electrode did not show the sufficient enhancement of the infrared signal so that the adsorption species were hard to detect. For these reasons, electrochemical deposition was chosen to prepare the PdPt electrodes. Strictly speaking, however, the deposited electrode is not exactly the

same as the sputtered electrode. In this section, the characterization, and nitrate reduction activity including those for deposited Pt and Pd to compare with results for the PdPt(sp) electrodes has been briefly discussed. The deposited electrodes are described as Pt(dep), Pd(dep) and PdPt(dep) electrodes. For the electrodes, of which the surface composition was determined, a Pd/Pt ratio is also added in the parenthesis.

4. 3.2.1 Characterization

The typical cyclic voltammograms of Pt(dep) and Pd(dep) electrodes prepared under the conditions described in the previous section are shown in Figure 4.9 The deposition charges correspond to 11 Pd or 4 Pt layers, respectively, assuming the deposition efficiency is 100% although it was reported to be 0.64 for Pd prepared at 0.425 V in 1 mM $PdCl_2$ + 0.1 M $HClO_4$ [21]. The surface oxide reduction peaks appeared at 0.358 ± 0.005 and 0.446 ± 0.003 V for the Pd and Pt, respectively. The peak potential for Pt(dep) is almost the same as that for Pt(sp), while it is somewhat higher for Pd(dep) than that for Pd(sp). It seems to be due to the difference of the surface fine structure. The cyclic voltammogram of PdPt(dep) deposited from 1 mM $PdCl_2$ + 0.5 mM K_2PtCl_6 in 0.1 M $HClO_4$ is also shown in the same Figure. The single oxide reduction peak shows that Pd and Pt are mixed at an atomic level. Using a linear relationship between the peak potential and the surface composition, the Pd/Pt ratio was determined to be 35/65 for the case shown in Figure 4.9. The thickness calculated from the deposition charge and the surface Pd/Pt composition (assuming that the composition is the same between bulk and surface) was 10 layers. By changing the concentrations of noble metal complex solutions during the deposition, the PdPt films ranging from Pd/Pt = 0.35 to 0.85 were prepared.

The cyclic voltammogram of PdPt(dep, 35/65) in the so-called hydrogen region is shown in Figure 4.10 a. In addition to the main hydrogen wave at the same potential as for PdPt(sp, 31/69), the reduction current, which is characteristic of hydrogen absorption into a bulk Pd (Figure 4.10, 4.1 & 4.2), was also observed at below –0.05 V for a wide range of a Pd/Pt ratio and PdPt layer thickness (deposition amount).

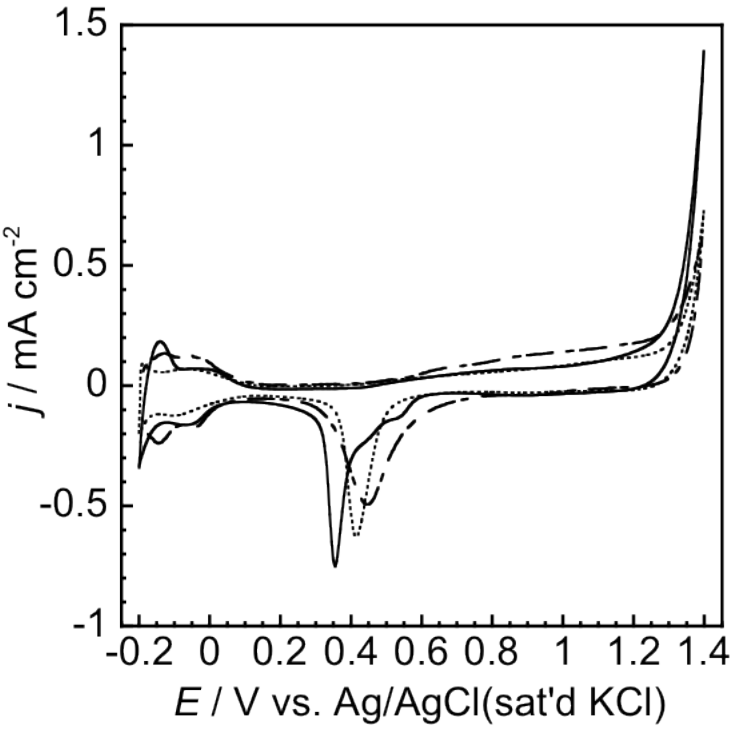

Figure 4.9 Cyclic voltammogram Pd (solid line) , Pt (dash line) and PdPt (dot line) in 0.1 M $HClO_4$. Scan rate: 0.05 V s^{-1}. The surface composition of Pd/Pt was 35/65.

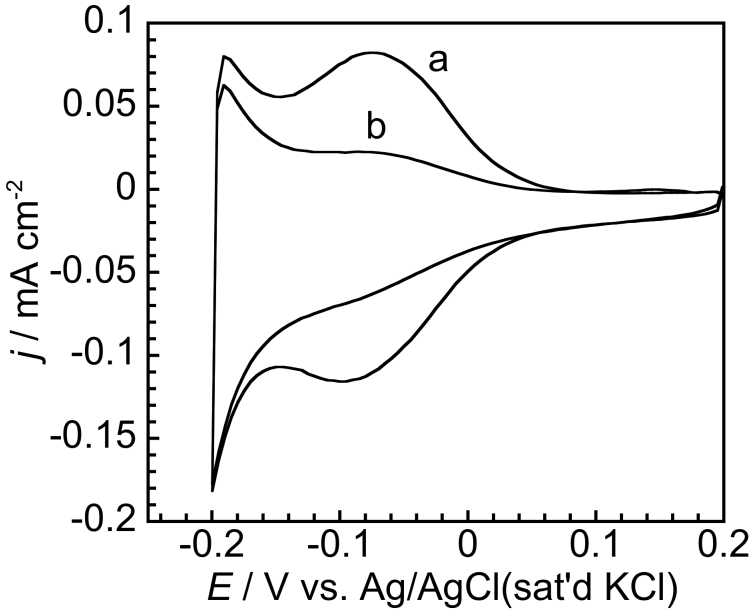

Figure 4.10 Cyclic voltammograms of PdPt (a) before and (b) after the immersion in a 0.1 M $HClO_4$ solution containing 0.05 mM $SnCl_2$ for 360s. The scan rate was 0.05 V s^{-1}. The surface Pd/Pt composition was 35/65 and the θ_{Sn} was 0.67.

Such characteristic can be more quantitatively expressed using the current ratio at –0.2 V and the peak potential (around –0.1 V). The ratio increased with the Pd/Pt ratio (Figure 4.11 e), but was almost independent of the PdPt layer thickness unless the layer was very thin (Figure 4.11 d)

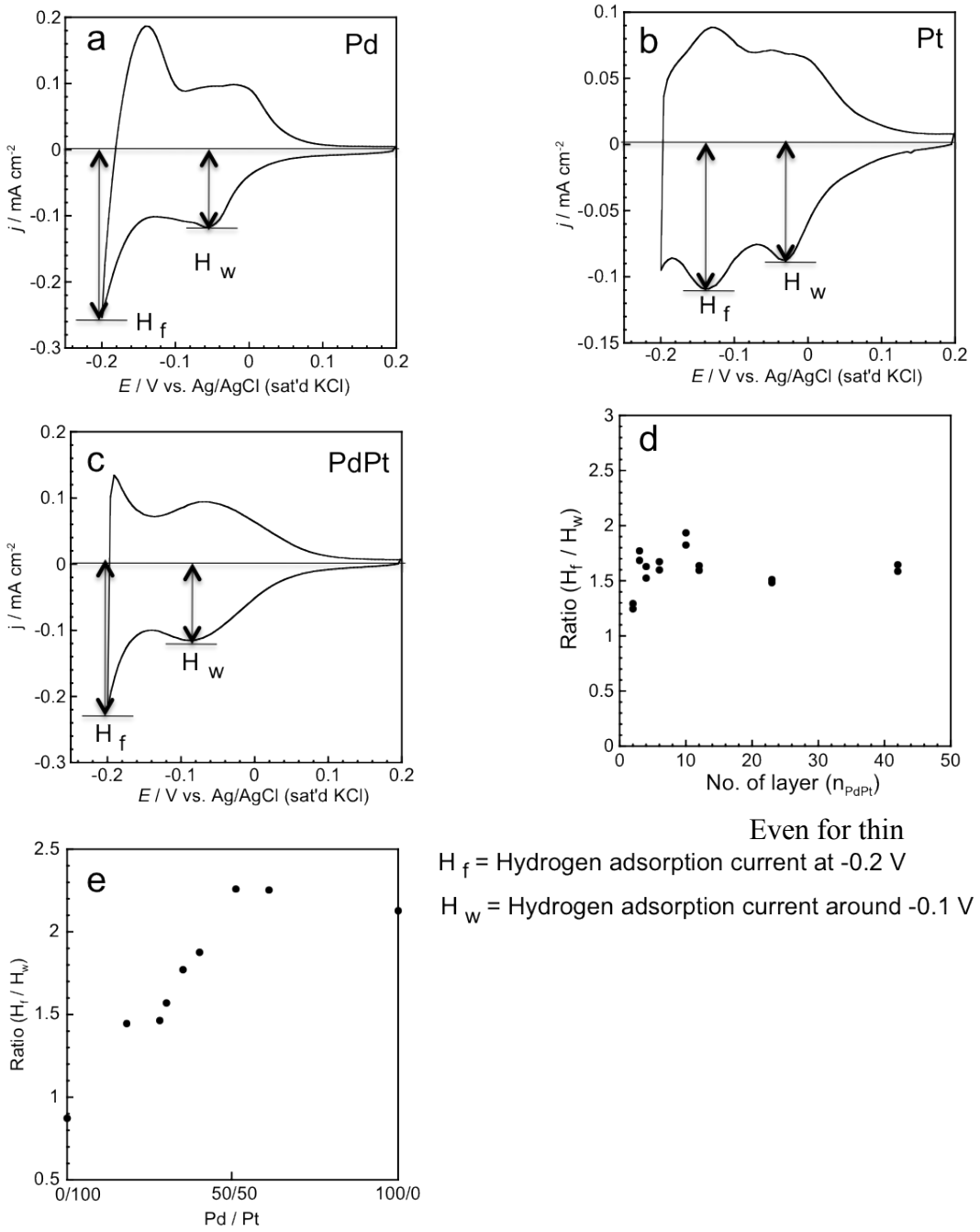

Even for thin

H_f = Hydrogen adsorption current at -0.2 V

H_w = Hydrogen adsorption current around -0.1 V

Figure 4.11 Cyclic voltammograms of Pd (dep), Pt (dep) and PdPt(dep, Pd/Pt = 31/69) in 0.1 M $HClO_4$ at a scan rate of 0.05 V s^{-1}. (d) Thickness dependence hydrogen adsorption behavior (Pd/Pt = 30/70) and (e) and composition dependence adsorption behavior of PdPt(dep) electrodes.

PdPt(dep, 40/60) electrodes of two layer thickness, however, the current ratio was about 1.2, and was still greater than 0.7 – 0.9 for Pt(sp) and Pt(dep). The ratio for the PdPt(dep, 30/70) electrode (1.6) is greater than that for the PdPt(sp, 31/69) electrode (1.0). Therefore, the codeposited PdPt electrodes leave the characteristic of a pure Pd.

The Sn adsorption was performed according to the aforementioned procedures. Figure 4.10 b shows the cyclic voltammogram in a hydrogen region for Sn/PdPt(dep, 40/60). As the case of the Sn/PdPt(sp) electrodes, hydrogen adsorption was greatly suppressed by the adsorption of tin, while the reduction current due to the hydrogen absorption was not. Particularly the currents at –0.2 V were the same before and after adsorption of tin. This has never been observed for Sn-modified PdPt(sp) electrodes (the current at –0.2 V after the tin adsorption was 75% of that before the adsorption). This observation also suggests that the Sn/PdPt(dep) electrodes retain the Pd characteristic more than Sn/PdPt(sp). As a result of this phenomenon, the tin coverage determined on the basis of the charges in the hydrogen region is underestimated particularly for a low tin coverage region. By immersing the electrode for more than 10 min, however, the tin coverage reached 1.0 (100%) (Figure 4.12).

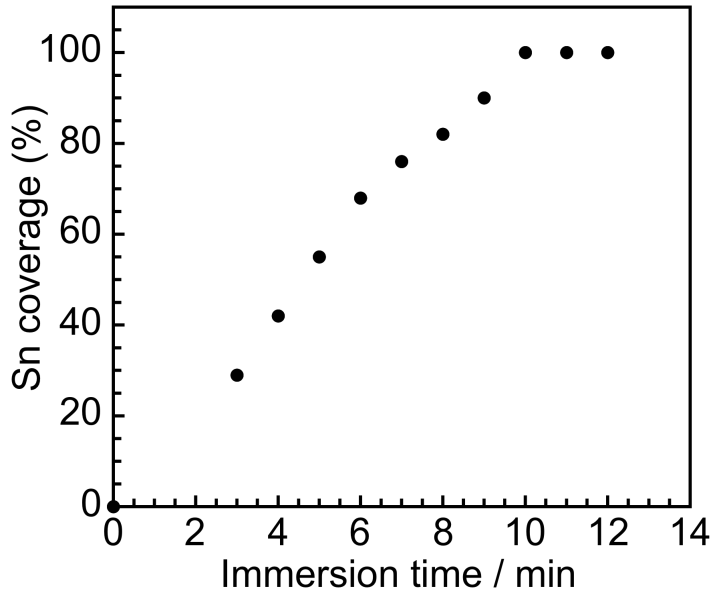

Figure 4.12 Immertion time dependence Sn coverage on PdPt electrodes. The surface composition of Pd/Pt was 35-40/65-60.

Table 4.4 is a list of the binding energies of XP Pd $3d_{3/2}$ and Pt $4d_{7/2}$ peaks for Pd(dep), Pt(dep) and PdPt(dep, 40-52/60-48) before and after the tin adsorption. They coincides with those reported for zero-valent Pd, zero-valent Pt and/or divalent Sn. The peak intensity of Pd and Pt became weaker after the modification by Sn. All binding energies were lower by 0.03 – 0.3 eV than the corresponding binding energies for the sputtered electrodes, showing that Pd and Pt are somewhat negatively charged compared with the sputtered electrodes. These results indicate the surface electronic state is very close to each other between the sputtered and deposited electrodes, but is not exactly the same.

Table 4.4 Binding energy of $Pd3d_{3/2}$, $Pt4f_{7/2}$ and $Sn3d_{3/2}$ in Pd, PdPt, Pt (dep) electrodes and their Sn modified derivatives.

	Binding energy / eV		
Electrode	$Pd3d_{3/2}$	$Pt4f_{7/2}$	$Sn3d_{5/2}$
Pd	340.47 ± 0.04		
PdPt	340.49 ± 0.03	71.08 ± 0.02	
Pt		71.15 ± 0.06	
Sn/Pd	340.44 ± 0.05		486.31 ± 0.14
Sn/PdPt	340.47 ± 0.10	71.07 ± 0.05	486.38 ± 0.20
Sn/Pt		71.14 ± 0.07	486.32 ± 0.22

Sn coverages were fixed in the range of 0.78-0.90 for Sn/Pd (dep), 0.80-0.95 for Sn/PdPt (dep) and 0.47-0.86 for Sn/Pt (dep). The Pd/Pt ratios were 32/68 and 40-52/60-48 for Sn modified and unmodified PdPt (dep) electrodes.

The STM image of the PdPt (dep) electrode shows that PdPt deposits apparently form relatively large-scale islands (diameter: 50 nm) (Figure 4.13). However, a close-up view shows that the islands consist of smaller particles (diameter: about 6 nm). The structure of such small particles almost disappeared by the tin adsorption to make the surface of the island smoother. Because it is considered that the secondary structure of this size (large-scale islands) does not affect the electrochemical reaction much, the surface structure is almost the same between the sputtered and deposited electrodes.

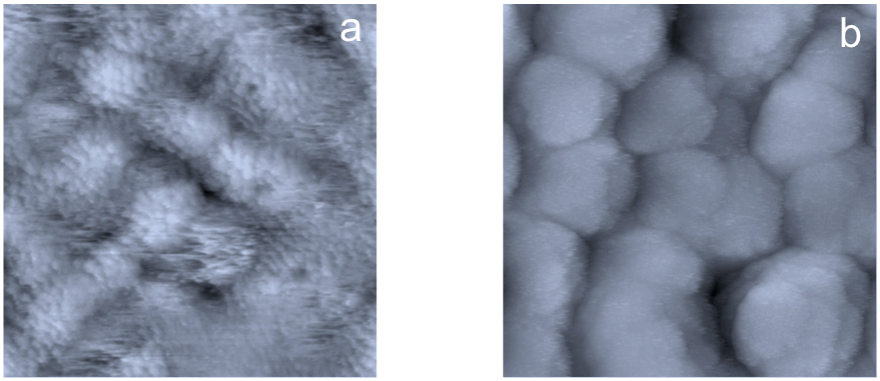

Figure 4.13 STM images of (a) PdPt and (b) Sn/PdPt electrodes. The scan size was 200 × 200 nm. A tip bias voltage of typically 800 mV and a tunneling current of 300 pA were used.

4.3.2.2 Nitrate reduction

Sn/PdPt(dep) electrodes show a similar tin coverage dependence of the electrocatalytic activity for the reduction of nitrate to that for the sputtered electrodes (Figure 4.14 & 4.15). Data were considerably scattered and thereby shown using an error bar. The maximum activity of the Sn/PdPt(dep, 35-40/65-60) obtained at θ_{Sn} = 0.85 was 4.5 mA cm^{-2} is almost the same as Sn/PdPt(sp, 31/69).

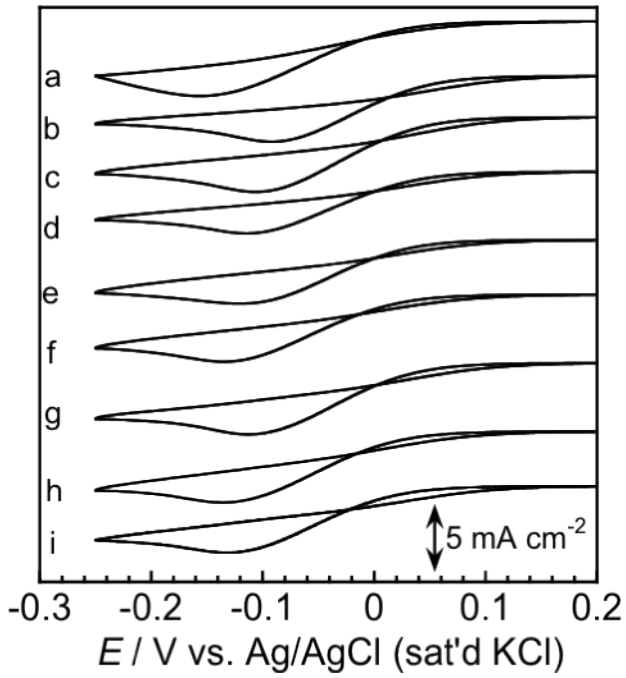

Figure 4.14 CVs for reduction of nitrate on Sn/PdPt electrodes in 0.01 M $NaNO_3$ + 0.1 M $HClO_4$. Surface compsition (Pd/Pt): (a) 0, (b) 18/82 (c) 28/72, (d) 30/70, (e) 35/65, (f) 40/60, (g) 51/49 (h) 61/39 and (i) 100/0. The Sn coverage was 0.80-0.90 and the scan rate was 0.01 V s^{-1}.

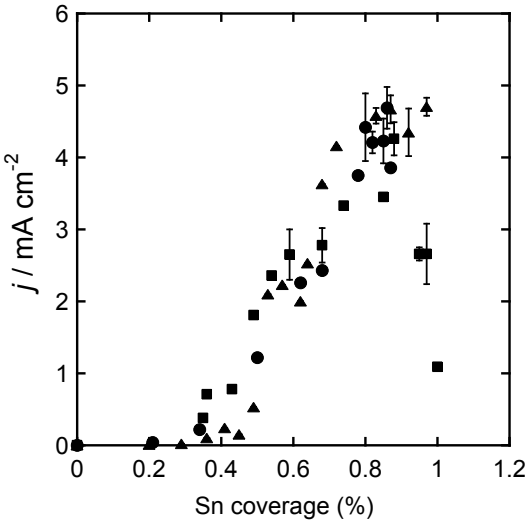

Figure 4.15 Tin coverage dependence nitrate reduction activity on Sn/Pd (circle), Sn/Pt (square), Sn/PdPt (triangle). The surface composition of Pd/Pt was fixed in the range of 35-40/65-70.

The Sn/Pt(dep) showed greater activity than Sn/Pt(sp). To examine the allying effect in more detail, the maximum activities on the basis of real surface area at –0.1 V and –0.05 V are plotted vs. Pd/Pt ratio (Figure 4.16), in which the θ_{Sn} was fixed in the range of 0.80 to 0.91 where the maximum activity was obtained. Data between Pd/Pt = 50/50 and 20/80 exist above a straight line connecting pure Pd and Pt, being indicative of synergy effect, although the effect is smaller compared with the sputtered electrode. No enhancement was observed for the electrodes with the Pd/Pt ratio below 50/50, for the preparation of which the sputtering method was not applicable.

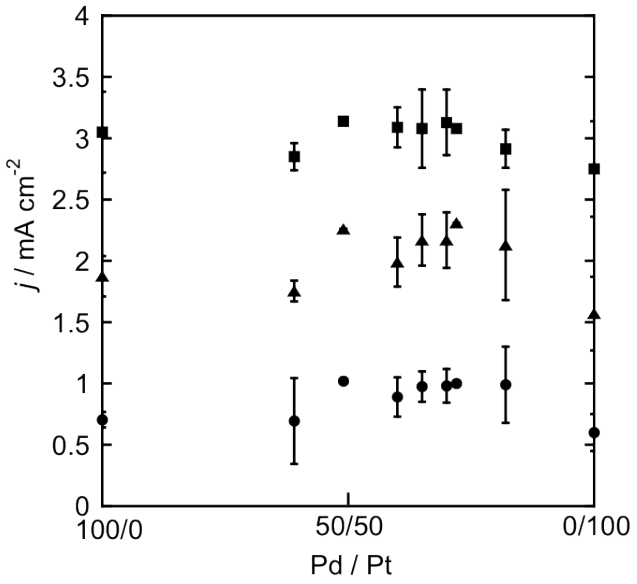

Figure 4.16 Composition dependence reduction current of Sn modified PdPt (dep) electrodes. The reduction current was measured from the cyclic voltammogram in 0.01 $NaNO_3$ + 0.1 M $HClO_4$ at 0.0 V (circle), -0.05 V (triangle) and -0.1V (square). Sn coverage was 0.80-0.91.

The product distribution for the reduction of nitrate on Sn/PdPt(dep, 41-49/59-51) is shown in Table 4.5.

Table 4.5 (a) Reduction products distribution on Sn modified Pt, PdPt and Pd (dep)

Electrode	Composition Pd/Pt	Sn coverage	Conversion (%)	Products (%)				
				NO_2^-	NH_3OH^+	NH_4^+	N_2O	N_2
Sn/Pt)[1]	0/100	0.4	12-17	10	46	11	7	26
Sn/PdPt	41-49/59-51	0.75-0.76	55	11	5	33	28	23
Sn/Pd)[2]	100/0	0.8-0.85	54	1	19	0	80	0
*Mixure	40/60			6	35	7	36	16

1) Piao et al. J. Electroanal. Chem. 629 (2009) 110.
2) K. Shimazu et al. J. Electroanal. Chem. 601 (2007) 161.
*Mixture) Calculated for the physical mixture of Sn/Pd and Sn/Pt

Table 4.5 (b) Reduction products distribution on Sn modified Pt, PdPt and Pd (dep)

Electrode	Composition Pd/Pt	N-O	N-N	N-H	P_{N2} (%)
Sn/Pt)[1]	0/100	2.45	0.44	0.32	87
Sn/PdPt	41-49/59-51	2.64	0.34	0.75	77
Sn/Pd)[2]	100/0	2.44	0.44	1.29	63
*Mixure	40/60	2.45	0.34	0.83	74

All values are calculated using the data shown in above table

The main product was NH_4^+, its selectivity (33%) was greater than that for Sn/PdPt(sp) (13%). Compared with that for Sn/PdPt(sp), NH_4^+ formation increased, while the N_2 decreased. Because the total selectivity of NH_3^+OH and NH_4^+ (38%) is greater than 26% for Sn/PdPt(sp), the hydrogenation ability of Sn/PdPt(dep) is stronger than that of Sn/PdPt(sp). On the contrary, the N-N bond formation was decelerated as shown by the decreased total formation of N_2O and N_2 (51%) compared with 69% for Sn/PdPt(sp). Because the product distribution is very sensitive to various factors, it is

hard to identify the origin for the difference in the product distribution between the sputtered and deposited electrodes. However, the characteristic observed for Sn/PdPt(sp) in the change in the product distribution by alloying, or the decrease in the hydrogenation ability and the increase in the N-N bond formation, was impaired by preparing the PdPt electrode using a deposition method.

4.3.3 Adsorbed species on the electrodes

Because the enhanced signal was not obtained for the sputtered electrodes, IR spectra of the adsorbed species were measured only for the deposited electrodes. As described in the previous section, however, a fundamental trend in the effect of alloying on the surface structure and the electrocatalytic properties is the same between both electrodes, although the effect was weaker for the deposited electrodes.

Figure 4.17 shows IR spectra at 0.3 V for the PdPt(dep) electrodes of various surface Pd/Pt compositions together with those for the Pd(dep) and Pt(dep) electrodes.

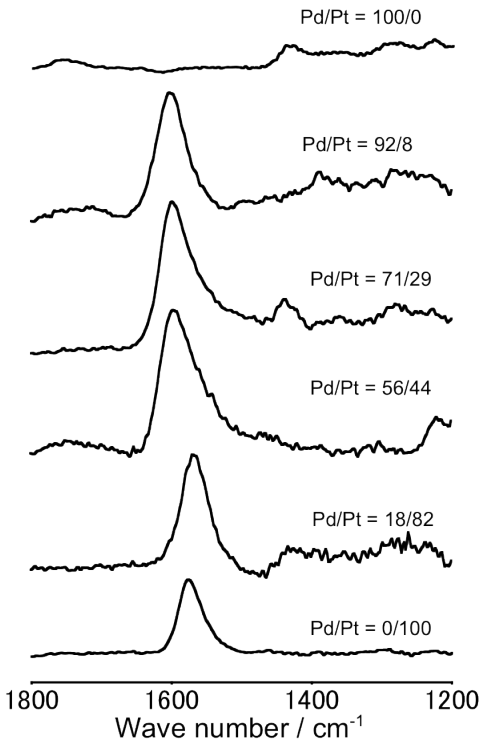

Figure 4.17 Composition dependence of N=O stretching bidentate nitrate adsorption on PdPt (dep) electrodes.

In these spectra, the band intensity was normalized to the same because the signal enhancement varied from electrode to electrode. Therefore, the change in the intensity with the surface Pd/Pt composition cannot be discussed. For the Pt electrode, a single band was observed at 1574 cm^{-1}, which is very close to previously reported 1572 cm^{-1} [34]. This band was assigned to the N=O stretching band of the bidentate nitrate adsorbed on the Pt surface [34]. For the PdPt(dep) electrodes, single band was observed. However, the bandwidth was always greater than that of Pt. The bandwidth increased with the increasing surface Pd/Pt composition and started decreasing after the maximum at Pd/Pt = 56/44.

These results may suggest that the observed band consists of the components due to the bidentates adsorbed on different adsorption sites such as PdPd, PdPt, and PtPt, or that the exchange between these bidentates is fast so that the observed band is the average of the N=O stretching modes of the bidentate nitrates. The band position was plotted versus the surface Pd/Pt composition in Figure 4.18. At low Pd/Pt ratios, it was lower and close to that for the Pt(dep) electrode, while it was about 1600 cm^{-1} at high Pd/Pt ratios. Although the band position looks jumped at the middle Pd/Pt ratio, it is hard to conclude so because data was rather scattering. In this study, therefore, it is only concluded that the band position shifted to the higher wave number (1601 cm^{-1} for Pd/Pt(dep, 92/8)) at high Pd/Pt ratios compared with 1574 cm^{-1} for the Pt electrode. Although the band position is also influenced by the surface coverage of the nitrate, the shift (ca. 10 cm^{-1} for the Pt electrode) was not so large. Therefore, the observed positive shift in the bidentate band reflects a real trend in the change in the adsorption state. The positive shift means the stronger N=O bond with more positive charge on N atom of the adsorbed nitrate, leading to weaken the metal-nitrate bonds. Consequently, the reduction of nitrate was more accelerated compared to the Pt electrode. On the other hand, no band was observed for the Pd electrode, showing that the adsorbed species are not IR active. Taking into account the surface selection rule, it is thought that the nitrate exists in a tridentate mode on the Pd surface, which is parallel to the surface.

On the tin-modified electrodes, the bidentate band was also observed even at the high Sn coverage, although the band intensity was weaker than those for unmodified electrodes, reflecting the higher electrocatalytic activity. The band position was again somewhat scattered, but it has a trend to show higher wavenumbers compared with unmodified PdPt electrodes. Such a shit was also observed for a Pt electrode. The positive shift means that the N=O bond is strengthened by Sn modification as the alloying of Pt with Pd.

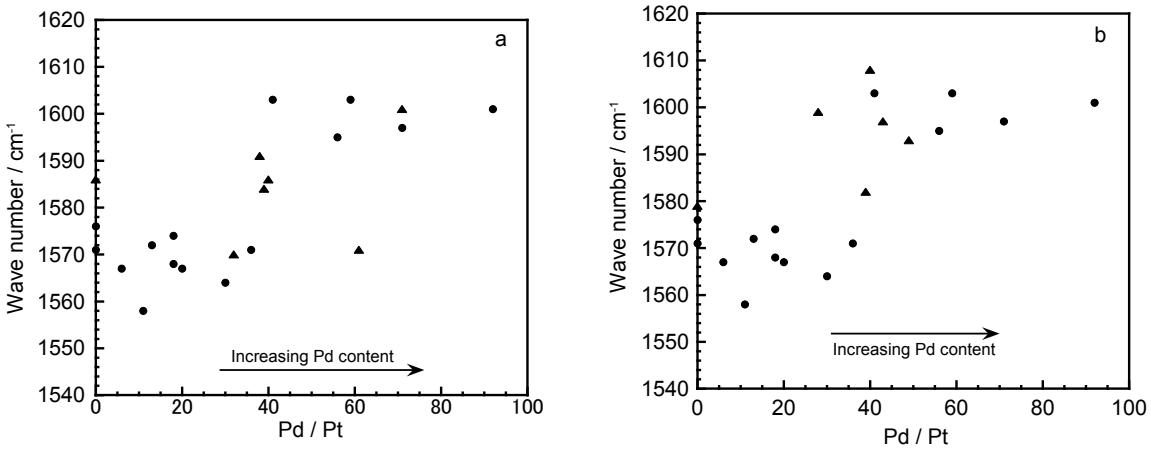

Figure 4.18 Compostion dependent band positions for the adsorbed species of N=O stretching of bidentate NO_3^- on PdPt (dep) electrodes before (circle) and after (triangle) adsorption of Sn. Tin coverage was (a) θ_{Sn} = 0.11-0.19 and (b) θ_{Sn} = 0.57-0.62.

4.3.4 Pretreatment effect of Sn/PdPt(sp) on nitrate reduction

In order to get the information about the effect of the electronic structure on the electrocatalytic activity for nitrate reduction, the pretreatment effect was investigated for Sn/PdPt electrode. Figure 4.19(A) shows the CVs for hydrogen wave for PdPt and Sn/PdPt electrodes before and after pretreatment. The electrode was pretreated at -0.35 V for 60 s. The hydrogen wave remained almost unchanged by the pretreatment. The same results were obtained for Sn/Pt electrode. Whereas the hydrogen wave for Sn/Pd electrode was entirely disappeared by the pretreatment. The electrocatalytic activity for Sn/PdPt electrode towards nitrate reduction was enhanced by the pretreatment (Figure

4.19 B). However, the enhancement current was very smaller than that of Sn/Pt and Sn/Pd electrodes. The binding energies of Sn 3d5/2 and 3d3/2 for Sn/PdPt electrodes

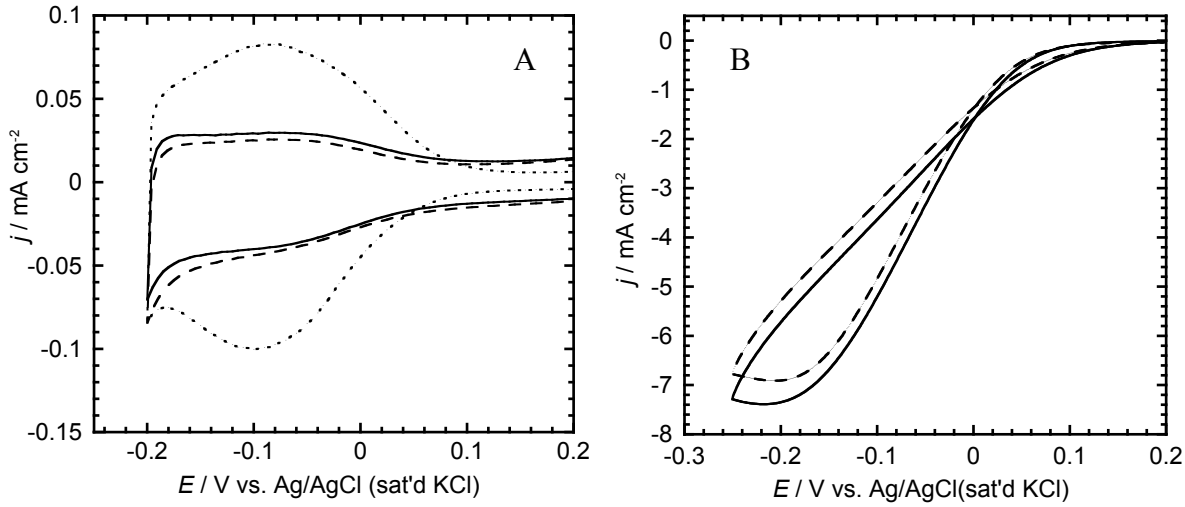

Figure 4.19 (A) Cyclic voltammograms of (dotted curve) PdPt, (dashed curve) as-prepared Sn/Pt, and (solid curve) pretreated Sn/Pt electrodes in 0.1 M $HClO_4$ at a scan rate of 0.05 V s^{-1}. Tin coverage was 0.87. (B) CVs of (dashed curve) as-prepared Sn/PdPt and (solid curve) pretreated Sn/PdPt electrodes in 0.01 M $NaNO_3$ + 0.1 M $HClO_4$ at a scan rate of 0.01 V s^{-1}. The electrochemical pretreatment was conducted at -0.35 V for 60s. The surface composition of Pd/Pt was 31/69.

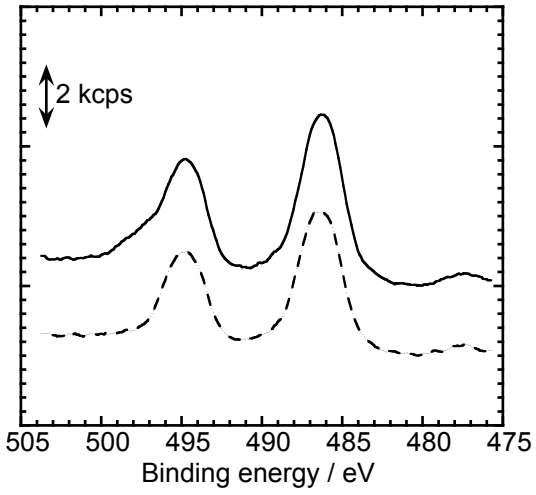

Figure 4.20 XP spectra of Sn3d of (dash curve) as-prepared Sn/PdPt and (solid curve) pretreated Sn/PdPt electrodes. Sn coverage before pretreatment was 0.87. The Sn/PdPt electrode was pretreated at -0.35 V for 60s. The surface composition of Pd/Pt was 31/69.

were 486.33 and 494.83 eV, respectively, (Figure 4.20), which are assigned to divalent tin as reported previously [16]. These binding energies remained unchanged by the pretreatment. On the other hand, as like for Sn/Pd surface, there is no shoulder appeared by the pretratment. These results proposition that the interaction between Sn and PdPt alloy is weaker than that of Sn/Pd. Therefore the effect of pretreatment on the electrocatalytic properties of Sn/PdPt is insignificant.

4. 4 Origin of the enhancement of the electrocatalytic properties

In various noble metal alloy systems, it was demonstrated that the *d*-band center with respect to Fermi level was a dominating factor to control the adsorption energy and thereby the reaction facility. The up-shift of the *d*-band center causes a stronger interaction of the *d*-band with antibonding orbital of the adsorbate such as CO, NO, O_2 etc., while the down-shift does a weaker interaction. Actually a linear relation between the adsorption energy and the shift of *d*-band center was reported for CO and O_2 adsorption on alloy electrodes. As usually observed for heterogeneous catalytic reactions, moderate adsorption would lead to the high reaction rate. Actually, a volcano-type relation was reported between the rate of electrochemical reduction of molecular oxygen and *d*-band center.

It is considered that this interpretation can be applicable for the nitrate adsorption and its reduction. Ruban et al. conducted density functional calculations and estimated shifts in *d*-band centers of surface impurities and overlayers. The overlayers showed insignificant shift, whereas the impurities, or isolated and/or small amount of atoms in the matrix of different metals, showed a visible *d*-band shift. For the combination of noble metals used in this chapter, the Pd *d*-band center shifted downward by -0.17 eV in Pd-Pt alloy, while the Pt *d*-band center shifted upward by 0.19 eV in Pd-Pt alloy. Therefore, a weaker interaction (adsorption) with adsorbate (nitrate) is expected for Pd in a PdPt alloy.

For Pt, on the other hand, a stronger interaction is expected. The positive shift of the bidentate band for Pt by alloying, or stronger N=O bond is consistent with this prediction. The nitrate reduction was conducted using Sn-modified electrodes. Therefore, the effect of Sn on the *d*-band center should be taken into account when considering the electrocatalytic properties of the alloy electrodes. As reported in a previous paper, alloying of Pd and Ni with the electropositive metal moves the *d*-band center faraway from Fermi level (down-shift). And our previous data (loss of the hydrogen adsorption ability by alloying) also supported this shift. The electronegativity of Pt is also greater than that of tin. Therefore, the same effect is expected for Pt. Based on this predicted trend, it is reasonably considered that *d*-band center for Pd would further shift downward by Sn-modification. On the other hand, the up-shifted *d*-band center for Pt would shift upward by Sn-modification, meaning that the Sn modification counteracts alloying with Pd to finally cancel the latter effect. Based on this consideration, the enhanced properties of Sn/PdPt electrodes would be mainly due to the *d*-band shift for Pd by both alloying with Pt and Sn-modification. As observed for electrochemically pretreated Sn/Pd electrode, the down-shift caused the accelerated activity for the nitrate reduction probably via weaker adsorption of nitrate. Thus, it is concluded that the *d*-band shift amplified by the alloying with Pt results in the acceleration of the reaction rate. The *d*-band down-shift also tends to decrease the hydrogen adsorption ability, resulting in the decrease in the formation of the hydrogenated products. It follows that the adsorbed intermediate has a greater chance to bind each other to form N-N bonds.

It is easy to understand from more organic chemistry viepoint that the positive charge of N increased by the interaction with Sn. In addition, the interaction between Sn and N causes the bent form of NO_3 plane to the surface. The approach of N to the surface and the increased positive charge on N in nitrate may assist the electron transfer. The Sn coverage dependence of the band position for the PdPt electrodes did not show a clear relationship because the shift by Sn modification is smaller than that caused by alloying.

4.5 Conclusions

The Sn-modified PdPt electrodes (Sn/PdPt), prepared by the sputtering of PdPt followed by the spontaneous adsorption of tin, showed higher electrocatalqytic activity for the reduction of nitrate, enhanced N_2 production, and suppressed NH_3OH^+ and NH_4^+ formation compared with the similarly prepared Sn/Pd and Sn/Pt electrodes, or that expected for a simple mixture of Sn/Pd and Sn/Pt electrodes. These results showed that the strong hydrogenation ability of Sn/Pt to produce NH_3OH^+ and NH_4^+ and the relatively weak N-O bond cleavage ability of Sn/Pd to produce N_2O rather than N_2 were harmonized by the formation of the PdPt alloy.

When the Sn/PdPt electrodes were prepared by the electrochemical deposition of PdPt and the adsorption of tin, similar effects were observed but the magnitude of the enhance was smaller. Distinct differences were neither observed for the binding energies of Pd, Pt and Sn in X-ray photoelectron spectra, nor the PdPt particle size between the electrodes prepared by the sputtering and deposition methods. The surface enhanced infrared spectroscopic (SEIRAS) measurements were performed for the deposited electrodes, because no significant signal enhancement was obtained for the sputtered electrodes. The SEIRA spectra showed a single band assigned to the bidendate mode of adsorbed nitrate. This band shifted to high wavenumbers with the increase of the surface fraction of Pd and by the Sn modification. This positive shift is indicative of the stronger N=O bond with more positive charge on N atom of the adsorbed nitrate. The change in the adsorption strength was interpreted based on the *d*-band center shift. The predicted d-band shift by Sn modification shows that the enhanced activity of Sn/PdPt electrodes is due to further downshift of *d*-band center for Pd.

4.6 References

[1] S. Horold, T. Tacke, K.D. Vorlop, Environ. Technol. 14 (1993) 931.

[2] A. Pintar, J. Batista, J. Levec, T. Jajiuchi, Appl. Catal. B. 11 (1996) 81.

[3] J. Warna, I. Turunen, T. Salmi, T. Maunula, Chem. Eng. Sci. 49 (1994) 5763.

[4] G. Strukul, R. Gawagnin, F. Pinna, E. Modoferri, S. Perathoner, G. Centi, Marella, M. Tomaselli, Catal. Today 55 (2000) 139.

[5] F. Deganello, L.F. Liotta, A. Macaluso, A.M. Venezia, G. Deganello, Appl. Catal. B 24 (2000) 265.

[6] U. Prusse, M. Hahnlein, J. Daum, K.D. Vorlop, Catal Today 55 (2000) 79.

[7] U. Prusse, J. Daum, C. Bock, K.-D. Vorlop, in: A. Corma et al. (Eds), Studies in Surface Science and Catalysis., Vol. 130 Elsevier, Amsterdam, 2000, p. 2237.

[8] G. Horanyi, E.M. Rizmayer, J. Electroanal. Chem. 188 (1985) 265.

[9] O.A. Petrii, T.Y. Safonova, J. Electroanal. Chem. 331 (1992) 892.

[10] A.C.A. de Vooys, R.A. van Santen, J.A.R. van Veen, J. Mol. Catal. A 154 (2000) 203.

[11] E. Epron, F. Gauthard, C. Pineda, J. Barbier, J. Catal. 198 (2001) 309.

[12] K. Nishimura, K. Machida, M. Enyo, Electrochim. Acta 36 (1991) 877.

[13] J.F.E. Gootzen, P.G.J.M. Peters, J.M.B. Dukers, L.Lefferts, W. Visscher, J.A.R. Van Veen, J. Electroanal. Chem. 434 (1997) 171.

[14] S. Wasmus, E.J. Vasini, M.Krausa, H.T. Mishima, W. Wielstich, Electrochim. Acta 39 (1994) 23.

[15] K. Shimazu, R. Goto, K. Tada, Chem.Lett. (2002) 204.

[16] K. Tada, K. Shimazu, J. Electroanal. Chem. 577 (2005) 303.

[17] K. Shimazu, R. Goto, S. Piao, R. Kayama, K. Nakata, Y. Yoshinaga, J. Electroanal. Chem. 601 (2007) 161.

[18] K. Tada, T. Kawaguchi, K. Shimazu, J. Electroanal. Chem. 572 (2004) 93-99.

[19] K. Shimazu, T. Kawaguchi, K. Tada, J. Electroanl. Chem. 529 (2002) 20-27.

[20] S. Piao, Y. Kayama, Y. Nakano, K. Nakata, Y. Yoshinaga, K. Shimazu, J. Electroanal. Chem. 629 (2009) 110.

[21] J. S. Garcia, E.A. Ticianelli, V. Climent, J.M. Feliu, Electrochim. Acta 54 (2009) 2094.

[22] H.A. Angerstein-Kozolowska, B.E. Conway, A. Homelin, L. Stoicoviciu, J. Electroanal. Chem. 228 (1987) 429.

[23] A. Capon, R. Parsons, J. Electroanal. Chem. 65 (1975) 285.

[24] D. A. Rand, R. Woods, J. Electroanal. Chem. 36 (1972) 57.

[25] B. G. Baker, D. A. Rand, R. Woods, J. Electroanal. Chem. 97 (1979) 189.

[26] K. Nakata, Y. Doi, S. Kubota, K. Shimazu, J. Electroanal. Chem. 647 (2010) 187.

[27] J.L. Shu, K. Otto, Appl. Surf. Sci., 32 (1988) 246

[28] C. D. Wagner, A. V. Naumkin, A. Kraut-Vass, C. J. Powell, J. R. Rumble, NIST X-ray Photoelectron Spectroscopy Database 20 (web edition), vers. 3.1.

[29] V. Rosca, M. Duca, M. T. de Groot, N. T. M. Koper, Chem. Rev., 109 (2009) 2209.

[30] M.U. Haque, M. Tariq, J. Chem. Soc. Pak., 32(2010)396.

[31] H. Miyake, S. Ye, M. Osawa, Electrochem. Commun. 4(2002)973.

[32] F.R. Rima, K. Nakata, K. Shimazu, M. Osawa, J. Phys.Chem. C 114 (2010) 6011.

[33] Osawa, M. Bull. Chem. Soc. Jpn. 70 (1997) 2861.

[34] K. Nakata, Y. Kayama, K. Shimazu, A. Yamakata, S.Ye, M. Osawas, Langmuir, 24 (2008) 4358.

[35] K. NakataY. Kayama, A. Okubo, A. Yamakata, S.Ye, M. Osawas, Langmuir, 24 (2008) 4352.

Chapter 5

Electrocatalyst of Tin-Modified Platinum Rhodium Alloy for Nitrate Reduction

5.1 Objective

Development of the efficient denitrification technology is one of most urgent environmental issues because the contamination of hydrosphere, particularly ground water and river, with nitrate becomes significant; for example, nitrate concentration in many wells exceeds admissible levels set by WHO, USA and Japan. As previously described, electrochemical denitrification is considered to be a superior method because of various advantages, particularly environmental compatibility (not to use chemicals except water and electron). In its development, it is a key to search electrodes, which reduce nitrate at fast reaction rate to selectively form N_2 [1-5].

Various electrodes such as metals, metal complexes etc. have been examined. Among them noble metal-based binary electrodes showed a high electrocatalytic activity Particularly CuPd and Sn-modified noble metals showed a very high activity [17, 18-20]. However, the production of harmless N_2 was limited to about 40%, and thereby the improvement of N_2 production is currently required. In order to develop electrodes, which entirely meet the requirement from denitrification technology, it is essential to understand the role of each electrode component, the key process to determine the product distribution, etc. In the previous of studies, Sn-modified noble metal electrodes have been examined. For all examined electrodes, the catalytic activity strongly depended on Sn-coverage. In detailed studies using Sn/Pd, it was found that the activity was dependent on the thickness of Pd layer [20] and the pretreatment electrode potential. The tin coverage dependence on noble metal

dependence was also examined. The activity decreased in the order of Sn/Pd > Sn/Pt > Sn/Rh≈ Sn/Ru > Sn/Ir [18]. A new parameter was introduced "the potential of the electrodes for the selective N_2 formation", which is calculated on the basis of the number of cleaved N–O bonds, and formed N–N and N–H bonds per reduced nitrate ion. As its name suggests, this parameter shows how much product distribution becomes close to the selective N_2 formation of N_2. It becomes 100% when only N_2 is produced. For the examined electrodes, it increased in the order of Sn/Ir≈Sn/Ru < Sn/Pt < Sn/ Rh < Sn/Pd [18].

To clarify the role of noble metal component for the electrocatalytic properties of these electrodes, Sn-modified PdPt electrodes have been examined in our previous study. Pd and Pt were selected because both showed high activity and high potential for the selective N_2 formation. The Sn/PdPt electrodes showed higher activity with greater potential for the selective N_2 formation. The results were interpreted in terms of *d*-band center shift. Namely *d*-band of Pd shifts downward and *d*-band of Pt shifts upward. Sn modification has an effect of decreasing *d*-band of Pd and Pt. For Pt, therefore, the *d*-band shift by alloying is cancelled by the Sn modification. Consequently, the *d*-band downshift of Pd may contribute to the enhanced electrocatalytic properties of Sn/PdPt.

To further examine the alloying effect, it is useful to examine the other noble metal alloys. The Pt/Rh alloy was chosen for the following reasons. The *d*-band center of Pt made downshift, which is reverse from the upshift in PdPt. Sn/Rh showed the second largest potential of the electrodes for the selective N_2 formation. It is also known that Rh shows a higher ability for nitrosyl dissociation, and hence it is used as main component of a three-way catalyst placed in the exhaust systems of motor vehicles to reduce the emission of pollutants.

To examine the effect of *d*-band shift on the adsorption state of nitrate, infrared spectra were measured using the surface enhanced infrared absorption spectroscopy (SEIRAS). The SEIRAS is highly sensitive to the electrode surface, and the contribution of the solution species is essentially neglected [6, 7]. In addition, the cell used for the SEIRAS measurements is free from any unexpected exhaustion and/or

accumulation because of the sufficient solution volume at the electrode. Several metal surfaces are available for SEIRAS measurements by direct metal deposition on prism [7-10] or electrochemical metal deposition on precoated Au surface [11]. Using SEIRAS technique with electrochemical measurements, adsorbed species on the electrode surface and their potential dependence has been successfully reported with respect to nitrate, nitrite, and nitric oxide [12-15]. Unfortunately, no study has been reported for the nitrate adsorption on a Rh electrode. Therefore, the spectra of the adsorbed nitrate on Rh, Pt/Rh as well as their Sn-modified electrodes using SEIRA have been reported.

5.2. Preparation of PtRh Electrodes

PtRh alloy wires (Nilaco corprotation, Japan) were used as working electrodes for the activity and product measurements. Prior to use, the wires were cleaned by immersing into a freshly prepared 50:50 vol.% mixture of concentrated nitric and sulfuric acids for 1 hour followed by a sufficient rinse with Milli Q water. The wire is referred to as a PtRh electrode.

The electrodes used for infrared measurements were prepared by the electroless Au deposition [7] followed by the electrochemical codeposition of Rh and Pt. In more detail, first the reflecting plane of the Si prism (non-doped semicylinder Si, Kyoto Pastec Co., Ltd.) was activated for metal deposition by contact with 40% NH_4F (Morita Chemical Industries Co., Ltd.) for 1 minute after successively polishing with 1 μm alumina followed by ultrasonication in acetone and water. Then Au was deposited at 60 °C for 1 minute by dropping a Au plating solution, which is a mixture of 30 mM $NaAuCl_4$ solution, reducing reagent solution (prepared by mixing Na_2SO_3, $Na_2S_2O_3$, NH_4Cl, and water [7]), and 5% HF solution (prepared from 50 % solution of atomic absorption spectrometry grade, Wako Pure Chemicals) in the ratio of 0.4 : 0.4 : 0.6 in volume. After setting the Au-coated Si prism to the glass or PCTFE cell and sufficient electrochemical cleaning in 0.1 M $HClO_4$, Rh deposition was carried out in X mM $RhCl_3$ + 0.1 M $HClO_4$ for 2100 s according to our previously reported method [2]. Considerably long deposition time was applied because Rh surfce was easily removed during spectroelectrochemical measurements.

5. 3 Results and discussion

5.3.1 Electrochemical and spectroscopic characterization of electrodes

5.3.1.1 Rh electrode

The cyclic voltammogram of Rh electrode in 0.1 M $HClO_4$ is shown in Figure 5.1 (a). The Rh electrode was prepared by electrochemical deposition of Rh on Au film at –0.1 V for 1200 s in 0.1 M $HClO_4$ + 0.1 mM $RhCl_3$ according to the reference [18]. The oxidation of the surface began at around 0.1 V. The oxidation wave is attributed to the formation of Rh(OH) and successive formation of $Rh(OH)_3$. Further oxidation leads to the formation of RhO(OH) and its reduction peak appears at 1.0 V vs. NHE (0.8 V vs. Ag/AgCl(sat. KCl))[16]. When the potential was scanned to 1.2 V, a broad reduction wave was observed at 0.8 V – 1.0 V, showing the formation of

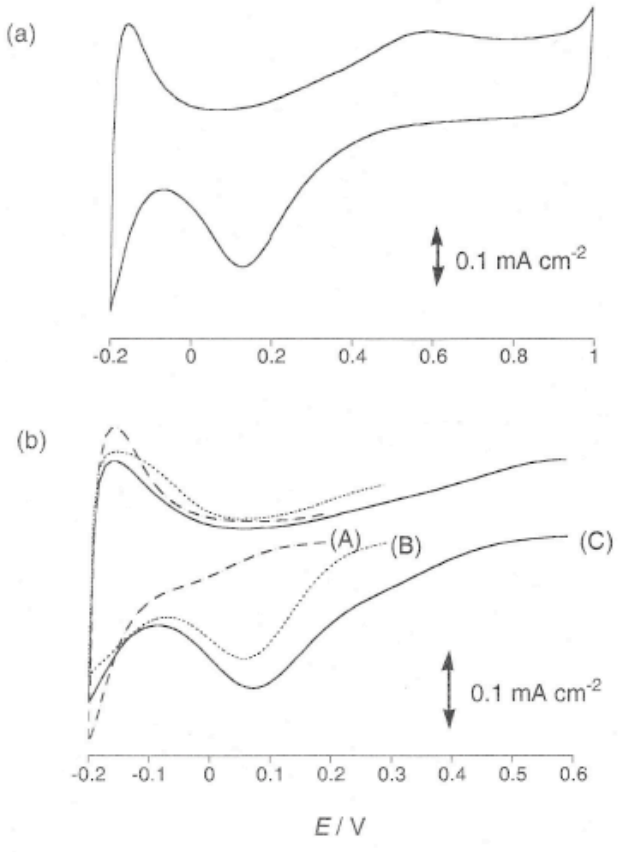

Figure 5.1 Cyclic voltammogram of a Rh electrode (a) between -0.2 and 1.0 V, and (b) the reduction waves started from 0.2, 0.3, and 0,6 V after holding the initial potential for 10 minutes. The cyclic voltammograms were measured at the scan rate of 0.1 V s^{-1} in 0.1 M $HClO_4$.

small amount of RhO(OH). However, no such wave was observed when the potential was scanned to 1.0 V. The oxide reduction peak was overlapped with the peak due to the formation of adsorbed hydrogen. The degree of overlapping and the magnitude and the potential of the oxide reduction peak were strongly dependent on the anodic potential limit.

As described later, the adsorption behavior (IR band intensity and position) of nitrate was a function of the electrode potential. Therefore, it is worth to estimate the amount of the surface oxide remaining at the specific potential. To do this, the electrode potential was kept at 0.2, 0.3 and 0.6 V for 10 minutes, then scanned in a negative direction (Figure 5.1 b). When the potential scan was held at 0.2 V, the oxide reduction peak appeared as a shoulder, showing that only a small amount of the surface oxide remains at this potential. As increasing the holding potential, the oxide reduction peak became greater. The charge due to the reduction of the surface oxide was estimated by subtracting the charge due to the oxidation of the adsorbed hydrogen from the total reduction charge. Thus obtained charge was normalized to the oxide reduction charge obtained from the cyclic voltammogram scanned up to 1 V (it was reported that the upper potential limit which gives the $Rh(OH)_3$ monolayer was ca. 1.25 V vs. NHE (1.05 V vs. Ag/AgCl (saturated KCl)). The surface oxide, which was not reduced and then remained on the surface, decreased from 56% at 0.6 V to 14 % at 0.2 V (Table 5.1).

Table 5.1 Remaining oxide amount for each potential based on the oxide amont until 1 V

Initial potential / V	Remaining oxide amount (%)
0.2	14
0.3	39
0.4	49
0.5	55
0.6	57

5.3.1.2 Pt/Rh electrodes

The surface oxide reduction peak of a Pt/Rh alloy electrode appeared at 0.16 V in-between 0.347 ± 0.002 for Rh and 0.517 ± 0.003 V for Pt in 0.1 M $HClO_4$ when the voltammograms were recorded in the potential range of -0.2 to 1.2V at a scan rate of 0.05 V s^{-1}. (Figure 5.2). The single oxide reduction peak instead of two separate peaks assigned to the Pt and Rh single domains is typical for alloy. Using the known linear relationship between the reduction peak potential of the surface oxide and the surface composition for the Pt-Rh electrodes [21, 24], the surface composition of the PtRh electrode shown in Fig. 5.2 was determined to be Pt/Rh = 25/75, which is quite different from the list composition given by the manufacture company (Pt/Rh = 78/22).

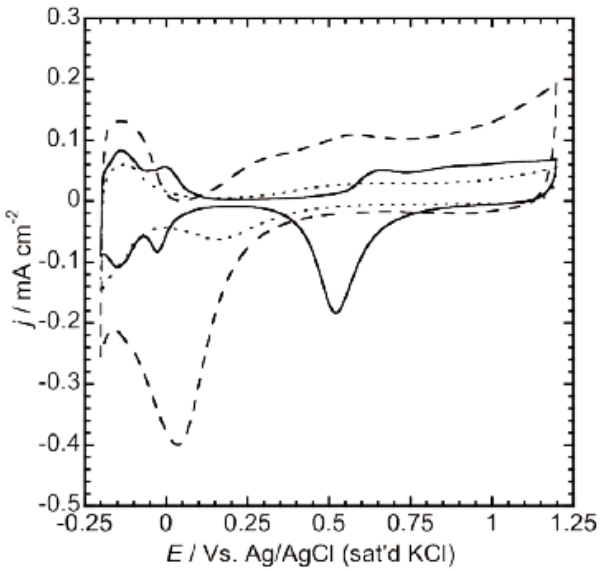

Figure 5.2 Cyclic voltammograms of (dashed curve) Rh, (solid curve) Pt, and (dotted curve) PtRh alloy electrodes in 0.1 M $HClO_4$ at a scan rate of 0.05 V s^{-1}. The surface composition of Pt/Rh was 25/75.

The surface composition of Rh and Pt in the PtRh alloy electrode was also determined from the XP intensities of $Rh3d_{5/2}$ and $Pt4f_{7/2}$ using the following equation.

$$In(d) = S \times I_x \times N_n \times \sigma_i \times \exp [-d/\lambda_i \cos \theta] \quad (5.1)$$

Here, S is machine function, I_x is intensity of incident X-ray, N_n is number of the target atoms, n per the certain surface area, σ_i = photoemission cross-section area of i-state in the certain atom, λ_i= mean free path length of i-state in the certain atom n and θ = angle between the detector and the sample = 90°. Only the $Rh3d_{5/2}$ and $Pt4f_{7/2}$ peak intensities were used because $Rh3d_{3/2}$ peak overlaps with Pt4d. The average surface composition for several individual experiments was Pt/Rh = 74/26, which is very close the list composition (Pt/Rh = 78/22), but is entirely different from the electrochemically determined average composition (Pt/Rh = 31/69). Such incongruity has been reported for Pt/Rh alloy electrode, and it was considered that the electrochemically determined composition most reliably reflects that of the outermost layer of the surface because [22]. In this study, therefore, the surface composition was estimated in PtRh alloy using the known linear relationship and experimentally determined the peak potentials for the Pt and Rh electrodes.

5.3.1.3 Sn-modified Pt/Rh electrodes

Sn modification was conducted by immersing the electrodes into 0.1 M $HClO_4$ containing 0.12 mM $SnCl_2$ for several minutes followed by rinsed with sufficient milli Q water. The prepared Sn-modified PtRh electrode is referred to hereafter as the Sn/PtRh electrode. Figure 5.3 (A) shows the cyclic voltammograms of PtRh in 0.1 M $HClO_4$ before and after Sn adsorption at a scan rate of 0.05 V s^{-1}. The Sn coverage (θ_{Sn}) was determined based on cyclic voltammograms in 0.1 M $HClO_4$ and using the equation $\theta_{Sn} = (Q_H^0 - Q_H)/Q_H^0$, where Q_H^0 and Q_H are the charge due to the oxidation of the adsorbed hydrogen atoms before and after the adsorption of Sn, respectively, as described in previous report [23]. In the Figure, the Sn coverage was 0.89. The immersion time dependence of Sn coverage for PtRh electrode is given in the Figure 5.3 (B), where the fixed concentration (0.12 mM) of $SnCl_2$ was used. It is clearly shown from the Figure 5.3 (B), that the Sn coverage increased with the increasing immersion time and reached the maximum coverage at ≥ 30 min.

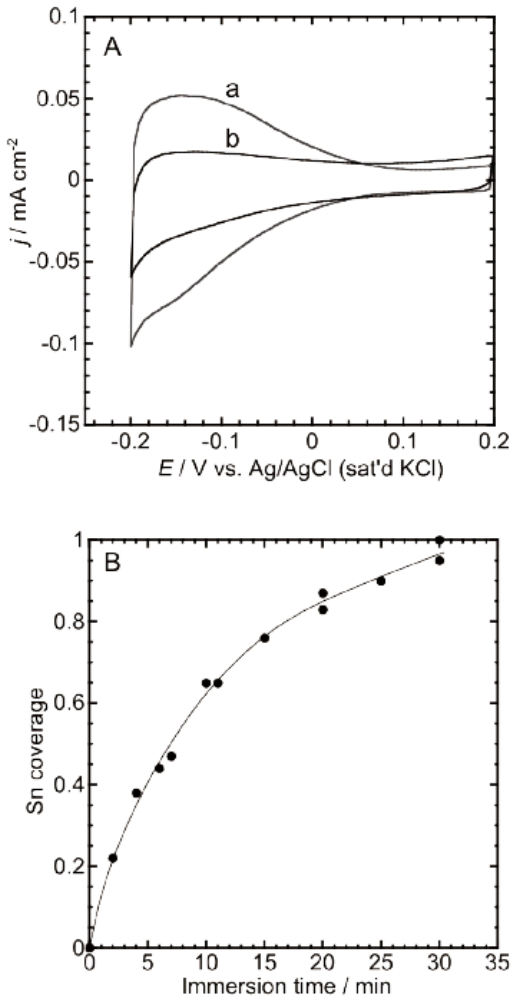

Figure 5.3 (A) CVs of PtRh electrodes in 0.1 M $HClO_4$ at a scan rate of 0.05 V s^{-1} (a) before and (b) after the immersion in 0.1 M $HClO_4$ solution containing 0.12 mM $SnCl_2$ for 20 mins. The surface composition of Pt/Rh was 24/76. (B) Plot of immersion time dependence Sn coverage on Sn/PtRh electrodes.

In order to evaluate the oxidation states of Rh, Pt and Sn in Sn modified PtRh electrodes (Sn/PtRh), the X-ray photoelectron spectra of PtRh alloy electrodes were analyzed before and after Sn adsorption. The $Pt4d_{5/2}$ and $Rh3p_{3/2}$ peaks were overlapped with $Rh3d_{3/2}$ and $Sn3d_{3/2}$, respectively; therefore only $Rh3d_{5/2}$ and $Sn3d_{5/2}$ peaks could be utilized to assign the oxidation state of Rh and Sn. The average binding energies of $Rh3d_{5/2}$, $Pt4f_{7/2}$ and $Sn3d_{5/2}$ in Rh, Pt, PtRh and their Sn modified electrodes are summarized in Table 5.2.

It was found that the binding energies of $Rh3d_{5/2}$ and $Pt4f_{7/2}$ are 307.28 ± 0.10 and 71.29 ± 0.21 eV, respectively for unmodified PtRh electrode. These values are very close to those reported for zero valent state of metals (307.0 ± 0.4 for Rh and 71.16 ± 0.26 for Pt) [23]. The binding energy of $Rh3d_{3/2}$ and $Pt4f_{7/2}$ remained unchanged before and after modification of the electrode by Sn. Therefore, the oxidation states of Rh and Pt are not influenced by the Sn adsorption. The binding energy for $Sn3d_{5/2}$ in Sn/PtRh was 486.25 ± 0.16 eV which is within the range reported for Sn(II) (485.6-487.4 eV) and at the edge of the range for Sn(IV) (486.1-488.2 eV) but much more positive than that for Sn(0) (484.3-485.2 eV) [23]. Therefore the most plausible oxidation state of the Sn on the surface is divalent.

Table 5.2 Binding energy of $Rh3d_{5/2}$, Pt4f7/2 and Sn3d5/2 for Rh, PtRh, Pt electrodes and their Sn modified derivatives

	Binding energy / eV		
Electrode	$Pd3d_{5/2}$	$Pt4f_{7/2}$	$Sn3d_{5/2}$
Rh	307.50 ± 0.04		
PtRh	307.28 ± 0.10	71.29 ± 0.21	
Pt		71.08 ± 0.06	
Sn/Rh	307.27 ± 0.03		486.53 ± 0.10
Sn/PtRh	307.25 ± 0.19	71.11 ± 0.04	486.25 ± 0.16
Sn/Pt		71.18 ± 0.02	486.45 ± 0.04

Sn coverages were fixed in the range of 0.86-0.91 for Sn/Rh , 0.90 – 0.93 for Sn/PtRh, 0.85-0.89 for Sn/Pt. The Pt/Rh ratios were 20-25/80-75 for unmodified and Sn modified PtRh electrodes.

5.4 Nitrate reduction activity of Sn/PtRh electrode

5.4.1. Sn coverage dependence

In order to get the information about the nitrate reduction activity on Sn modified PtRh alloy electrode, the cyclic voltammograms were taken in 0.1 M $HClO_4$ containing 0.01 M $NaNO_3$ at a scan rate of 0.01 V s^{-1}. Figure 5.4 shows those of PtRh

alloy electrodes with different Sn coverage. The PtRh electrode exhibited insignificant activity for the reduction nitrate. As usually observed for Sn-modified

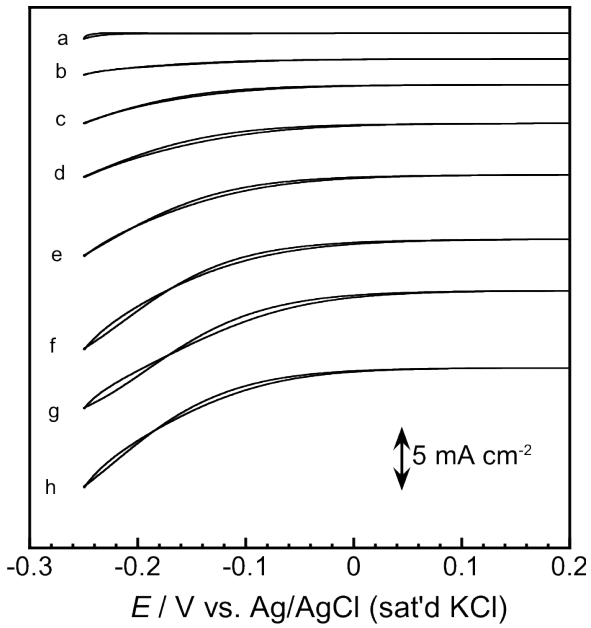

Figure 5.4 Cyclic voltammograms for the reduction of nitrate on as-prepared Sn/PtRh electrodes in 0.1 M $NaNO_3$ + 0.1 M $HClO_4$ at the scan rate of 0.01 V s^{-1}. Sn coverage: (a) 0, (b) 0.22, (c) 0.38, (d) 0.47 and (e) 0.65. (f) 0.76, (g) 0.87 and (h) 1.0. The surface composition of Pt/Rh was 25-20/75-80.

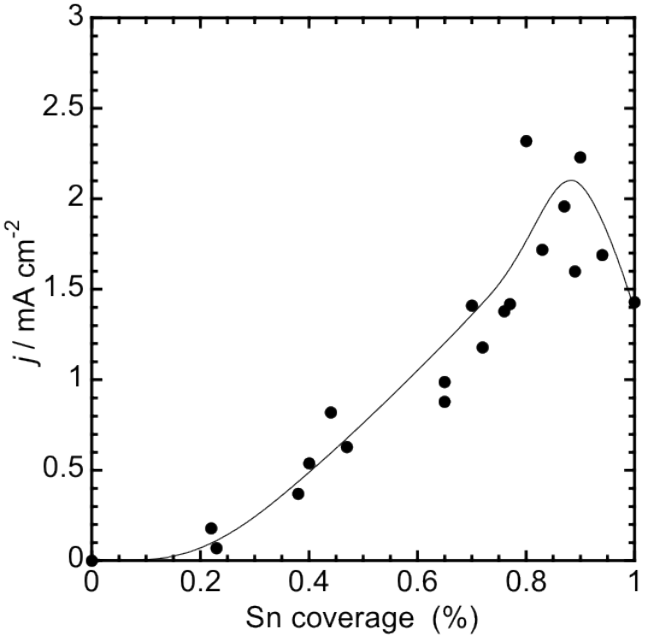

Figure 5.5 Tin coverage dependence of the reduction current at -0.1 V on Sn/PtRh electrodes. Data were collected from cyclic voltammograms in 0.1 M $NaNO_3$ + 0.1 M $HClO_4$ at a scan rate of 0.01 V s^{-1}. The surface composition was Pt/Rh = 25-20/75-80.

noble metal electrodes, the reduction current increased with the Sn coverage. The Sn coverage dependence of the reduction current at -0.1 V on Sn/PtRh electrodes is shown in the Figure 5.5. The surface composition was fixed in the range of Pt/Rh = 25-20/75-80. The maximum reduction current was obtained at about θ_{Sn} = 0.85, which resembles Sn coverage dependences of the activity for Sn/Rh and also Sn/Pt [18, 20].

5.4.2. Surface composition dependence on the reduction activity.

The nitrate reduction was also conducted on Sn/PtRh of different Pt/Rh compositions. Although the same Pt/Rh wire electrode was used, the surface Pt/Rh composition is tunable because of preferential dissolution of Rh, or the Pt/Rh electrode of higher Pt/Rh ratio was prepared by cycling the electrode potential. In order to simplifying the system, the Sn coverage was fixed in the range of 0.85-0.90.

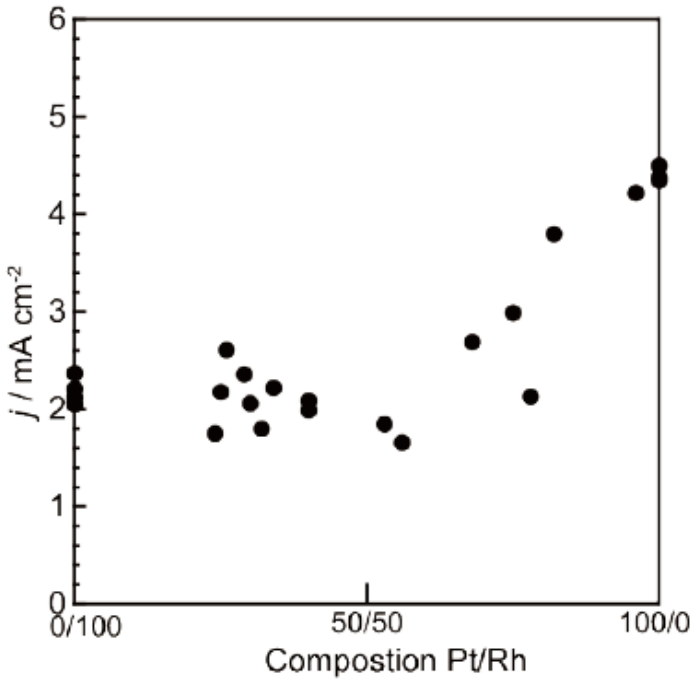

Figure 5.6 Surface composition dependence of the reduction current at -0.1 V on Sn/PtRh electrodes. Data were collected from cyclic voltammograms in 0.1 M $NaNO_3$ + 0.1 M $HClO_4$ at a scan rate of 0.01 V s^{-1}. Sn coverage was fixed 0.85-0.91.

Figure 5.6 shows the surface Pt/Rh composition dependence of the electrocatalytic activity (reduction current at –0.1 V during the potential sweep at the sweep rate of 0.01 V s^{-1}). It is clear that the reduction current of Rh and PtRh was almost the same at Pt/Rh < 40/60. At higher Pt/Rh ratios, the reduction current linearly increased. No maximum current was observed at any ratio of Pt/Rh. From these results and the fact that the real surface area of the electrodes was almost the same, it can be concluded that there is negative rather than positive synergy effect between Pt and Rh.

5.5 Products distribution

To analyze product distribution, the electrolysis was conducted on the Sn/PtRh electrode for 5 hours at a constant potential of -0.2V and compared with Sn/Pt and Sn/Rh electrodes (Pt/Rh=30/70, Sn coverage = 0.82–0.86). The average product distribution for several experiments is summarized in the Table 5.3.

Table 5.3 (a) Distribution of products for nitrate reduction at -0.2 V

Electrode	Composition Pt/Rh	Sn coverage	Conversion (%)	Products (%)				
				NO_2^-	NH_3OH^-	NH_4^-	N_2O	N_2
Sn/RhPt	30/70	0.82-0.86	11-15	30.86	8.12	24.14	10.32	26.56
Sn/Rh	0/100			-	22	19	59	-
Sn/Pt	100/0			10	46	11	7	26
Mixture[1])	30/70			3	29.2	16.6	43.4	7.8

For Sn/Rh and Sn/Pt, the Sn coverage was fixed where the maximum activity obtained.
1) Calculate for physical mixture of Sn/Rh and Sn/Pt

Table 5.3 (b) Average number of formed and cleaved bonds pre reduced nitrate and the potential for the selectivity N2 production (P_{N2})

Electrode	Composition Pt/Rh	N-O	N-N	N-H	P_{N2} (%)
Sn/RhPt	30/70	2.41	0.27	0.71	70.27
Sn/Rh	0/100	2.49	0.37	0.77	77.15
Sn/Pt	100/0	2.45	0.25	1.29	62.82
Mixture[1])	30/70	2.48	0.34	0.91	73.37

Data were taken from above table 5.3 (a)

The conversion of the reactant nitrate was only 11-15 % and much lower than the other Sn-modified electrodes such as Sn/Pd, Sn/Pt etc. (typically 40-60%). This reflects lower activity of Sn/PtRh and relatively fast activity-decrease with time.

The major reduction products on the Sn/PtRh electrode were N_2 (27%) and NH_4^+ (24%). In addition, a considerable amount of NO_2^- was formed. This makes comparison with the component single metal electrodes (Sn/Rh and Sn/Pt) more difficult because NO_2^- usually behaves as an intermediate. Assuming the distribution of products formed from the nitrite is the same as that shown in Table 5.3 but excluding nitrite, just simply estimate the distribution (see in the parenthesis of Table 5.3). This distribution can be compared with that expected for a physical mixture of Sn/Rh and Sn/Pt (Table 5.3). Apparently these distributions are different from each other. However, a sum of the hydrogenated products (NH_3OH^+ + NH_4^+) is the same; 45.8% and 46.6% for the physical mixture and Sn/PtRh, respectively. Similarly, the ability to form N-N bond, estimated from a sum of N_2O and N_2, is the same; 51.2% and 53.3% for the physical mixture and Sn/PtRh, respectively. Therefore, the hydrogenation ability and the N-N formation ability are essentially unchanged by the formation of alloy. However, the decrease in the formation of NH_3OH^+ and N_2O compared with that expected for a physical mixture is indicative of the increase of N-O cleavage ability.

5.6 Adsorption species from NO_3^-

5.6.1 Adsorption of nitrate on Rh

The SEIRA spectra during the adsorption and reduction of nitrate and the assignment of the bands are described in detail in SUPPLIMENTAL section. Briefly, the SEIRA spectra at 0.6 V show the band due to the unidentate nitrate. This is easily understood because a considerable part of the surface is covered by the oxide at this potential, and then most of Rh sites must be isolated. When the oxide is reduced, more Rh sites becomes available, resulting in the formation of more stable bidentate. Simultaneously, the unidentate nitrate is reduced to form nitrite of the nitrito form.

This reduction is easy to understand because both compound are adsorbed via one oxygen atom and structural change is small. At more negative potentials the adsorbed nitrate and/or nitrite are more reduced to nitric oxide. A variety of the adsorbed species may owe to the higher activity for nitrate reduction of Rh. The recovery of the intensity by the reverse scans of the negative and positive-going scans indicates the presence of the potential dependent configuration change of the adsorbed NO_3^- in these processes.

5.6.2 Pt electrode

The SEIRA spectra of the adsorbed species formed from nitrate has been conducted in the previously published paper [25]. Here the experimental results were briefly described and compared to those on Rh and hereafter Pt/Rh electrodes. During the adsorption of nitrate from nitrate-containing 0.1 M $HClO_4$ at 0.2 V and reduction and/or desorption of the adsorbed nitrate in nitrate-free 0.1 M $HClO_4$, only the bidentate nitrate was observed in 1547-1568 cm^{-1} without the formation of any other adsorbed species. The bidentate band intensity started to decease at 0 V, and completely disappeared at –0.1 V. This potential range is very close to that in which the bidentate band on Rh decreases.

5.6.3. PtRh electrode

Figure 5.7 shows the SEIRA spectra of the adsorbed species on PtRh(47/53). Compared with those on Pt and Rh, the band due to linear NO (1772 cm^{-1}) was large, showing that the activity of this electrode for the reduction of the adsorbed nitrate. The broad band at 1385 cm^{-1} can be assigned to the unidentate nitrate and the nitrito NO_2^- as did for the spectra of Rh. The band at 1590 cm^{-1} is due to the bidentate nitrate, but is probably overlapped with the band due to the bridged NO because the linear NO is almost always accompanied by the bridged NO on various noble metal electrodes. For this reason, the shift of band position by alloying was not evaluated using the SEIRA spectra.

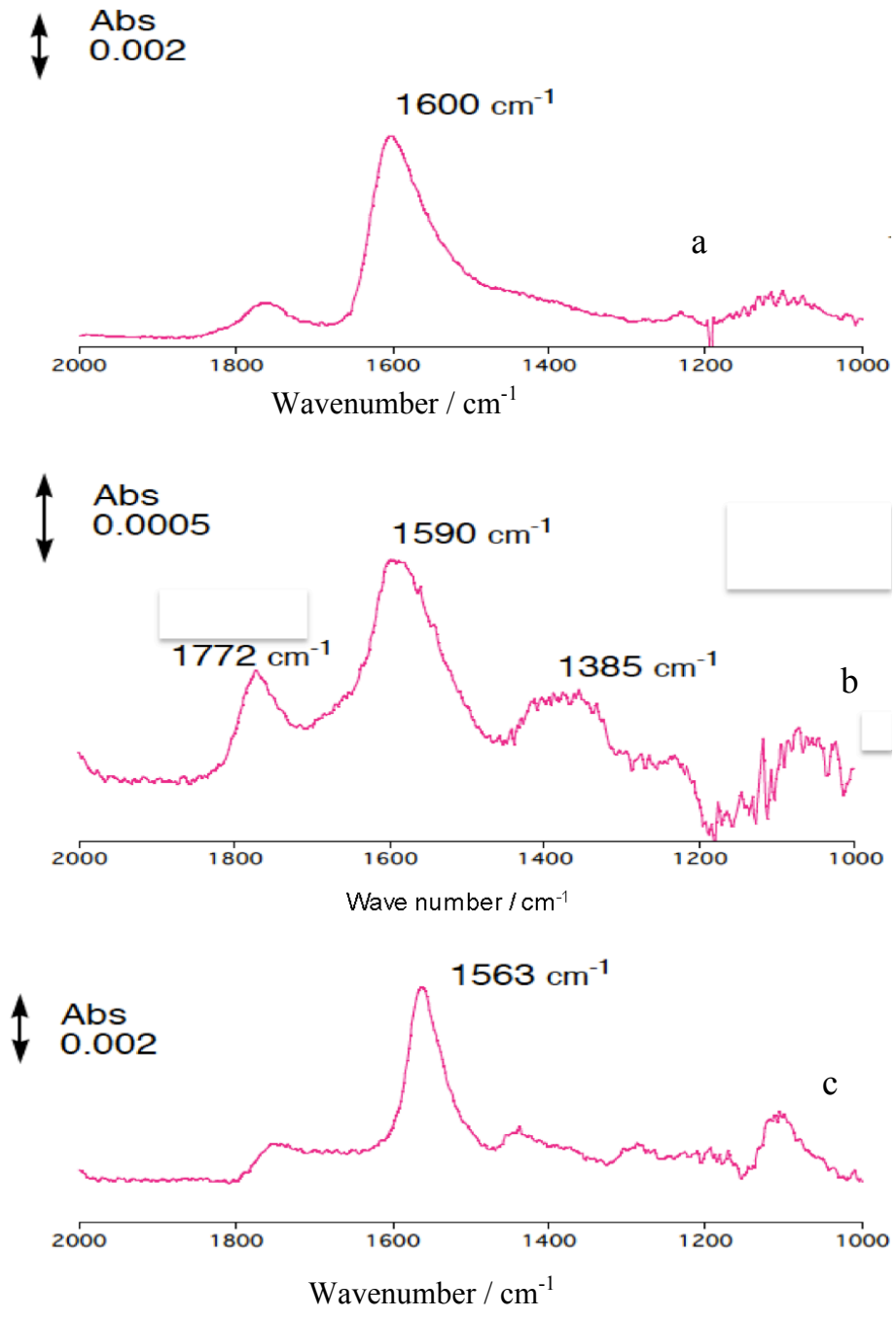

Figure 5.7 The SEIRA spectra of NO_3^- on (a) Rh, (b) PtRh, and (c) Pt electrodes in 0.1 M $HClO_4$. The adsorption was conducted at 0.2 V. The surface composition was Pt/Rh = 43/57.

5.6.4 Sn/ Rh and Sn/ PtRh electrodes

As shown in Figure 5.8, only bands assigned to linear and bridged NO were observed both on Sn/Rh (θ_{Sn} = 0.45) and Sn/PtRh (43/57, θ_{Sn} = 0.93). This is reasonable because of the enhanced activity. These results also suggest that the observed adsorbed nitrate species can be reduced on these electrodes, and thereby it is concluded that the adsorbed nitrate is active surface species.

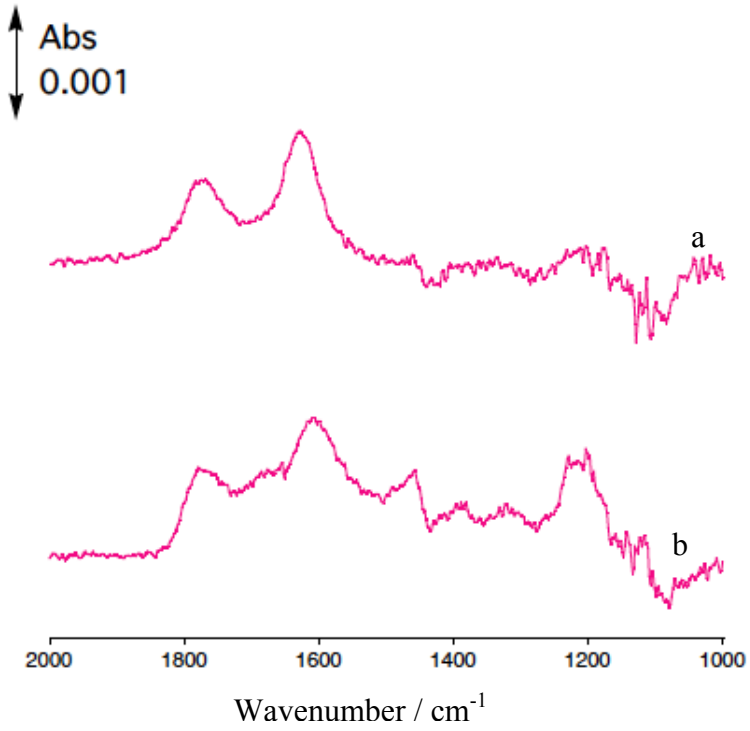

Figure 5.8 The SEIRA spectra of NO_3^- on (a) Sn/Rh (θ_{Sn} = 0.45) (b) Sn/PtRh ((θ_{Sn} = 0.93) electrodes in 0.1 M $HClO_4$. The adsorption was conducted at 0.2 V. The surface composition was Pt/Rh = 43/57.

5.7 Pretreatment effect on Sn/PtRh for electrocatalytc properties for nitrate reduction

In order to get the information about the pretreatment effect on Sn/PtRh for electrocatalytic properties towards nitrate reduction, Cyclic voltammograms were taken in 0.01 M $NaNO_3$ + 0.1 M $HClO_4$ at a scan rate of 0.01 V s^{-1} for Sn modified PtRh alloy before and after pretreatment (Figure 5.10). The electrode was pretreated

at -0.35 V for 60 s. The electrocatalytic activity for reduction of nitrate remained constant by the pretreatment.

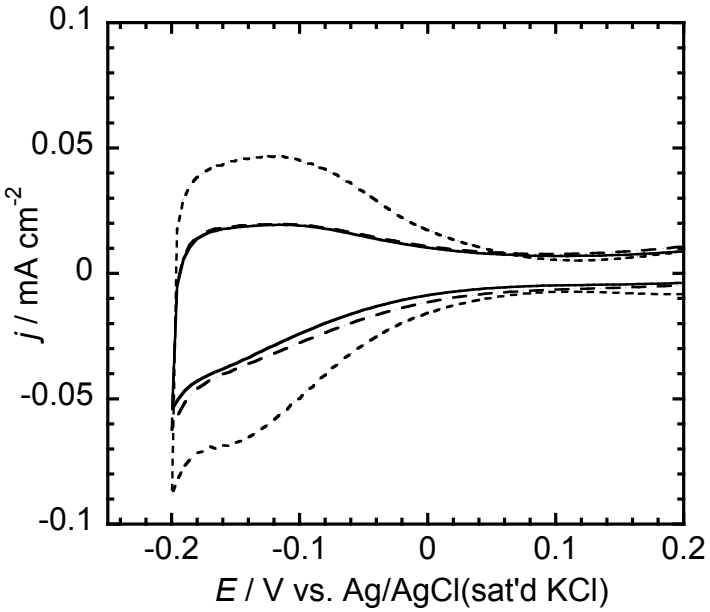

Figure 5.9 Cyclic voltammograms of (dotted curve) PtRh, (dashed curve) as-prepared Sn/PtRh, and (solid curve) pretreated Sn/PtRh electrodes in 0.1 M $HClO_4$ at the scan rate of 0.05 V s^{-1}. Tin was adsorbed by immersing a PtRh electrode in a 0.12 mM $SnCl_2$ solution for 15 min. The tin coverage was 0.78. The electrochemical pretreatment was conducted at -0.35 V for 60 s.

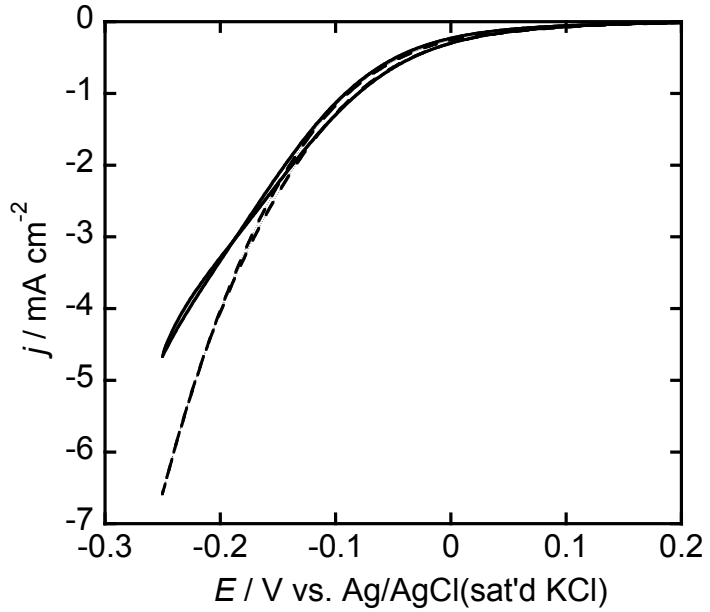

Figure 5.10 Cyclic voltammograms of (dashed curve) as-prepared Sn/Pd, and (solid curve) pretreated Sn/Pd electrodes in 0.01 M $NaNO_3$ + 0.1 M $HClO_4$ at the scan rate of 0.01 V s^{-1}. The tin coverage was 0.89. Electrochemical pretreatment was conducted at -0.35 V for 60 s.

The hydrogen adsorption and desorption wave in the cyclic voltammogram in 0.1 M $HClO_4$ remained also unchanged after the pretreatment at -0.35 V for 60s (Figure 5.9). It is predicted that the electronic interaction between Sn and PtRh alloy was very weak by the pretreatment. Therefore pretreatment effect on this electrode for nitrate reduction was insignificant.

5.8 Conclusion

The electrocatalytic properties of tin-modified rhodium-platinum alloy electrodes (Sn/PtRh) for the reduction of nitrate ions were examined in 0.1 M $HClO_4$. as a function of Sn coverage. The reduction current is strongly dependent on the tin coverage on the electrode surface. The reduction activity for nitrate reduction for Sn/PtRh is identical with for Sn/Rh, but smaller than Sn/Pt. The Sn/PtRh alloy accelerated N-O bond cleavage, suppressed N-H bond and enhanced the ability N-N bond formation and consequently a considerable amount of N_2 (27%) was formed as one of the most desirable, feasible and environment friendly reduction products, even though there is no N_2 obtained for Sn/Rh electrode.

5.9 References:

[1] Grden, M., Piascik, A., Koczorowski, Z., Czerwinski, A., J. Electronal. Chem. 532 (2002) 35.

[2] Lukaszewski, M., Kusmierczyk, K., Kotowski, J., Siwek, H., Czerwinski, A., J. Solid State. Electrochem. 7 (2003) 69.

[3] Lukaszewski, M., Grden, M., Czerwinski, A., J. Electroanal. Chem. 573 (2004) 87.

[4] Zurowski, A., Lukaszewski, M., Czerwinski, A., Electrochem. Acta 51 (2006) 3112.

[5] Wood, R. in: A. J. Bird (Ed.) Electrochemical Chemistry, vol 9, Marcel Dekker, New York, 1976, pp 2-162.

[6] Rand, D. A. J., Woods, J. Electroanl. Chem. 36 (1972) 57.

[6] Rand, D. A. J., Woods, Surf. Sci. 41 (1974) 611.

[7] Gossner, E., Mizera E., J. Electronal. Chem. 98 (1979) 37.

[8] Gossner, E., Mizera E., J. Electronal. Chem. 140 (1982) 35.

[9] Lukaszewski, M., Czewinski, A., J. Solid State Electrochem. On line.

[10] Solla-Gullon, J., Vidal-Iglesias, F. J., Montiel, V., Aldaz, A., Electrochim. Acta 49 (2004) 5079.

[11] Kabbabi, A., Faure, R., Durand, R., Beden, B., Hahn, F., Legger, J. – M., Lamy, C., J. Electroanal. Chem. 444 (1998) 41.

[12] Siwek, H., Lukaszewski, M., Czerwinski, A., Polish J. Chem. 78 (2004) 1121.

[13] Grden, M., Paruszewska, A., Czerwinski, A., J. Electroanal. Chem. 502 (2001) 91.

[14] Nishimura, K., Machida, K., Enyo, M., J. Electroanal. Chem. 251 (1988) 103.

[15] Beden, B., Lamy, C., Leger, J. M., Electrochim. Acta 24 (1979) 1157.

[16]. B. Gurau, R. Viswanathan, R. Liu, T. J. Lafrenz, K. L. Ley, E. S. Smotkin, E. Reddington, A. Sapienza, B. C. Chan, T. E. Mallouk, S. Sarangapani, J. Phys. Chem. B, 102 (1998) 9997.

[17] G. E. Dima, A. C. A de Vooys, M. T. M Koper, J. Electroanal. Chem. **2003,** 554, 15.

[18] Piao, S.; Kayama, Y.; Nakano, Y.; Nakata, K.; Yoshinaga, Y.; Shimazu, K. J. Electroanal. Chem. **2009,** 629, 110.

[19] K. Tada, K. Shimazu, J. Electroanal. Chem. 577 (2005) 303.

[20] K. Shimazu, R. Goto, S. Piao, R. Kayama, K. Nakata, Y. Yoshinaga, J.Electroanal. Chem. 601 (2007) 161.

[21] D. A. Rand, R. Woods, J. Electroanal. Chem. 36 (1972) 57.

[22] B. G. Baker, D. A. Rand, R. Woods, J. Electroanal. Chem. 97 (1979) 189.

[23] K. Shimazu, R. Goto, S. Piao, R. Kayama, K. Nakata, Y. Yoshinaga, J. Electroanal. Chem. 601 (2007) 161.

[24] A. Capon, R. Parsons, J. Electroanal. Chem. 65 (1975) 285.

[25] K. Nakata, Y. Kamaya, K. Shimazu, A. Yamakata, S. Ye, M. Osawasa, Langmuir 24 (2008) 4358.

Chapter 6

Summary and conclusion

Groundwater is the main source of drinking water in many countries and about more than one-half of the Nations population is dependent on groundwater for their daily activities. Nowadays groundwater is significantly contaminated with nitrate and spread out all other the world. The increasing contamination of ground, potable and wastewater by nitrate is an alarming issue due to its adverse health and environmental effect. In order to invent a new method, which has a high catalytic activity for denitrificaiton and selectivity to N_2, basic information on the reduction activity and products distribution is necessary. Activity and selectivity depends on properties of the electrode surfaces (such composition, electronic state of surface etc.). In the previous reports, Sn modified novel metal alloy exhibit highest catalytic activity for nitrate reduction compared to so far binary novel metals [1]. Therefore, the role of electronic state of novel metals according to the collective band model (*d* band model) in Sn alloys has been examined to develop a good electrocatlysts. This chapter describes the foremost findings of this study.

In chapter 3, Pd is formed alloy with Sn due to charge transfer from Sn to Pd d orbitals by the electrochemical pretreatment of Sn modified Pd electrodes at -0.35 V. In addition, divalent Sn^{2+} was partially reduced to Sn^0, and consequently *d* band center of Pd shifts downward due to the formation of Pd-Sn alloy. The pretreated Pd-Sn electrodes was lost hydrogen sorption ability because of the *d* band is being filled by electrons. This result is reflecting alter in the surface electronic state and reconstruction the electrode surface. The hydrogenation ability was decreased and N-N bond formation ability was increased, resulting enhances the N_2 selectivity. The activity and selectivity of the pretreated Pd-Sn electrodes for nitrate reduction can be explained by the following scheme.

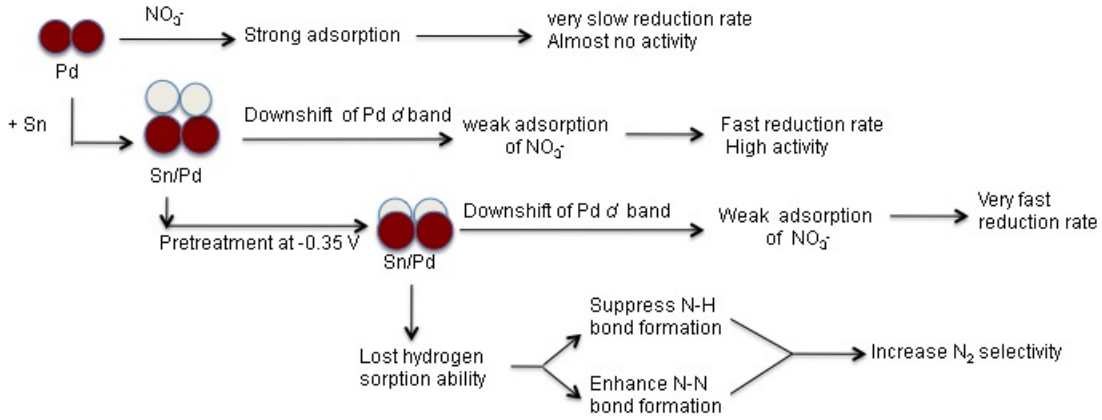

Scheme 6.1: Schematic representation of Pd-Sn electrodes for nitrate reduction and N_2 selectivity.

In chapter 4, the Sn modified PdPt alloy electrodes prepared by sputtering method followed by the spontaneous Sn adsorption exhibits higher catalytic activity and N_2 selectivity than those of Sn/Pd and Sn/Pt electrodes. The SEIRA spectra of N=O stretching of bidentate NO_3^- on PdPt electrodes observed at higher wavenumber with increasing the Pd content on the surface and by the Sn modification. This positive shift is indicative of the stronger N=O bond with more positive charge on N atom of the adsorbed nitrate. The change in the electronic state of the adsorbed species is the consequence of shifting of *d* band center of metals. The *d* band center of Pd and Pt shifts downward and upward respectively in PdPt alloy, resulting enhances the nitrate reduction activity and selectivity to N_2 on the Sn/PdPt electrodes. The activity and product selectivity of Sn/PdPt electrodes can be explained as follows:

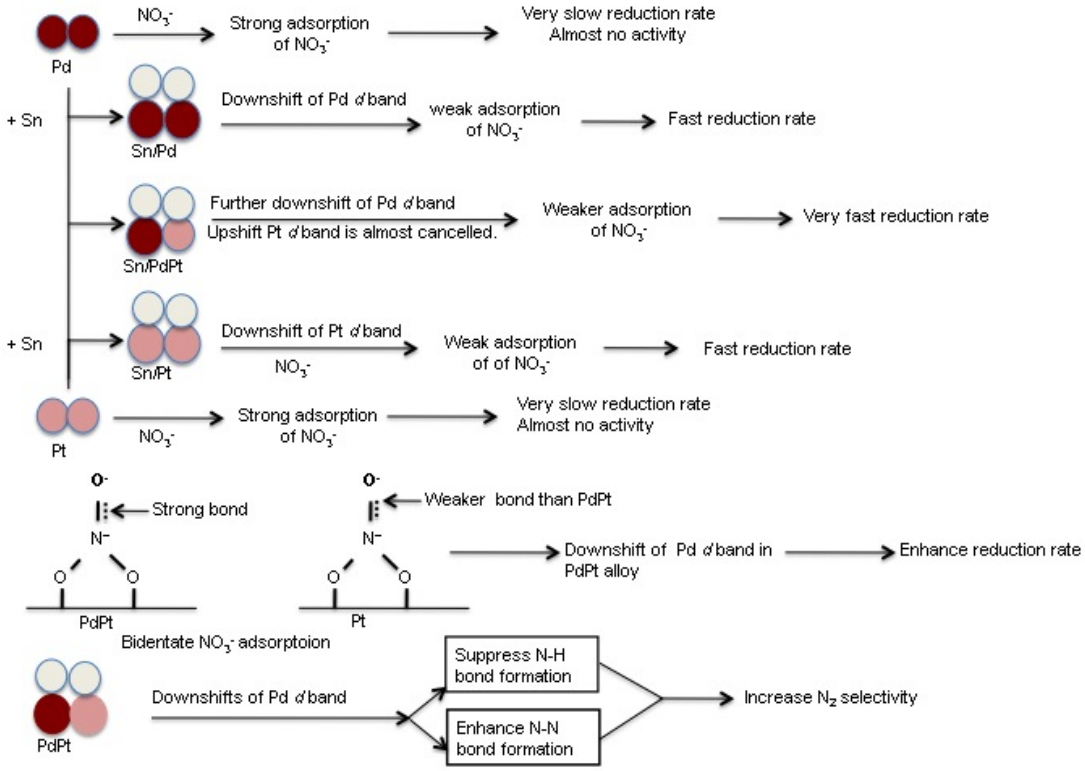

Scheme 6.2: Schematic representation of PdPt electrodes for nitrate reduction and N_2 selectivity.

In chapter 5, the preparation method for Sn modified PtRh alloy is very simple. The reduction activity is dependent on the Sn coverage and the maximum activity was observed at $\theta_{Sn} \geq 0.85$, is consistent with previously reported for Sn modified Pd and Rh electrodes. N_2 selectivity was increased for Sn/PtRh alloy, however there is no N_2 selectvity for Sn/Rh alloy. The increased N_2 selectivity was observed due to change in the electronic state of PtRh alloy, which suppressed hydrogenation ability and enhanced N-N bond formation ability. The role of novel metal (shifting of *d* band center) in PtRh and Sn modified electrodes for the reduction of nitrate and selectivity to N_2 can be elucidated by the following scheme:

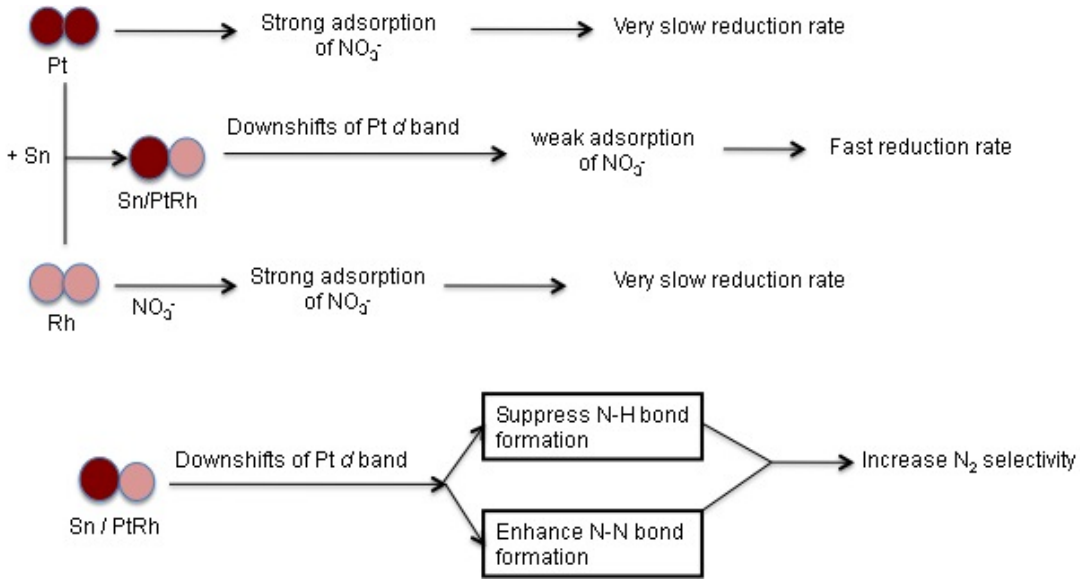

Scheme 6.3: Schematic representation of Sn/PtRh electrodes for nitrate reduction and N_2 selectivity.

From the experimental results on activity and product selectivity for nitrate reduction the following points are concluded:

- The trend of electrocatalytic properties can be interpreted by *d* band center shift.
- Downshift of *d* band center causes
  (i) enhancement of activity for nitrate reduction.
  (ii) decrease in the hydrogenation ability to reduce the formation of hydrogenated species, consequently improves N_2 selectivity

This study demonstrated the electrocatalytic activity and the N_2 selectivity for the reduction of nitrate on Pd electrodes were enhanced by pre-reduction of the electrode and alloying with Pt as well as Sn-modification. It is confirmed that *d* band center of noble metal in alloys plays an important role for its electrocatalytic properties. It is concluded that the downshift of the *d*-band weakens the nitrate adsorption and the hydrogen sorption ability, resulting in the improvement of the activity and the product distribution.

Noble metal alloys exhibit higher catalytic activity compared to individual metals, so noble metal alloy are extensively used in various purpose as catalysts. But Noble metal alloys are very expensive, therefore there is a pressing need to develop other metal alloys, which can be substitute as catalyst instead of noble metal alloys. Recently, the computer simulation based on the molecular orbital such as LCAO, plane-wave, APW etc has been rapidly developed. In addition, the computer simulation can also predict the information about *d*-band center of metal alloys that have a better catalytic property than novel metal alloys. Since the valence band of alloys can also be directly measured by near-IR, X-ray photoemission spectroscopy or High-resolution ultraviolet photoelectron spectroscopy etc, it can be confirmed by the spectroscopic method. However the number of combination of metals in alloy is infinity, the present results provide a clear guidance for the electrode design for the denitrification in the hydrosphere. Furthermore this knowledge provides a path how to develop *d*-band metal alloys (except noble metal alloys), which can be effective for fuel cell and other practical purposes.

6.1 References

[1] S. Piao, Y. Kayama, Y. Nakano, K. Nakata, Y. Yoshinaga, K. Shimazu, J. Electroanal. Chem. 629 (2009) 110.

Supplemental

Infra-red Spectra of Nitrate on Rh Electrode

S1.1 Objective

In order to examine the adsorption state of nitrate on Sn/PtRh electrodes using SEIRA, it is essential to know the spectra of adsorbed nitrate on the component metals such as Pt and Rh. For Pt electrodes, it is reported from the group I belong to that the bidentate nitrate was formed during the adsorption at 0.2 V. The infra-red peak due to this species decreased at more negative potentials. And kinetics of the decrease in this surface species has been discussed [1, 2]. However, no infra-red study has been reported for the adsorbed nitrate on Rh. To assign the peaks and to compare results between the alloy electrodes and component electrodes, I will give more detailed information as to the spectra and its potential-dependence in this supplemental section.

S1.2 Adsorption species from NO_3^-

S1.2.1 Rh electrode

S1.2.1.1 Adsorption of nitrate

The time dependences of the SEIRA spectra during the adsorption of NO_3^- at the fixed potential were shown in Figure S1. At 0.6 V, a broad band was observed at 1375 cm^{-1}. Its intensity was very low (Abs < $5x10^{-4}$). At 0.3 V, this broad band was observed at 1350 cm^{-1} with greater intensity. The band position and shape are close to those observed at 0.6 V. A new band began to appear at 1575 cm^{-1} at around 50 s after the nitrate injection with the decreasing intensity of the broad band at 1350 cm^{-1}.

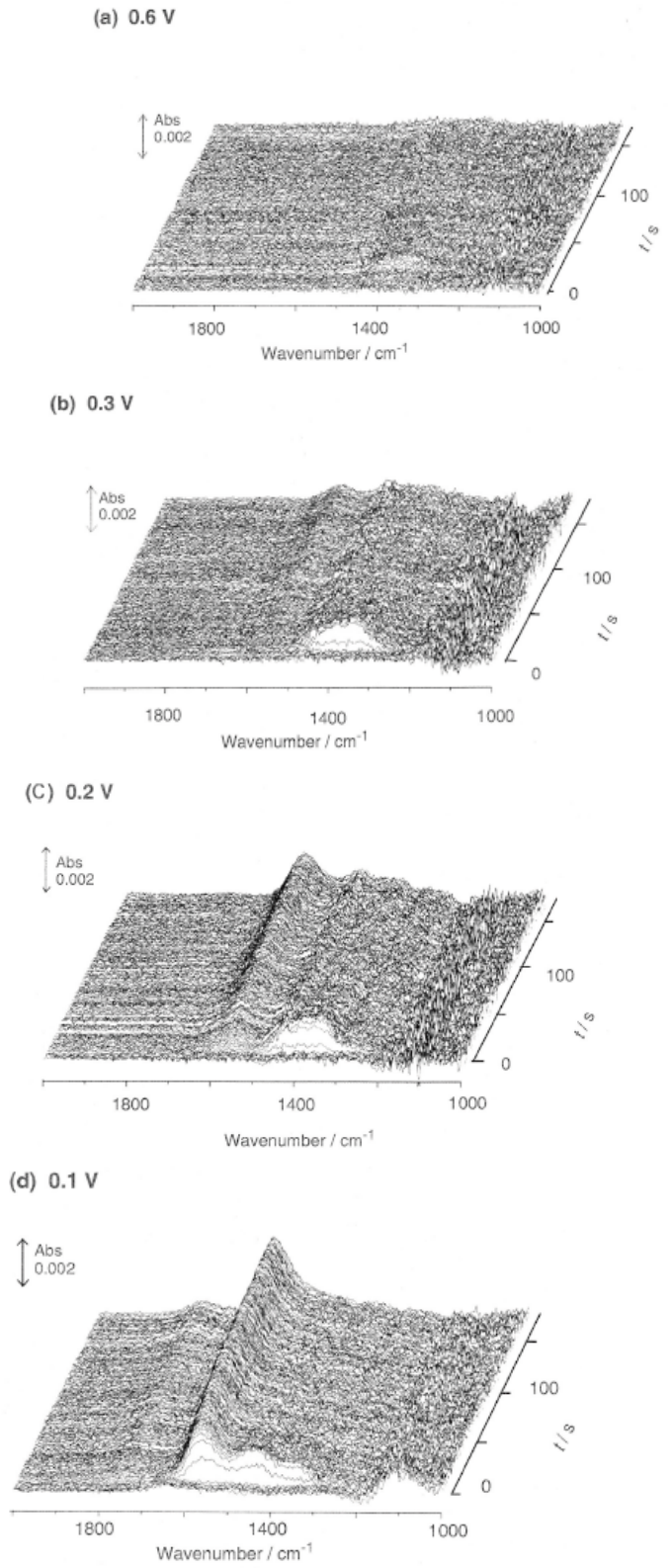

Figure S1 The time courses of the SEIRA spectra by the addition of a NO_3^- at (a) 0.6 V, (b) 0.3 V, (c) 0.2 V, and (d) 0.1 V, in 0,1 M $HClO_4$.

The growth of the band at higher wavenumber accompanied by the degradation of the broad band at around 1400 cm^{-1} was accelerated at 0.2 V. The decrease of the band started within 15 s. Figure S2 shows the comparison of the spectra at 15 s and 180 s with their deconvoluted spectra, which were obtained by the Quasi-Newton method [3].

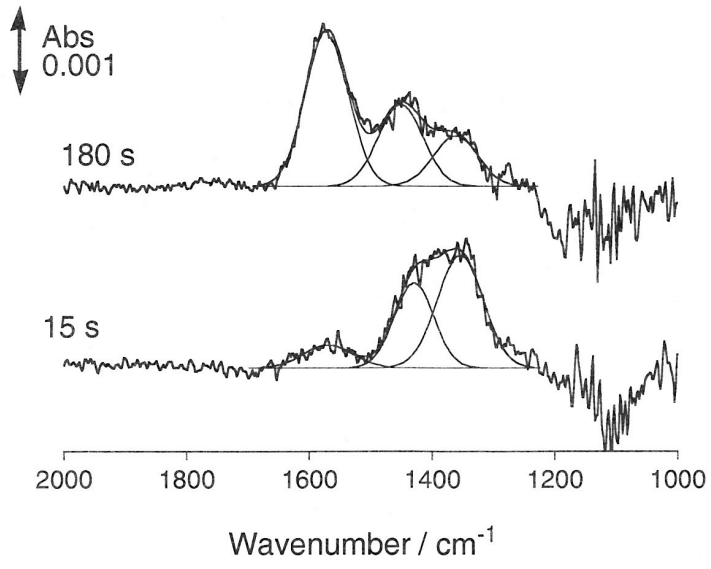

Figure S2 The SEIRA spectra at 15 s and 180 s after NO_3^- injection with their deconvolution spectra. The present data were obtained from the spectra shown in Figure S1 (c).

The spectra showed the existence of two bands in the range of 1350-1450 cm^{-1}. The intensity of lower wavenumber band was larger than that of higher wavenumber band at 15 s. At 180 s, the order of the intensity of these bands was reversed. Based on such deconvoluted spectra, the time course of the band position and the relative band intensity were shown in Figure S3. The intensity of the band at 1350 cm^{-1} steeply increased in the initial stage (0-15 s) and gradually decreased with time, whereas that of the band at 1440 cm^{-1} increased until 50 s. The band intensity of both bands became almost constant after 50 s. A band at 1575 cm^{-1} also appeared at the initial stage (0-15 s) and its intensity was gradually increased with time. The band position of these bands was not changed with time. At 0.1 V, a broad band at 1760 cm^{-1} appeared in addition to three bands observed at 0.2 V. The intensity of this band

was weak and gradually increased from 50 s. The relative intensity of the other bands was close to that at 180 s at 0.2 V.

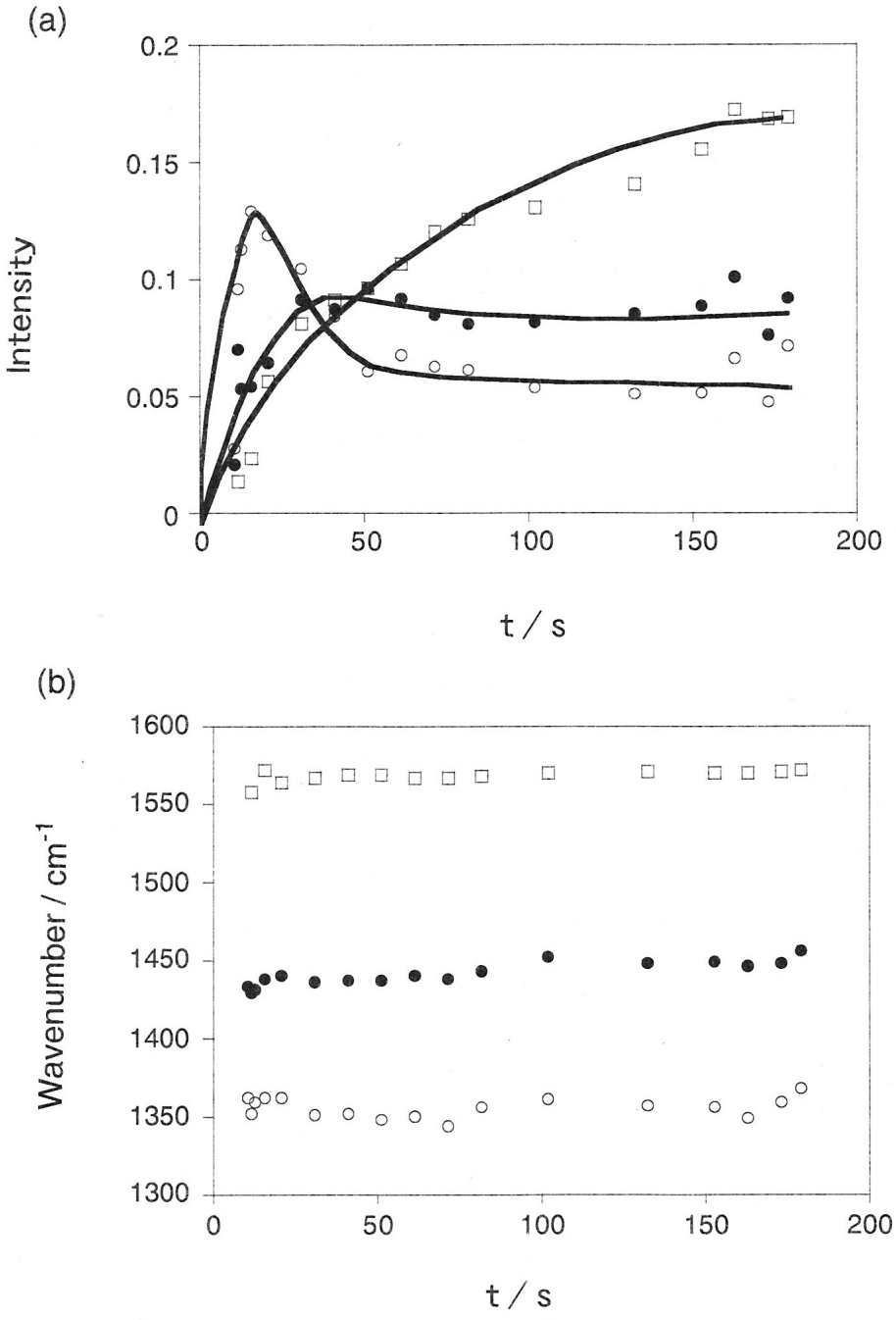

Figure S3 (a) Band positions and (b) band intensities for the observed bands. Band at 1575 cm^{-1} (open square), band at 1440 cm^{-1} (solid circle) and band at 1350 cm^{-1} (open circle) as a function of time. The present data were obtained from the spectra shown in Figure S1.

S1.2.1.2 Assignment of observed bands

(i) The band at 1350 cm^{-1}

The possible adsorption states of NO_3^- are unidentate, chelating bidentate, and tridentate, which are adsorbed through one, two and three oxygen atoms, respectively, as shown in Scheme. According to the report for the nitrate-coordinated complexes [4], the symmetric NO_2 stretching mode of the unidentate NO_3^- and asymmetric NO_2 stretching mode of the chelating bidentate NO_3^- appear in the wavenumber range of 1160 – 1300 cm^{-1}. The latter band and symmetric and asymmetric NO stretching modes of the tridentate are IR inactive due to the surface selection rule. Consequently, the observed band is assigned to the symmetric NO_2 stretching mode of the unidentate NO_3^-.

(ii) The band at 1575 cm^{-1}

This band position is within the region (1480-1630 cm^{-1}) reported for the N=O stretching mode of the chelating bidentate and the asymmetric NO_2 stretching mode of the unidentate (Scheme S1). Because the latter mode is IR inactive, the band at 1575 cm^{-1} is reasonably assigned to the N=O stretching mode of the bidentate NO_3^- adsorbed on Rh. This bidentate nitrate was only adsorbed nitrate species on a polycrystalline Pt in 0.1 M $HClO_4$ containing 0.01 M $NaNO_3$ (band position: 1547-1568 cm^{-1} at 0.2 V) [2].

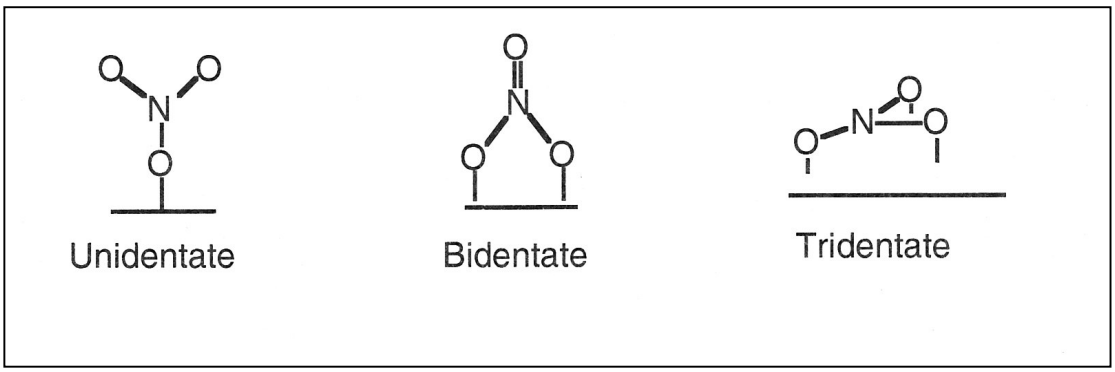

Scheme S1 Adsorption mode of nitrate ion on metal surface.

(iii) The band at 1440 cm^{-1}

The unidentate and bidentate NO_3^- do not have the band in the wavenumber range close to 1440 cm^{-1} except for the N=O stretching mode of the bidentate NO_3^- (1480-1630 cm^{-1}). However, this mode was already assigned to the band at 1575cm^{-1}. Another candidate is adsorbed NO_2^- because pure Rh has the NO_3^- reduction activity [5, 6], and this band appeared and grew at negative potentials. It is reported that nitrite can be coordinated to the metal surface in the three different mode as in metal complexes; i.e., nitro (coordinated via nitrogen atom), nitrito (coordinated via one oxygen atom), and chelating nitrito forms (coordinated via two oxygen atoms) as shown in Scheme [4]. The observed wavenumber of 1440 cm^{-1} is within the range of the N=O stretch of the nitrito form and the asymmetric NO_2 stretch of the nitro form. The latter band is IR inactive [7, 8]. Therefore, it is concluded that the band at 1440 cm^{-1} is assigned to the N=O stretching mode of the nitrito form in NO_2^- formed by the reduction of NO_3^-. Although the nitrito form has another IR active band assigned to N-O stretching mode in the range of 1084 - 1114 cm^{-1}, it was not clearly observed because of the overlapping with the band due to ClO_4^-.

(iv) The band at 1760 cm^{-1}

This band is assigned to the linear NO for the following reasons. First, the band was only observed in negative potentials, indicating that it is originated from the reduction product. Second, there is no band, which can be assigned to NO_3^- in this region. Third, the adsorbed linear and bridged NO gives bands at 1775 and 1620 cm^{-1} on Rh [9], respectively. The 1760 cm^{-1} band is close to the band assigned to the linear NO.

S1.2.1.3 Potential dependence of the bidentate band

SEIRA spectra during negative and positive-going potential scans from 0.2 V in a NO_3^--free 0.1 M $HClO_4$ solution are shown in Figure S4 (a) and (b), respectively. Figure S5 (a) and (b) show the position and the relative integrated intensity of the bidentate NO_3^- band as a function of the electrode potential. The intensities of the

other bands were so small that it was difficult to estimate the correct band position and change in the intensity. The potential dependence of the amount of the surface oxide determined in a previous section is also shown in Figure S5(b).

The band position of the bidentate NO_3^- shifted to lower or higher wavenumbers with the decrease or increase of the potential (Figure S5(a)), respectively, which is characteristic to the adsorbed species. In a negative-going potential scan, the band intensity decreased with the decreasing potential to reach ca. 20% of the initial intensity at -0.2 V. It is reasonably considered that the adsorbed species are reduced because Rh has the ability to reduce the nitrate [5, 6]. In a reverse scan, however, about one third of the decreased intensity was recovered, showing a part of the bidentate was not reduced to convert to a different form of nitrate. In a positive-going potential scan, the band intensity gradually decreased up to 0.6 V and more steeply decreased at > 0.6 V. Only a 18% of initial intensity remained at 1.0 V, and reappeared in a reverse scan. As the case of reduction, some part of the adsorbed bidentate may change its configuration to be IR inactive; for example the change from perpendicular to parallel to the electrode surface. The disappearance of the band by the potential-dependent configuration change was observed for the adsorbed NO_2^- on Pt electrode [10]. It is worthwhile to mention that the band intensity started to increase at 0.6 V in a negative-going potential scan from 1.0 V. This potential (0.6 V) corresponds to that at which the reduction of the surface oxide started.

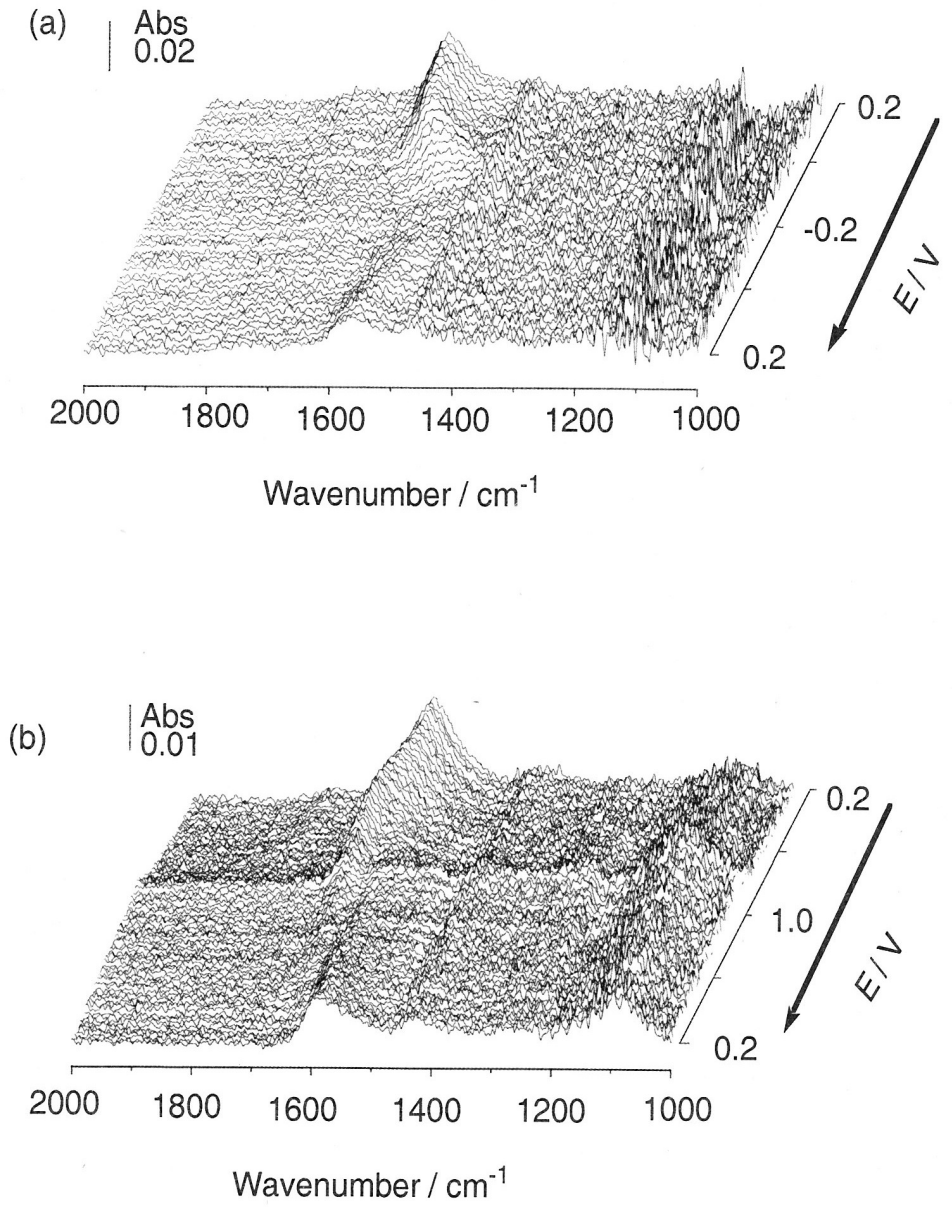

Figure S4 The potential dependence of SEIRA spectra in 0.1 M $HClO_4$. The electrode potential was scanned from 0.2 V to (a) negative and (b) positive potentials at the sweep rate of 0.02 V s^{-1}.

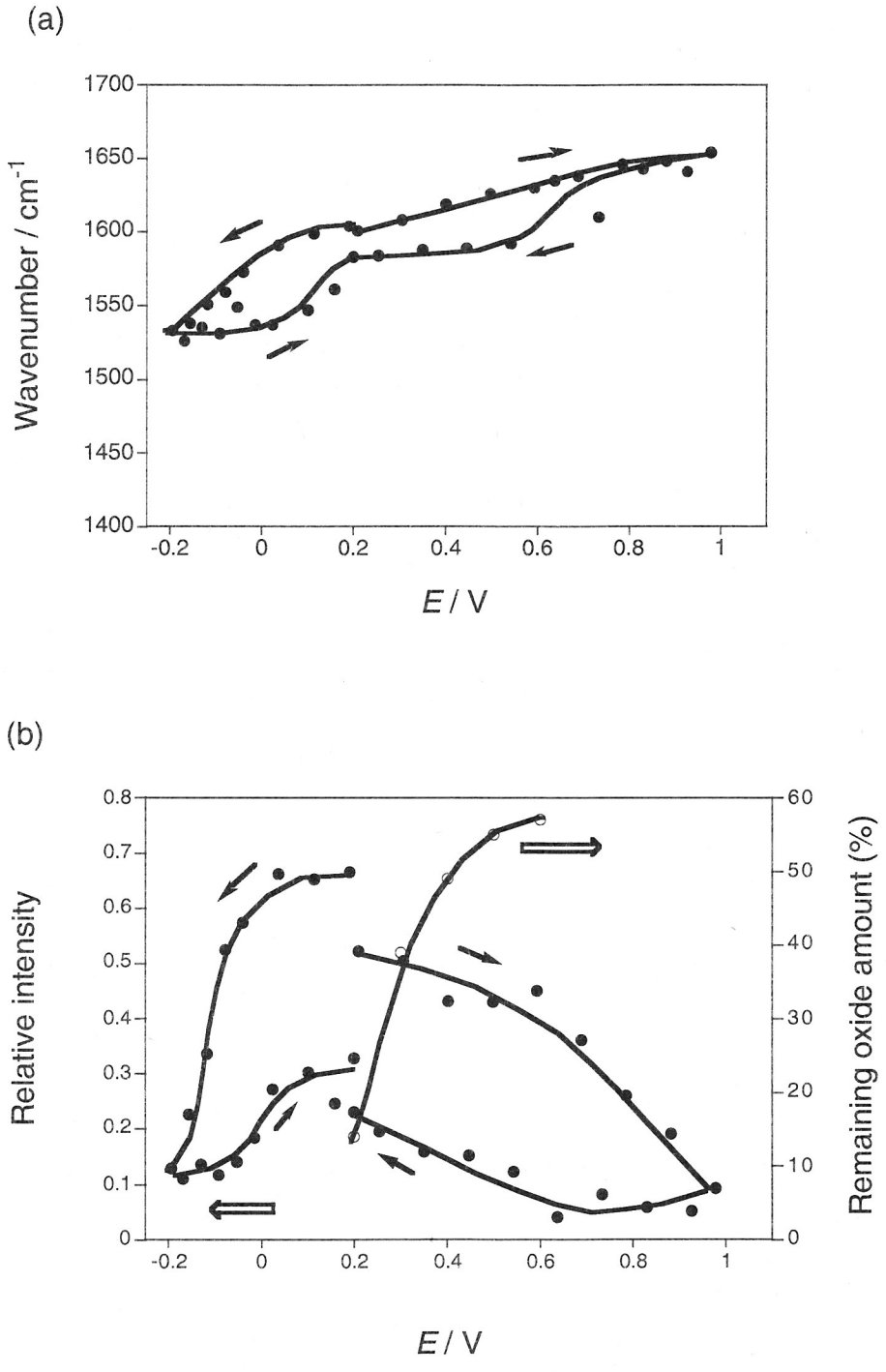

Figure S5 The potential dependence of (a) the band position and (b) the integrated band intensity for bands at 1575 cm^{-1} (solid circle), which were obtained from the spectra shown in Figure S4. The potential dependences of the remaining oxide amount cited in Table 1 (open circle) shown in (b). The integrated area was normalized to the total band intensity at -0.2 V.

S1.3 Overall adsorption scheme of nitrate on Rh

At 0.6 V where a considerable part of the surface is covered by the oxide, only the unidentate nitrate is formed. This makes sense because most of Rh sites must be isolated. When the oxide is reduced, more Rh sites become available, resulting in the formation of more stable bidentate mode. Simultaneously, the unidentate nitrate is reduced to form nitrite of the nitrito form. This reduction is easy to understand because both compound are adsorbed via one oxygen atom and structural change is small. At more negative potentials the adsorbed nitrate and/or nitrite are more reduced to nitric oxide. A variety of the adsorbed species may owe to the higher activity for nitrate reduction of Rh. The recovery of the intensity by the reverse scans of the negative and positive-going scans indicates the presence of the potential dependent configuration change of the adsorbed NO_3^- in these processes.

S1.4 Summary

The adsorbed states of nitrate on the Rh electrode and their potential dependence were examined by the surface-enhanced infrared absorption spectroscopy (SEIRAS) in 0.1 M $HclO_4$. The bands of adsorbed NO_3^- were observed at 1350 cm^{-1} and 1575 cm^{-1} at 0.2 V vs. Ag/AgCl (saturated KCl), which are assigned to the symmetric NO_2 stretching mode of unidentate NO_3^- and the N=O stretching mode of the chelating bidentate NO_3^-. In addition to these two type of NO_3^- bands, another band at 1440 cm^{-1} was appeared and it is assigned to the N=O stretching mode of the nitrito form of adsorbed NO_2^-, which can be formed by the reduction of NO_3^- at 0.2 V. At 0.1 V, the band of adsorbed NO was also observed at 1760 cm^{-1}. On the other hand, no band was observed at 0.6 V because of the increase of the surface oxide. The potential dependence of the band intensity for the adsorbed NO_3^- at 1575 cm^{-1} shows that the adsorbed NO_3^- disappeared by reduction and surface oxidation by negative and positive-going scans, respectively.

S1.5 References:

[1] K. Nakata, Y. Doi, S. Kubota, K. Shimazu, J. Electroanal. Chem 647 (2010) 187.

[2] K. Nakata, Y. Kamaya, K. Shimazu, A. Yamakata, S. Ye, M. Osawasa, Langmuir 24 (2008) 4358.

[3] Conway, B. E., Angerstein-Kozlowska, H., Czartoryska, G., Z. Phys. Chem. N. F. 112 (1981) 195.

[4] Kadirgan, R., Beden, B., Leger, J.-M., Lamy, C., J. Electroanal. Chem. 125 (1981) 89.

[5] Grden, M., Piascik, A., Koczorowski, Z., Czerwinski, A., J. Electronal. Chem. 532 (2002) 35.

[6] Lukaszewski, M., Kusmierczyk, K., Kotowski, J., Siwek, H., Czerwinski, A., J.

[7] Rand, D. A. J., Woods, Surf. Sci. 41 (1974) 611.

[8] Lukaszewski, M., Czewinski, A., J. Solid State Electrochem. On line.

[9] B. Gurau, R. Viswanathan, R. Liu, T. J. Lafrenz, K. L. Ley, E. S. Smotkin, E. Reddington, A. Sapienza, B. C. Chan, T. E. Mallouk, S. Sarangapani, J. Phys. Chem. B, 102 (1998) 9997.

[10] Beden, B., Lamy, C., Leger, J. M., Electrochim. Acta 24 (1979) 1157.

Acknowledgement

First and foremost, I would like to express my sincere gratitude to my supervisor Professor Katsuaki Shimazu for the continuous support of my Ph.D study and for his patience, motivation, enthusiasm, and immense knowledge. I could not have imagined having a better advisor and mentor for my Ph.D study. Ever since, He has supported me not only by providing a research assistantship during my study but also academically and emotionally through the rough road to finish this thesis. And during the most difficult times when writing this thesis, he gave me the moral support and the freedom I needed to move on. His effective guidance also helped me in all the time of research and writing of this thesis. Besides my advisor, I would like to thank the rest of my thesis committee members: Professor Katsuaki Konishi, Professor Ichizo Yagi, Associate Professor Kawaguchi Toshikazu and Dr. Kou Nakata (Assistant professor) for their encouragement, insightful comments, and hard questions.

I would like to thank Dr. Toshikazu Kawaguchi (Associate professor) for the thoughtful comments, wonderful support and the constructive criticism during project evaluation, which helped me to make necessary improvements.

I am greatly indebted to Dr. Kou Nakata (Assistant professor) for the support he has extended to me throughout my work towards this thesis, and for his informed guidance and advice. He always offered me good advice and brought previously unrecognized aspects of each situation to my attention.

I specially would like to thanks the members of Shimazu group for their kind help and cooperation during my work and mental support. I am grateful to my parent for giving me life I ever deemed and their unconditional love has been my greatest strength. The constant love, encourage and optimistic mental support, from my wife is sincerely acknowledged. Finally, my greatest regards to my Almighty for bestowing upon me the courage to face the complexities of life and complete this project successfully.